Geochronology and geochemical characteristics of sediments

at the Jeongokri archaeological site, Korea

Jin Cheul Kim

A dissertation submitted to Graduate School of

Seoul National University in partial fulfillment of

the requirements for the degree of Doctor of Philosophy

School of Earth and Environmental Sciences

Graduate School

Seoul National University

August, 2009

ABSTRACT

Geochronology and geochemical characteristics of sediments at the Jeongokri

archaeological site, Korea

Jin Cheul Kim

School of Earth and Environmental Sciences

The Graduate School

Seoul National University

This study presents the depositional ages and geochemical characteristics of unconsolidated Quaternary sediments collected from the Jeongokri archaeological area, Korea. For decades, many paleolithic artifacts have been excavated from this area, which provided important data for the East Asian Lower Palaeolithic with occurrence of the so-called "Acheulian-like" handaxe (Yi and Clark, 1983; Bae, 1988). Unconsolidated sediments from a total of 12 localities at the Jeongokri were collected from the sediment sequence overlying unconformably the Quaternary Jeongok Basalt. Among them, 25 samples were selected from three places for age dating. Age estimate was made by applying of optically stimulated luminescence (OSL) dating, with results showing a large range of age distribution. The samples collected from fluvial sandy sediments at locality 1 have an age range of 34 to 66 ka, while those from fine-grained silty-clay sediments (localities 2 and 3) are with a range of 100 to 200 ka. Localities 2 and 3 do not show ages younger than 100 ka. The altitude of the Jeongok Basalt beds indicates the possible existence of least three different basalt levels at 48~49 m, 52 m, 53~54 m above the sea-level. Previous age-dating suggested that the lava flow could have occurred during a prolonged period between 0.1 and 0.5 Ma (Kojima, 1983; Danhara et al., 2002; Yi et al., 2005). The current study demonstrates that the deposition of the

unconsolidated fine-grained sediments on the basalt bed began at least 200,000 years ago. Re-measurement of the artifact horizon by OSL dating suggests that a hominin occupation could be younger (less than 200 ka) than previously suggested. The results of geochemical analyses suggest that the most dominant sources of the deposit could the Chinese loess and local material of fluvial origin from the Korean Peninsula. A possible source area of deposition of wind-blown materials is the Yellow Sea locating between China and Korea. Also, geochemical compositions of the deposit indicate the influence of monsoonal activities on the Quaternary paleoenvironment in Korea, which are closely related with sediments origin.

CONTENTS

CHAPTER 7. Re-evaluation of the chronology of the palaeolithic site at Jeongokri, Korea, using OSL and TT-OSL signals from quartz -------------- 127

CHAPTER 8. Geochemical characteristics of Jeongokri sediment as indicators of provenance --- 139

CHAPTER 1. Introduction

1-1. Purpose of this study

Since the late 1970's, paleolithic artifacts have been excavated from fine-grained sediments in the Jeongokri area, located in the central part of the Korean peninsula (Yi, 1984). The palaeolithic site of Jeongokri is one of the best known archaeological sites in the Korean Peninsula. The Jeongokri Paleolithic site has been considered an important Lower Palaeolithic site in East Asia with the discovery of the so-called "Acheulian-like" handaxe (e.g. Yi and Clark, 1983; Bae, 1988). This led to an age estimation of 0.3 Ma based on some morphological similarity of artifacts (Yoo, 2007), which provides evidence against the Movius' hypothesis that there was no culture of handaxes in East Asia (Movius, 1948; Yi and Clark, 1983). The timing of manufacture of these artifacts is important to understand the prehistoric cultural evolution in East Asia. However, there has been a lack of reliable age dating, because of the lack of suitable material for dating and the age limit of conventional dating methods such as radiocarbon dating. Therefore, despite the archaeological significance of the site and almost 30 years of research, its chronological framework has remained unclear still today.

In this study, optically stimulated luminescence (OSL) dating method was applied to determine the timing of the deposition of the fine-grained sediments containing archaeological remains. This method measures OSL signals from certain mineral grains (e.g. quartz) in sedimentary deposit and the environmental dose-rate to derive the age of the last exposure of the sediment to sunlight. The main advantages of the OSL dating over other conventional methods in Quaternary materials are: (1) quartz grains, which is a commonly used dosimeter for OSL

dating method, are present in almost all sediments, and (2) the age range datable by the OSL method is relatively wider than others, coverings from several years up to hundreds of thousands years.

Over the last decade, OSL studies have been applied to a range of depositional environments. However, some cases are not an ideal for OSL dating. Insufficient or/and uneven exposure to daylight prior to burial is a potential problem in OSL dating, which may not have been sufficient to completely reset the OSL signal of all grains prior to deposition (Murray et al., 1995; Olley et al., 1998; Zhang et al., 2003). Nevertheless, OSL technique shows a great potential for use in accurate determination of the timing of deposition for Quaternary sediments.

In this study, we used the quartz grain samples collected from the fine-grained sediments overlying the Quaternary Jeongok Basalt. We carried out various experiments to check the problems in OSL ages, including preheat plateau test and dose recovery test. Also, more detailed analysis of the component separation of OSL decay curve was measured for investigate component defined behaviour. Also, we applied OSL dating to fine grain (4-11μm) sediments. In order to extend the age range of OSL dating of Jeongokri sediments, a thermally transferred optically stimulated luminescence (TT-OSL) signal was investigated. From these various experiments, this study assesses the suitability of OSL dating techniques and develops the most suitable OSL dating method for Jeongokri sediments. These results also allow the development of chronologies of the Jeongokri archaeological sites.

Following age-dating, there were made geochemical analyses of the Jeongokri sediments. After examining the variations of geochemical compositions, there were developed geochemical proxies to identify the provenance of sediments, and a comparison was made with those of Chinese
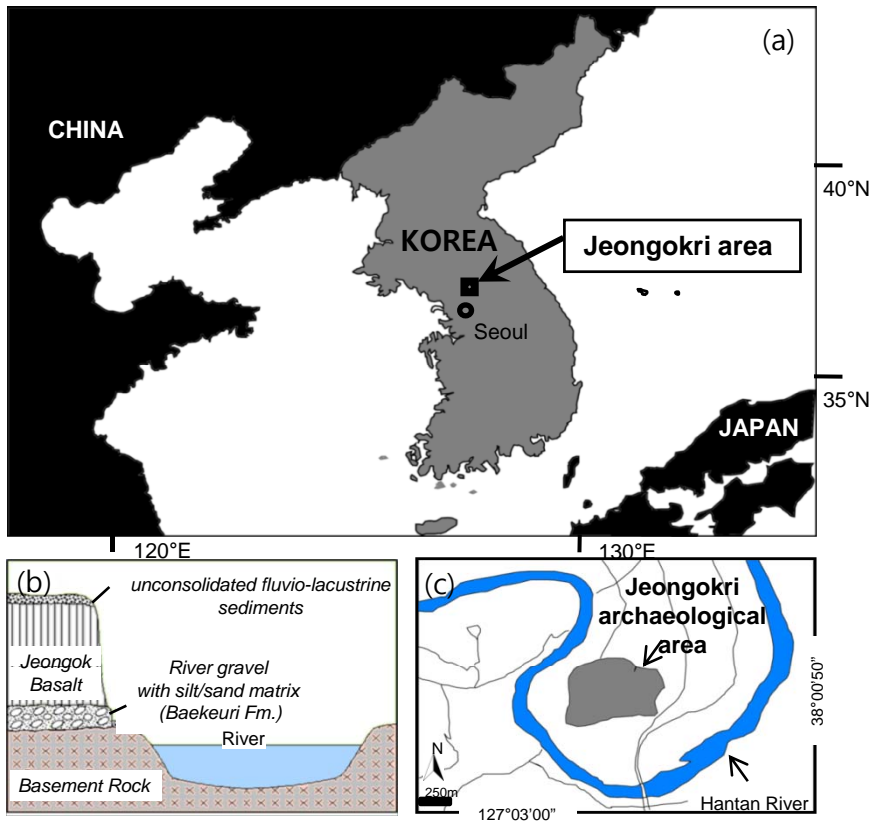
Fig. 1-1. (a) The location of Jeongokri, (b) a schematic geological section illustrating the major units discussed in the text (from Bae, 1989), and (c) the position of the archaeological area relative to the Hantan river.

Loess Plateau. Finally, geochemical indices were also applied to interpret the Quaternary paleoenvironmental changes in Jeongokri sediments.

1-2. Geology and review of previous researches of the Jeongokri area

1-2-1. An overview

The Jeongokri archaeological area is located in the central part of the Korean Peninsula, 37 km northeast of Seoul (Yi, 1984) on the inside of a meander of the Hantan River (Figs. 1-1a and c). The geology of this study area is composed of Precambrian gneiss, Jurassic granite, gravel and sand layers (Baekeuri Formation), Quaternary basalt, unconsolidated fluvial sediments and paleosols with decreasing age (Fig. 1-1b). The Baekeuri Formation consists primarily of quartzite, gneiss and granite, all of which originated from the Precambrian bedrock below (Bae, 1988). The Jeongok Basalt is usually found overlying the Baekeuri Formation and its thickness is about 10 to 20 m. The number of lava flows is estimated to be more than three and, up to eleven (Lee et al., 1983). The unconsolidated fluvial sediments are interpreted to have been deposited from the Hantan or Imjin rivers on Quaternary Jeongok Basalt plateau. Although poorly supported, Shin et al. (2004) interpreted that upper 4m of the unconsolidated sequence is made of loess-paleosol deposits, while the lower 3m consists of fluvial or lacustrine sediments. The loess-paleosol sequence is different from the fluvial sediments in grain-size distribution pattern, which is composed of silt-clay sized sediments (Shin et al., 2004). Lower part of the sequence is composed of thick layer of coarse and fine-grained sand sediments.

Over the years, there have been made some petrographical studies of the volcanic rocks, tectonic episode of this region and development of the Hantan river

4

basin have been assessed (Lee et al., 1983; Won, 1983; Kim et al., 1984; Bae, 1988; Won et al., 1990; Wee, 1996). There also have been many efforts to establish chrono-stratigraphy of the Jeongokri Palaeolithic site in the regional context (Lee et al., 1983; Yi, 1984; Bae, 1988; Yi et al., 1998; Danhara et al., 2002; Shin, 2004; Shin et al., 2004). However, controversies on the chronology have continued, and general consensus has not been reached for the explanation of formation processes of unconsolidated sediments overlying the Jeongok Basalt.

1-2-2. Previous geochronological studies

The age estimation of the Jeongokri Palaeolithic site has been discussed from the early 1980's and a number of dating methods have been applied to rocks and sediments in the vicinity of Jeongokri. But, there have been several problems concerning the age calculation of this study area. Fission track (FT) dating has been undertaken on zircon grains from the Baekeuri Formation underlying the Jeongok Basalt which had been baked when the basalt flowed. FT ages of 510 ± 70 ka (Danhara et al., 2002) and 420 ± 170 ka (Yi et al., 2005) have been obtained. There were additional ESR and luminescence dates from the underlying Baekeuri Formation (Yi, 2005). Especially, thermoluminescence (TL) dating on the Baekeuri Formation revealed 148 ± 10 ka (Choi et al., 2004), which was significantly younger than previously reported fission track (FT) ages as mentioned above (0.5~0.4 Ma; Danhara et al., 2002; Yi et al., 2005). Therefore, no clear consensus has been reached regarding the age of the Baekeuri Formation. The Jeongok Basalt overlying these gravels has been analysed repeatedly using K-Ar methods. These have given ages from ca.10 ka to over 1 Ma (Yi, 1984, 1986, 2005; Bae, 1988; Danhara et al., 2002). Many of these ages were determined on whole rock samples, and Danhara et al. (2002) found evidence for a variety of problems with such an

approach including xenoliths giving age overestimates, and the possibility that glassy materials may not have retained radiogenic argon. Additionally, Norton et al. (2006) suggest that a number of different basalts may have been dated in these studies, but no clear consensus has been reached, and so these underlying materials provide little constraint on the age of the overlying unconsolidated sediments in which the archaeological finds have been made. Direct dating of the artifact-bearing layers have been attempted by applying ^{14}C and luminescence techniques at various localities with results ranging between >30 ka and ca. 150 ka. Nevertheless, a conclusive evaluation of their age is premature as a comprehensive stratigraphic correlation is yet to be made for them.

Glass shards have been reported from two horizons, 10-45cm and 100-110cm below the surface and identified as AT and K-Tz tephra (Yi et al., 1998; Danhara et al., 2002), with ages of 25.1±0.3^{14}C ka BP (Miyairi et al., 2004) and 90-95 ka, respectively (Machida and Arai, 1992; Machida, 1999). However, only two shards of K-Tz tephra were recovered (Danhara et al., 2002) making it difficult to be confident in the identification of the tephra.

1-2-3. Archaeological discovery

The Jeongokri is famous for the discovery of the hand-axe. It was discovered in 1978, providing important archaeological evidence not only for Korea but also for East Asia. Artifacts are chiefly made of crude quartz and quartzite, which can be easily acquired from the outcrops of old bedrock and river cobbles deposited by the river flow (Yoo, 2007).

Among the artifacts, hand-axe is the most important element of the palaeolithic industry. Its discovery ignited discussion on the characteristics of the paleolithic industry in East Asia. Also, it has been made many controversies in the

archaeological society. It is conclusive opposite evidence against the Movius'
hypothesis (Movius, 1948; Kim et al., 1981; Yi and Clark, 1983; Bae, 1988).

Movius' hypothesis is a theory first proposed by the American archaeologist
Hallam L. Movius in 1948 to demonstrate a technological difference between the
early prehistoric tool technologies of the east and west of the Old World
(http://en.wikipedia.org/wiki/Movius_Line). He noticed that assemblages of
palaeolithic stone tools from east sites of northern India never contained handaxes
and tended to be characterized by less formal implements known as chopping tools.
He drew a line to show where the difference occurred, dividing the tools of Africa,
Europe and western Asia from those of eastern Asia. His hypothesis also suggests a
difference in the evolutionary course of the people who made different tool types
across the Movius Line. Researchers (e.g. Chung, 1996; Bae, 1988, 1992) tend to
argue that handaxes from Jeongokri site are the clear evidence against Movius'
attribution of the East Asian Lower Palaeolithic to the "chopper-chopping tool
tradition". However, morphological resemblances of the Korean samples may be
explained in various terms (Yi, 1989; Yoo, 1997; Yoo, 2007).

1-3. Paleoclimates through the late Quaternary in East Asia

The astronomical theory of paleoclimates aims to explain the climatic variations occurring with quasi-periodicities situated between tens and hundreds of thousands of years. Such variations are recorded in deep-sea sediments, in ice sheets and in continental archives. Globally, climatic variations are driven by orbital cycles of different periodicity; eccentricity has ~100ka cycles, tilt has ~41 ka cycles, and precession has ~23 ka cycles. During the Quaternary, these orbital cycles are thought to have been the cause of glacial and interglacial cycles that are seen in the $\delta^{18}O$ records of benthic marine foraminifera and in the δD records of ice cores from Vostok, Antartica.

The middle to late Pleistocene (MIS 5-7) paleoclimates are related with this study, so the following introduction of paleoclimate focuses on this time period (Fig. 1-2), which shows that the paleoclimatic variations of the eastern Asia. During interglacial (MIS 5 and 7), the climate in the eastern part of Asia was relatively warm and humid. Interglacial environments on the sediments are characterized by summers, enhanced precipitation, and elevated soil-moisture under the influence of the East Asian summer monsoon. Increased summer monsoon precipitation leads to high stream discharge and associated erosion of alluvial deposits along valley floors. Strong pedogenic activity during peak interglacial conditions produced well-developed organic-rich soils. A relatively warm and humid climate has continued at least until the appearance of a colder phase in MIS 6. During glacial period, dust accumulation rate and the fluxes of eolian grain-size sediments increased. The chemical and mineralogical parameters of these dust deposits are used to document the effects of the winter and summer monsoon. Pedogenic activity substantially reduced. The increased dust deposition

8
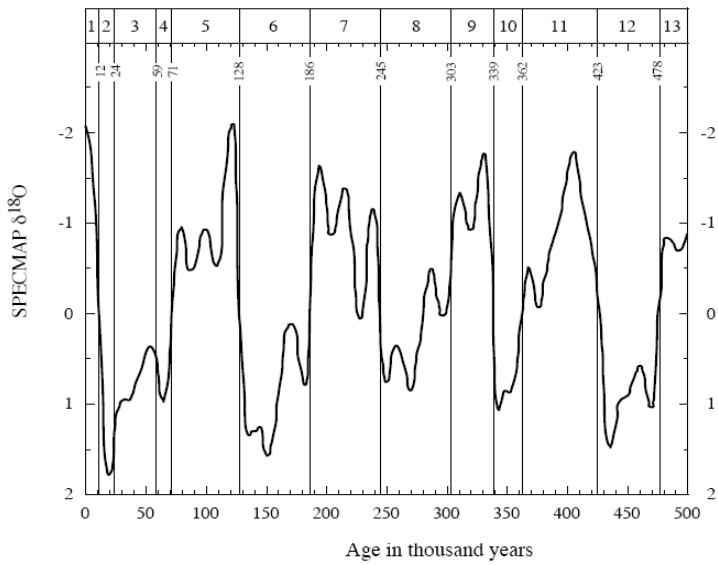
Fig. 1-2. The orbital theory of Pleistocene climate; support from a revised chronology of the marine $\delta^{18}O$ record (Imbrie et al., 1984).

had a diluting effect on soil formation and resulted in a substantial decrease in the volume percent of pedogenically produced fine-grained magnetic minerals in the accumulating loess, and a related reduction in its magnetic susceptibility (Porter et al., 2001). The North Atlantic Heinrich events and the Asian winter monsoon are closely related through the Mongolian high pressure system as indicated by the increased loess deposition in the Chinese Loess Plateau (Porter and An, 1995; Lee et al., 2008).

CHAPTER 2. Optically Stimulated Luminescence (OSL) dating

OSL dating of sediments was first proposed by Huntley et al. (1985). Quartz or feldspar minerals are commonly used for OSL dating. During geological burial period, the OSL signal builds up at a rate related to the environmental dose-rate. From these accumulated OSL signal we can estimate the burial age.

2-1. Basic Concepts of Luminescence Dating

After sedimentation, grains of quartz and feldspar are buried and exposed to low-level ionizing radiation, which is produced by the decay of naturally occurring radionuclides. During this exposure to ionizing radiation, free charge carriers (electrons and holes) are produced, and some of them are trapped at defects in the crystal lattice. In natural quartz grains, impurities present in the crystal lattice may cause defects (Fig. 2-1). Charge trapped in the OSL traps is stable over long periods of time until the mineral is exposed to light. Hence, the total amount of charge in these traps will increase with burial time. However, trapped charge is released when the sediments containing mineral grains are eroded and transported in daylight (Wallinga, 2002). Luminescence occurs from the recombination of electrons released from traps and holes (McKeever and Chen, 1997). If heating is applied to release the trapped charges, the luminescence is called thermoluminescence (TL); if light exposure is the releasing agent, the light emission is called optically stimulated luminescence (OSL). OSL is generally much more rapidly reset than TL (Godfrey-Smith et al., 1988), thus making it more suitable for dating sediments where the bleaching occurs by exposure to light. The brightness of the luminescence signal reflects the amount of charge trapped.
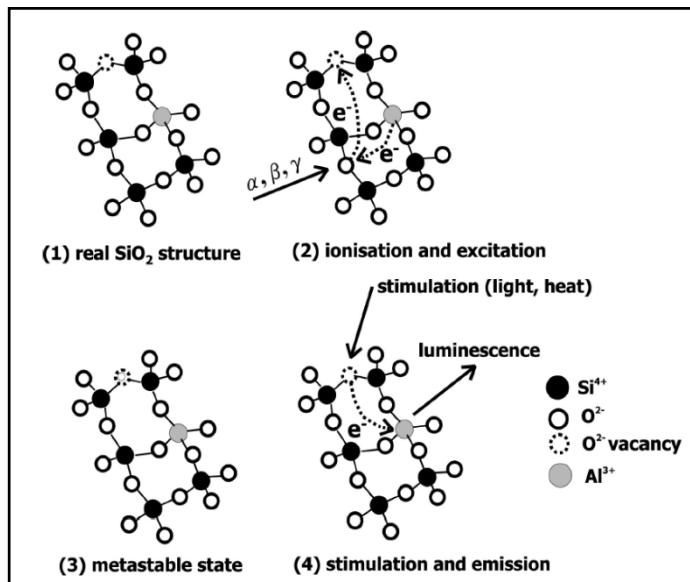
Fig. 2-1. Traps are defect in the lattice and trapped electrons are the 'memory' of the accumulated exposure to nulcear radiation. Luminescence centres are certain types of centre, gives rise to the emission of light (Wagner, 1998; Modified by Choi et al., 2004).

Age (a) = Equivalent dose (Gy) / Dose rate (Gy/year)

The maximum age for application of OSL dating is determined by saturation of the traps in the crystal. The limitation of the saturation of the quartz OSL is approximately 300Gy, which usually limits its application to the last 150ka, whereas for feldspar dating up to 1 Ma is possible in principal (Wallinga, 2002). Although, feldspar dating is useful for old age samples, feldspar dating can be troubled by anomalous fading (Wintle, 1973; Spooner, 1994b; Lamothe and Auclair, 1999; Huntley and Lamothe, 2001) and changes in trapping sensitivity (Wallinga et al., 2000). Also, Wallinga et al. (2001) found severe underestimation in the feldspar infrared stimulated luminescence (IRSL) ages, which was attributed to changes in the trapping probability of the feldspars during preheating. On the other hand, quartz signal is more rapidly reset than that of feldspar. Also, physical properties are much simpler to general understanding. This led to use quartz for luminescence dating more frequently.

2-2. Instrumentation for OSL dating

The Risø TL/OSL automatic measurement system enables measurement of both thermoluminescence (TL) and optically stimulated luminescence (OSL). The system allows up to 48 samples to be measured. Individual irradiation sources are by radioactive beta or alpha ($^{90}Sr/^{90}Y$ or ^{241}Am). Also, optical stimulation is used by various light sources. The emitted luminescence is measured by a light detection system comprising a photomultiplier tube and suitable detection filters (Fig. 2-2).

2-2-1. Optical stimulation system

Optical stimulation is achieved using an array of light emitting diodes (LEDs), which are compact, fast and enables electronic control of the illumination power density. The array of LEDs is equipped with an optical feedback servo-system to ensure the stability of the stimulation power. The LEDs are arranged in 7 clusters each containing 7 LEDs (i.e. a total of 49 LEDs). The distance between the diodes and the sample is approximately 20 mm.

1) Infrared (IR) LEDs emitting at 875 nm arranged in three clusters each containing seven individual LEDs. The maximum power from the 21 IR LEDs is approximately 135mW/cm^2 at the sample position.

2) Blue LEDs emitting at 470 nm (FWHM = 20 nm) arranged in four clusters each containing seven individual LEDs. The total power from these 28 LEDs is approximately 40mW/cm^2 at the sample position. A green long pass filter (GG-420) is incorporated in front of each blue LED cluster to minimise the amount of directly scattered blue light reaching the detector system (extracted information is from the Risø TL-OSL reader brochure).

2-3. The Single-Aliquot Regenerative Dose Protocol (SAR method)

During the last few years, OSL dating has been developed by SAR procedure. This measurement was described by Murray and Roberts (1998) and further developed by Murray and Wintle (2000). The most important modification is insertion of a fixed test dose following measurement of the natural and regeneration doses, in which the "sensitivity-corrected" natural OSL signal is compared with equivalent sensitivity-corrected signals regenerated by laboratory irradiation of the same aliquot of quartz. Prior to measurement of the test dose, a

thermal treatment termed the 'cut-heat' is applied, instead of preheat. This cut-heat is same purpose as preheat, however, in order to minimize sensitivity change of OSL signal, the heating step applied during the cut-heat is less severe than the preheat. Also, cut-heat operated as that sample is cooled immediately once the desired temperature has been reached.

Simplified SAR protocol is represented in Table 2-1. After preheating and subsequent measurement of the natural OSL signal (L_0) at 125^oC, the aliquot is given a small beta irradiation (test dose). A test-dose is given (usually about 10% of the expected equivalent dose (D_e)), the sample heated again, and then the OSL (T_0) is measured. These measurement cycles provide the sensitivity-corrected natural OSL ($R_0 = L_0/T_0$). The complete measurement cycle is repeated with increasing regeneration doses (D_i). Corrected regenerated OSL signals (R_i) are calculated by dividing each regenerated OSL signal (L_i) by $R_i = L_i/T_i$. After finish increasing regeneration dose step, regeneration dose (0 Gy) is given to test whether the curve of R_i against D_i passes close to the origin. To confirm that the sensitivity correction is working suitably, the final regeneration dose, termed the recycling point, is the same as the initial dose (D_1). The "recycling ratio" should be close to unity if the sensitivity correction is satisfactory (Choi, 2004).

The SAR procedure has now been applied to quartz grains from a wide range of sediments of different ages and from different geographic areas. Using the SAR protocol, OSL ages have been obtained in good agreement with independent age control for a wide range of depositional environments including aeolian, lacustrine, marine, and fluvial (Murray and Olley, 2002). OSL dating of quartz using the SAR procedure is probably the best available method for luminescence dating for various environmental sediments. In this study, SAR protocol is fundamentally used to obtain high precision estimates of equivalent dose (D_e).

Step	Treatment	Observed
1	Give dose, D_i	-
2	Preheat (160~300°C for 10s)	-
3	Stimulate for 100s at 125°C	L_i
4	Give test dose, D_t	-
5	Cut heat to 160°C	-
6	Stimulate for 100s at 125°C	T_i
7	Return to 1	-

Table 2-1. Single-Aliquot Regenerative-Dose (SAR) (Murray and Wintle, 2000, 2003)
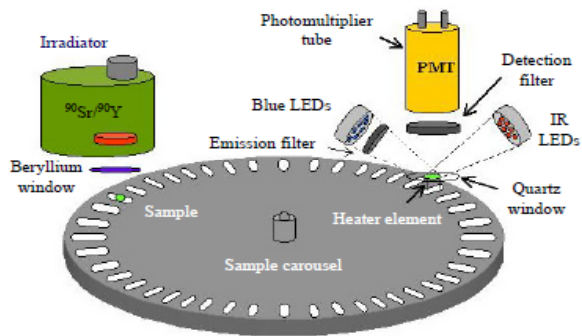
Fig. 2-2. Photo and schematic drawing of the Risø TL/OSL Luminescence reader.

2-4. Resetting of the OSL signal

The trapped charge in the mineral is reduced by light exposure, which is normally referred to as bleaching or zeroing (Fig. 2-3). The OSL signal from quartz is reset more quickly than that of feldspar when the minerals are exposed to sunlight (Godfrey-Smith et al., 1988). Incomplete zeroing of OSL signal prior to deposition is caused by the limited light exposure of sediment grains during transport. Poorly bleached sediments will almost certainly consist of a mixture of poorly bleached and well-bleached grains. If quartz grains were optically bleached to different degrees, and OSL measurements on each grain would give a different equivalent dose (D_e). Because luminescence measurements cannot distinguish between charge trapped before and after burial. Where partial bleaching is present, careful assessment of the distribution of D_e values is necessary to obtain the correct D_e. Simply taking some measure of the average from the D_e values for a partially bleached sample may lead to a significant overestimation of the luminescence age (Wallinga, 2002).

2-5. OSL dating of fluvial sediments

Radiocarbon dating is the most widely used geochronological tool, however it is often not applicable because of the lack of organic material and the limited age range (approximately <35ka). Accordingly, OSL dating is now increasingly used to determine the timing of sediments deposition, especially for fluvial sediments. However, incomplete zeroing of OSL signal prior to deposition is arguable for fluvial deposits owing to the limited light exposure of sediment grains during transport (Murray et al., 1995; Olley et al., 1998; Wallinga, 2002; Zhang et al.,
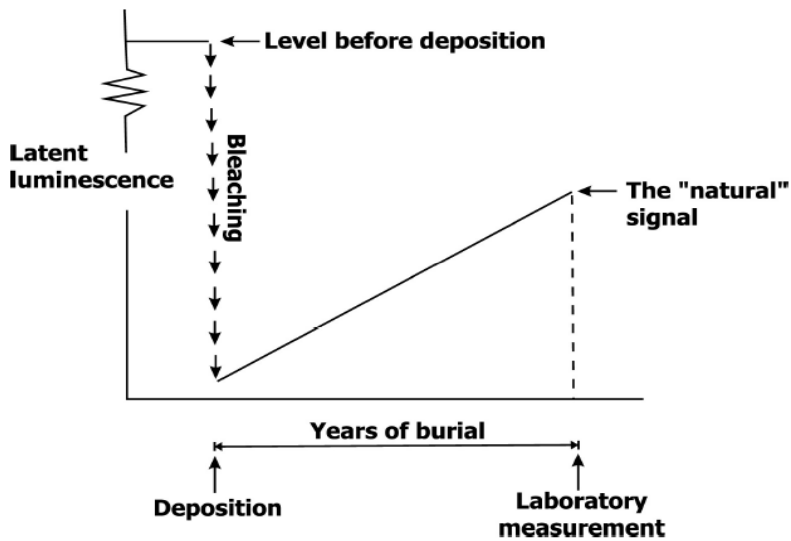
 Fig. 2-3. Bleaching event is the setting to zero of the latent signal. Subsequent latent signal builds up again through exposure to the weak natural flux of nuclear radiation (Aitken, 1998).

2003). In recent years, many studies have been undertaken to investigate the presence of partial bleaching in fluvial sediments. Murray et al. (1995) found that whilst modern overbank deposits were well bleached, channel deposits contained partially bleached grains. In heterogeneously bleached sample, each grain has been exposed to sunlight of differing strength and/or duration, causing varying amounts of residual trapped change to remain in the grains (Duller, 1994). Owing to the mechanisms of river transport, whereby each grain will follow a different path during transport, it is likely that grains in fluvial sediments will usually be heterogeneously bleached, thus causing scatter in the D_e values. Various statistical techniques to calculate an appropriate D_e value from heterogeneously bleached sediments were applied to fluvial sediments. The recent research into dating of fluvial sediments uses the shape of the D_e distribution to detect heterogeneous bleaching (e.g. Thomas et al., 2005), or uses a comparison with an independent age (Helena, 2006).

Most of the bleaching will occur when the grains are close to the water surface where the light intensity is greater and the light spectrum is wider (Wallinga, 2002). As mentioned above, Murray et al. (1995) suggested that overbank deposits are more likely to be well bleached as they must have been close to the water surface when the channel flooded while channel deposits contained partially bleached grains. Under turbid water in a fluvial environment the intensity of the light is greatly reduced, and the spectrum of the light is restricted (e.g. Berger and Luternauer, 1987). As a consequence, some trapped charge might remain at the time of deposition and burial of the grains. From Stokes et al. (2001), large aliquots of quartz from the river bed of the Loire indicate a decreasing trend of equivalent dose with transportation distance. Serious age overestimation has been found for deposits where transport distances are very short (Wallinga, 2002). However,

Murray and Olley (2002) presented a review where they collected results from various studies on fluvial samples which showed good correspondence between the OSL ages and those obtained from independent age. Jain et al. (1999) also suggest that the modern sample from the Luni channel (India) is well-bleached since the local climatic circumstances causes prolonged dry periods during which fluvial material is locally reworked by wind.

In all cases, large scattering of OSL age is not simply derived from partial bleaching. In addition, the different luminescence properties of grains such as different mechanical resetting rate and experimental error contribute to the scatter of OSL dating (Zhang et al., 2003).

2-6. Grain size effect

Recently, new possibilities of the OSL dating from fluvial sediments are explored and highlighted by some examples of geological applications. In a fluvial environment, finer grains are more likely to be carried on the upper part of the water column than coarser grains. Therefore, fine grains (4-11 μm) are more likely to be thoroughly exposed to light, and thus better bleached (Fuller et al., 1994). It seems to have a benefit to fluvial deposits. However, OSL dating of polymineral fine grains (4-11 μm) is usually suffered from the same problems as IR-OSL dating on sand-sized feldspar minerals. Recently, methods have been proposed (Banerjee et al., 2001; Roberts and Wintle, 2001) to obtain a quartz-dominated OSL signal from polymineral fine-grains by measuring the blue-stimulated OSL signal after exposure to infrared light (post IR blue OSL) (Wallinga, 2002). However, all kinds of fluvial sediment couldn't be satisfied with this method. Olley et al. (1998) reported that equivalent doses obtained on coarse quartz grains yielded lower

results than those obtained on finer grains. Similar results have since been reported by Colls et al. (2001) for two grain sizes from a modern fluvial deposit from the Loire (France). We will discuss these problems in the following section with our results.

CHAPTER 3. Assessment of diagnostic tests for evaluating the reliability of SAR D_e values from polymineral and quartz fine grains

Abstract

In this study, we applied optically stimulated luminescence (OSL) dating to two fine grain sediment samples collected at Jeongokri, Korea. A single aliquot regenerative dose (SAR) procedure was applied to both polymineral grains and to chemically isolated (H_2SiF_6) quartz grains of 4–11 μm diameter. For polymineral fine grains, the OSL IR depletion ratio and the equivalent dose (D_e) plateau test appear to be equally sensitive indicators of appropriate IR stimulation time for use in the 'double SAR' protocol. Additionally, the OSL IR depletion ratio test gives an indication of the relative mineral composition of the samples, hence providing an assessment of the likelihood of obtaining a quartz-dominated [post-IR] OSL signal. Use of higher preheat temperatures would assist in thermally eroding the non-quartz component of the [post-IR] OSL signal from polyminerals. The double SAR method cannot be applied ubiquitously, even after careful and rigorous study of one sample from a section. Quartz OSL dating using a range of preheat temperatures is suggested to be the most suitable method for OSL dating of fine grain sediments.

3-1. Introduction

Recently, luminescence measurement of fine-grained sediments is widely explored using various geological samples. Luminescence measurements of fine-grained sediments have traditionally been made using 4-11μm diameter polymineral grains because fine grain sediments have a difficulty to mineral seperation; however, use of these mixed-mineralogy (quartz and feldspar) grains can lead to age underestimations due to anomalous fading of the signal from

feldspars (e.g. Wintle, 1973; Spooner, 1994b; Huntley and Lamothe, 2001; Wallinga et al., 2001). In contrast, widespread success has been reported in optically stimulated luminescence (OSL) dating of coarse-grained quartz (e.g. summaries by Murray and Olley, 2002; Rittenour, 2008) following the development of the Single Aliquot Regenerative dose (SAR) technique for quartz (Murray and Wintle, 2000; Wintle and Murray, 2006). Recent efforts in dating fine-grained sediments have therefore focused upon using a signal from fine-grained quartz for dating, with the aim of circumventing problems caused by anomalous fading of feldspar signals.

Isolating pure quartz from coarse-grained (sand-sized) materials is relatively simple, involving physical and chemical laboratory treatments; however, the procedure to isolate pure quartz of fine-silt size is less straightforward and more time consuming (e.g. discussed in Roberts, 2007). The 'double SAR' method was proposed (Banerjee et al., 2001) and developed (Roberts and Wintle, 2001; 2003) to obtain a quartz-dominated OSL signal from polymineral (i.e. quartz and feldspar) grains without the need for chemical isolation of quartz. The double SAR method uses infra-red (IR) stimulation to deplete the signal from feldspar grains, prior to stimulation with blue diodes which yields a [post-IR] OSL signal that should then be dominated by a signal from quartz. Several studies (e.g. Banerjee et al., 2001; Roberts and Wintle, 2001; Stokes et al., 2003; Watanuki et al., 2003, 2005; Wang et al., 2006c) have utilised this method; however, there is a concern that a substantial OSL signal can still be observed from feldspar grains even after IR exposure, as noted by Duller and Bøtter-Jensen (1993). Recently, several workers (e.g. Thomas et al., 2003; Watanuki et al., 2003; 2005; Roberts, 2007; Zhang et al., 2007) have compared the D_e value obtained using the polymineral [post-IR] OSL signal and that obtained using the OSL signal from pure quartz; these studies noted that the D_e

value obtained using the polymineral [post-IR] OSL signal can significantly underestimate that obtained for measurements made on pure quartz using OSL. Using the double SAR protocol applied to loess sediments from China, Wang et al. (2006c) also noted that after a short duration of IR stimulation ($\leq$ 200 s, ~ 45 mW/cm^2 power) the D_e value obtained using the subsequent measurement of the [post-IR] OSL signal underestimated the D_e value derived from measurement of a pure quartz OSL signal using the SAR protocol. However, after longer IR exposure, between 300 and 500s, Wang et al. (2006c) observed a plateau for the [post-IR] OSL-derived D_e values that was in good agreement with the D_e value from the pure quartz OSL signal. They concluded that investigation of the IR stimulation duration was important in order to determine the appropriate measurement conditions for the double SAR protocol; this conclusion was also reached by Zhang and Zhou (2007).

The test proposed by Wang et al. (2006c), to define the appropriate IR stimulation duration for each sample examined using the double SAR technique, appears to hold the key to obtaining agreement between quartz OSL and polymineral [post-IR] OSL age determinations, by ensuring that 'sufficient' IR stimulation takes place to deplete the signal from feldspars prior to measurement of the [post-IR] OSL signal. The purpose of this study is to compare the D_e values obtained using the polymineral [post-IR] OSL and quartz OSL signals for dating of fine grain (4-11μm) sediments from a study site located at Jeongokri. To optimise the [post-IR] OSL signal used for dating, the measurement parameters for the double SAR technique are determined using the IR stimulation duration plateau test of Wang et al. (2006c); the suitability of this test is assessed, and other diagnostic tests are proposed and examined. Finally, the reliability of the two OSL methods (i.e. [post-IR] OSL from polyminerals using the double SAR protocol, and

OSL from pure quartz using the SAR protocol) is assessed, in order to determine the most appropriate method for OSL dating of fine-grained sediments from this site.

3-2. Samples and Methodology

A total of seven polymineral fine grain samples were taken from units (38°00'33.1''N, 127°03'54.8''E) that overlie the Quaternary Jeongok Basalt. From these samples, we mainly used the upper most two fine-grained samples (0519-5 and 6) for detailed investigation. There is no independent age control for these loess-like sediments.

The samples were prepared in the laboratory under standard dim-red lighting conditions. Due to the very fine-grained nature of the sediments, samples were washed repeatedly in sodium pyrophospate decahydrate ($Na_4P_2O_7 \cdot 10H_2O$) to remove clay minerals which would otherwise act as a barrier to chemical digestion treatments. Samples were then washed with a 10% v.v. dilution of concentrated (37%) hydrochloric acid (HCl), followed by treatment with 20 vols. hydrogen peroxide (H_2O_2), to remove carbonates and organic matter respectively. Fine grains (4-11μm diameter) were then isolated from the sediments using standard methods, settling according to Stokes' Law over a depth of 20cm in 0.01M solution of sodium oxalate ($Na_2C_2O_4$). These 4-11μm diameter grains were divided into two sub-samples; one sub-sample was used for dating using the double SAR technique (Roberts and Wintle, 2001) applied to polyminerals, whilst the second sub-sample was taken for further chemical processing to isolate quartz grains prior to dating using the SAR protocol (Murray and Wintle, 2000). Fine grains of quartz were isolated from this polymineral sub-sample using hydrofluorosilicic acid (H_2SiF_6)

treatment as described by Roberts (2007), using a treatment duration of two weeks to encourage complete dissolution of feldspars. Aliquots of both quartz and polymineral fine grains were prepared by settling 1 mg of material in acetone onto a 9.7 mm diameter aluminium disc.

All OSL measurements were made using a Risø TL/OSL automatic reader. The stimulation sources were arrays of blue LEDs (470Δ30 nm, ~3.5 mW/cm^2) and IR LEDs (880Δ80 nm, ~14.5 mW/cm^2). The reader was also equipped with a ^{90}Sr/^{90}Y beta source delivering 0.045 Gy s^{-1}. Photon detection was achieved with an EMI 9635QA photomultiplier tube, with the light passing through 5 mm thickness of Hoya U-340 filter and a neutral density filter (N.D. 1.0).

For both samples, the SAR protocol (Murray and Wintle, 2000) was applied to the sub-sample of fine-grained quartz and the double SAR protocol (Roberts and Wintle, 2001) was applied to the fine-grained polymineral sub-sample. In both measurement protocols, the change in sensitivity of all OSL measurements is monitored and corrected for by the OSL response to a test dose applied throughout the measurement sequence. The double SAR protocol involves exposure to infra-red (IR) in order to reduce the OSL contribution from feldspars, prior to the measurement of the OSL signal obtained on stimulation with blue light, termed the [post-IR] OSL signal, which is the signal used for dating. The SAR protocol applied to the quartz grains uses exposure to blue diodes only.

To deplete the signal from feldspars in the double SAR protocol, IR stimulation was conducted at a temperature of 50°C, i.e. a low temperature as advocated by Zhang and Zhou (2007). For both the SAR and the double SAR protocols, a number of checks were made on the behaviour of the various OSL signals and on the suitability of the method of D_e determination. For example, the efficacy of the sensitivity correction was monitored using the recycling ratio, and tests for

recuperation were employed. For each aliquot examined, including those measured using the double SAR protocol, the purity of the quartz signal was assessed using the 'OSL IR depletion ratio' (Duller, 2003). Sensitivity-corrected dose-response curves were constructed for each individual aliquot examined in this study, using a minimum of six regeneration doses to define each curve; these dose-response curves were fitted by an exponential-plus-linear function.

3-3. Results

3-3-1. Application of the double SAR protocol to polymineral fine grains

3-3-1-1. Determining the appropriate duration of IR stimulation

In this study the optimal IR stimulation duration (Wang et al., 2006c) was investigated for the two samples, 0519-5 and -6, using the [post-IR] OSL signal from the polymineral fine grains. IR stimulations of between 100 and 1500s were carried out, at a temperature of 50°C; higher temperatures were not used because they cause depletion of the quartz OSL signal (Spooner, 1994a), particularly the fast component (Singarayer and Bailey, 2004; Jain et al., 2005; Zhang and Zhou, 2007). Figure 3-1 demonstrates that for both samples, the [post-IR] OSL D_e values show a slight increase with increasing IR stimulation time from 100 - ~250 s; the D_e value obtained using the OSL signal only (i.e. with 0 s IR stimulation preceding the OSL measurement) is also shown in Figure 3-1 for comparison. Following 500-1500 s IR stimulation for both samples, slightly higher and more consistent [post-IR] OSL D_e values are typically obtained. These data suggest that IR stimulation of 500 s duration is appropriate for dating of other samples from Jeongokri using the double SAR method.

The increase in [post-IR] OSL D_e values with increasing IR stimulation

duration (Fig. 3-1) can be interpreted as an increase in the relative contribution of quartz to the [post-IR] OSL signal used for dating. Sample 0519-5 shows an increase of ~ 30% in D_e values with increasing IR stimulation time, whereas for sample 0519-6 the increase in D_e values is smaller, being ~ 13%; this different response suggests that they contain differing amounts of feldspar. The pattern of [post-IR] OSL decay curve shapes obtained for the two samples following different durations of IR stimulation supports this suggestion (Fig. 3-2), and can be used to help identify the presence, and assess the significance, of a signal from feldspars. Typically, decay curves from feldspars exhibit a slow decay form, and a more rapid decay form is associated with a signal from quartz (e.g. Roberts, 2007). For sample 0519-5, the initially slow decay curves visibly steepen with increasing IR stimulation time, although after only 2 s stimulation (i.e. the signal used for D_e determination), the curves with IR pretreatment ≥ 250 s are indistinguishable from those of pure quartz. The dramatic change in [post-IR] OSL decay curve shape with increased IR stimulation time, and the slow decay form compared to that of pure quartz (Fig. 3-2a), suggests that the [post-IR] OSL signal from sample 0519-5 still contains a mix of signals from both quartz and feldspar even after long stimulation durations when a plateau in D_e values is observed (Fig. 3-1); this emphasises the need to use the initial portion of the signal for D_e determination, thereby maximizing the contribution from the fast OSL component. In contrast, sample 0519-6 shows little change in the [post-IR] OSL decay curve shape regardless of IR stimulation time, and the rapid decay form using IR stimulation times of ≥ 250 s is indistinguishable from that of pure quartz for the same sample (Fig. 3-2b), implying that for this sample the [post-IR] OSL signal is dominated by quartz regardless of the IR stimulation time.

An appropriate IR stimulation time for use in the double SAR sequence can
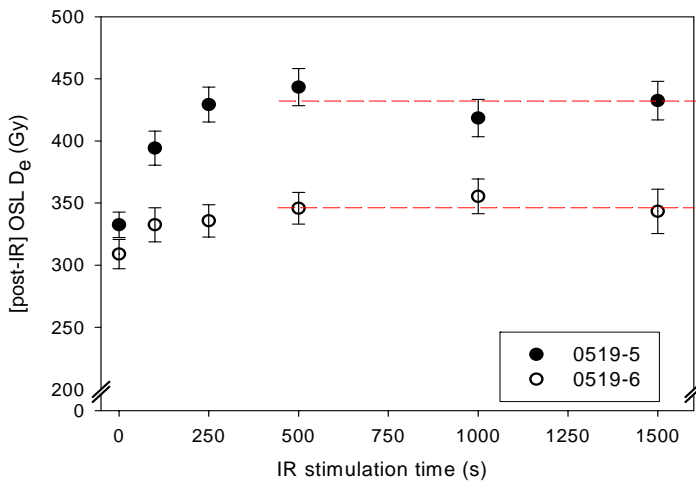
Fig. 3-1. Post-IR OSL D_e values for polymineral samples 0519-5 and 0519-6, determined for various IR stimulation times using a preheat of 220°C for 10 s. Note the break in the y-axis scale. Each point shown is the result from one aliquot, and the error shown is calculated using *Analyst* version 3.24 (Duller, 2007). The dashed line is the mean of the three data points between 500 and 1500 s (sample 0519-5 = 431 Gy; sample 0519-6 = 348 Gy).
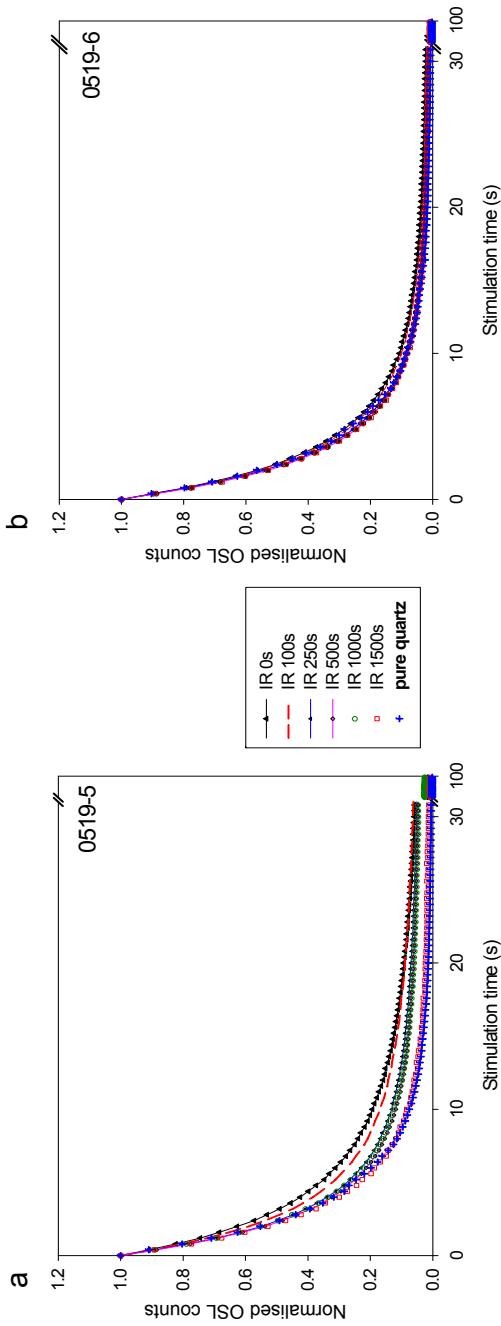
Fig. 3-2. The [post-IR] OSL decay curves for the data shown in Fig. 3-1, from polymineral samples a) 0519-5 and b) 0519-6, following IR stimulation of different durations from 0 to 1500 s (as indicated by the key). The OSL decay curve (stimulation with blue light only) from fine-grained quartz is also shown for comparison and shows the greatest decay. All data are shown as raw counts per 0.4 s stimulation normalised to the first data point. Note the break in the x-axis scale, which highlights the first 30 s of the 100 s (250 channel) stimulation.

also be identified using the 'OSL IR depletion ratio' (Duller, 2003) in conjunction with different IR stimulation times. The OSL IR depletion ratio is calculated as outlined in equation 1, and is displayed in Figure 3-3 (for measurements made on the same aliquots shown in Figure 3-1) using different durations of IR exposure prior to measurement of the [post-IR] OSL signal.

$$\text{OSL IR depletion ratio} = \frac{L_x (\text{[post-IR] OSL}) / T_x (\text{OSL})}{L_x (\text{OSL}) / T_x (\text{OSL})} \qquad \text{(Eq. 1)}$$

Sample 0519-5 shows a large and rapid decrease in the OSL IR depletion ratio with increasing IR stimulation time for short stimulations ($\leq$ 250s), suggesting that this sample is not dominated by quartz but instead contains a large proportion of material that is responsive to IR as well as blue light (Fig. 3-3). The OSL IR depletion ratio is normally used to assess the presence of contaminants within a quartz-rich sample, where a value of unity is obtained if the sample is pure quartz, and falls below unity in the presence of contaminants that respond to IR stimulation (e.g. feldspar). However, in the case of the polymineral samples in this study which are not dominated by quartz, it is not the proximity to unity which is important (because a short IR stimulation may have little or no effect on the subsequent [post-IR] OSL signal), but rather the region in which a plateau in the 'OSL IR depletion ratio' is obtained that is significant (Fig. 3-3). A plateau in OSL IR depletion ratio values (within errors) is observed for sample 0519-5 for IR stimulation time $\geq$ 500 s (note that for the [post-IR] OSL D_e values shown in Figure 3-1, a plateau was also observed for IR stimulation times $\geq$ 500 s). In contrast, sample 0519-6 shows a small decrease in the OSL IR depletion ratio with increasing IR stimulation duration (Fig. 3-3), giving values that are consistently

greater than 0.9 regardless of IR stimulation duration (100-1500 s); this compares with Figure 3-1 where a plateau was observed for IR stimulation times $\geq$ 500 s. The OSL IR depletion ratio values for sample 0519-6 are within 2σ error of unity (Fig. 3-3), suggesting that this sample contains a higher proportion of quartz than sample 0519-5.

Examination of the different D_e values obtained using different IR stimulation durations (Fig. 3-1), coupled with observations of the [post-IR] OSL decay curve shape (Fig. 3-2) and the OSL IR depletion ratio with increased durations of IR exposure (Fig. 3-3), suggests that sample 0519-6 has a higher proportion of its OSL signal derived from quartz compared to 0519-5 from the same sample profile. It is concluded from these tests, that an IR stimulation duration of 500s at 50°C would be appropriate for use in the double SAR protocol applied to other samples from Jeongokri. The OSL IR depletion ratio test (Fig. 3-3) appears to be an equally sensitive indicator of appropriate IR stimulation time as the D_e plateau test (Fig. 3-1). Additionally, the OSL IR depletion ratio test gives an indication of the relative composition of the samples by assessing the impact of IR stimulation (Fig. 3-3).

3-3-1-2. Preheat plateau test for polymineral fine grains using the double SAR protocol

Preheat plateau tests were conducted for both samples in this study using the double SAR measurement protocol across a range of temperatures from 160 to 280°C, holding for 10 s; this would be expected to induce differing amounts of sensitivity change in the quartz OSL signal (Wintle and Murray, 1999). A cut-heat of 160°C was used following application of the test dose. An IR stimulation duration of 500s applied at a temperature of 50°C was employed, as discussed in section 3-3-1-1. Figure 3-4a shows the D_e values obtained using both the [post-IR]
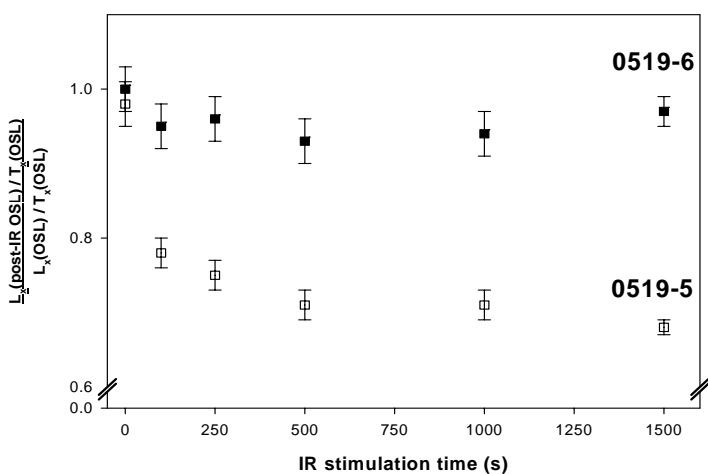
Fig. 3-3. OSL IR depletion ratio versus IR stimulation time (s) for the data shown in Fig. 3-1, polymineral samples 0519-5 and -6. Each point shown is one aliquot, and the error shown is calculated as a recycling ratio using *Analyst* version 3.24 (Duller, 2007).

OSL signal and the IRSL signal using different preheat temperatures, for sample 0519-5, which was the sample containing a significant proportion of non-quartz signal. The [post-IR] OSL D_e values and the IRSL D_e values show a similar trend, with D_e values increasing progressively with increasing preheat temperature (Fig. 3-4a). This increase in IRSL D_e is not surprising; Blair et al. (2005) has previously noted such a pattern for museum feldspar specimens when using a fixed cut-heat. However, the lack of a distinctive plateau in the [post-IR] OSL D_e values (Fig. 3-4a) is not expected given the tests to determine a suitable IR pretreatment (section 3-3-1-1). Similar D_e values are observed for the [post-IR] OSL data between 180-220°C, but this forms part of a general trend of increasing D_e values with increasing preheat temperature. A clue as to the cause of this trend is provided by the similarity to the pattern of IRSL D_e values. The temperature-dependent behaviour observed for both the [post-IR] OSL and IRSL D_e values implies that a significant non-quartz signal, such as feldspar, still remains even if an 'appropriate' IR stimulation value is determined using an IR stimulation duration test (section 3-3-1-1). These ideas are supported by the data from sample 0519-6, which contained a larger proportion of quartz, where the pattern of [post-IR] OSL D_e values versus preheat temperature is distinctly different to the IRSL D_e values (Fig. 3-4b). In contrast to the data for sample 0519-5, relatively quartz-rich sample 0519-6 shows a plateau in [post-IR] OSL D_e values for preheat temperatures between 200-240°C and the trend of D_e values across the preheat range is one that is commonly observed in quartz. These behaviours of temperature dependence of post-IR OSL and IRSL signal implies that feldspar signal still remains after sufficient IR stimulation, and is eroded by increasing preheat temperature, therefore, high preheat temperature is necessary to remove the feldspar signal.

Feldspar OSL signals come from a range of traps (Duller and Bøtter-Jensen,

1993) and the signal is eroded by increasing preheat temperature (e.g. as illustrated in Fig. 5-6b of Roberts and Duller, 2004). This effect can also be seen by plotting the OSL IR depletion ratio (Eq. 1) measurements versus preheat temperature (Fig. 3-5) for the aliquots of both samples shown in Figure 3-4. The OSL IR depletion ratio values for sample 0519-6 are all between 0.9 and 1.0, suggesting that the sample is largely dominated by quartz. In contrast, the OSL IR depletion ratio for sample 0519-5 increases steadily over the preheat temperature range 160 - 260°C for this polymineral sample, indicating that the relative importance of the quartz component of the [post-IR] OSL signal increases with increasing preheat temperature (because the feldspar signal is eroded thermally).

The highest OSL IR depletion ratio value for sample 0519-5 is 0.85 (far from the value of unity that would suggest the presence of a pure quartz signal), obtained for a preheat temperature of 260°C/10s (Fig. 3-5); thus, thermal erosion of the feldspar [post-IR] OSL signal is not on its own sufficient to generate a pure quartz signal from polymineral samples. In some circumstances, however, it might be possible to exploit the behaviour shown in Figure 3-5 for sample 0519-5, by using a high preheat temperature to further deplete the OSL signal from contaminants such as feldspar. For this study, given the inability to obtain any plateau in the [post-IR] OSL D_e values as a function of preheat temperature for sample 0519-5 (Fig. 3-4a), it is difficult to know which, if any, of the [post-IR] OSL D_e values obtained for this sample are correct. For this reason, the D_e values determined for fine-grained quartz were also examined, and are discussed in the following section.

3-3-2. Comparison of polymineral [post-IR] OSL and quartz OSL D_e values

Although both of the samples in this study were collected 1m apart from the same sample section, received the same pre-treatment, and were measured using
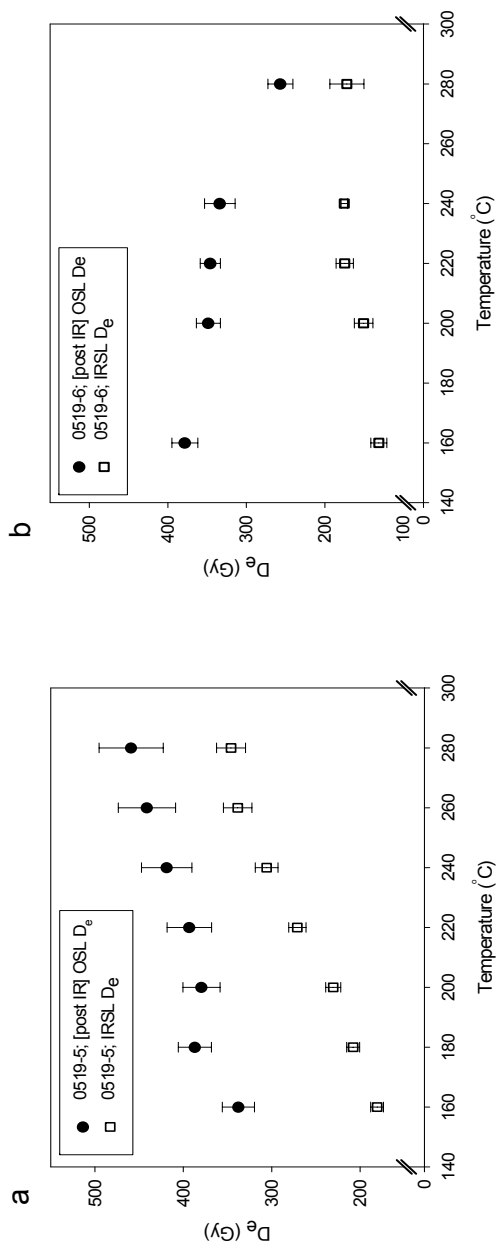
Fig. 3-4. Preheat plot showing [post-IR] OSL and IRSL D_e values obtained for polymineral samples a) 0519-5 and b) 0519-6, using the double SAR protocol with preheat temperatures from 160 to 280°C, and using IR stimulation of 500 s at a temperature of 50°C. Each point shown in a) is the mean of 3 aliquots, and the errors for the three aliquots were combined in quadrature to give the error shown; in b) each point is the result from one aliquot and the errors were calculated using *Analyst* version 3.24 (Duller, 2007).
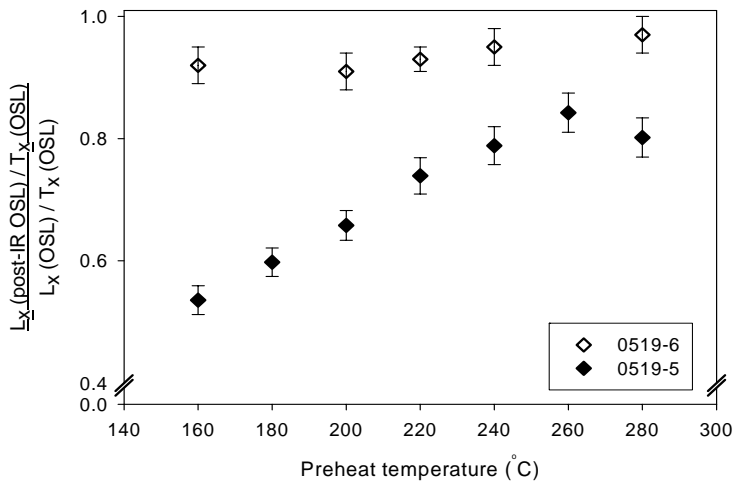
Fig. 3-5. The OSL IR depletion ratio as a function of increasing preheat temperature for polymineral samples 0519-5 and -6, assessed using the same aliquots shown in Fig. 3-4. For sample 0519-5, each point shown is the mean of three aliquots, whilst sample 0519-6 has one aliquot per data point. The errors were calculated by combination in quadrature.

the same [post-IR] OSL method, different levels of success are achieved when comparing the [post-IR] OSL D_e values with those obtained using the OSL signal from quartz prepared from the same samples. For sample 0519-6, using IR stimulation times of 100-1500s, the [post-IR] OSL D_e values show good agreement with the D_e values derived from the quartz OSL signal (Fig. 3-6b, using quartz data from preheat temperatures 200-240°C). In contrast, sample 0519-5 shows that the [post-IR] OSL D_e values underestimate those D_e values derived from quartz OSL by ~7% across the range of IR stimulation durations which define a plateau in [post-IR] OSL D_e values (i.e. from 500-1500 s) (Fig. 3-6a; [post-IR] OSL D_e = 431 Gy, quartz OSL D_e = 468 Gy). A plateau in [post-IR] OSL D_e values with IR stimulation time was obtained for both samples (Fig. 3-6), as recommended by Wang et al. (2006c). However, for sample 0519-5 the observation of this plateau was shown to be no guarantee of the dominance of quartz in the [post-IR] OSL signal. This observation agrees with the findings of Duller and Bøtter-Jensen (1993) and Thomas et al. (2003), which suggest that even after prolonged IR exposure, the [post-IR] OSL signals may still contain a contribution from feldspars and hence may give rise to underestimated D_e values, possibly due to anomalous fading. This finding may initially appear to be in contradiction to a number of studies that suggest that the [post-IR] OSL signal gives a quartz-dominated signal appropriate for dating (e.g. Banerjee et al., 2001; Roberts and Wintle, 2001; Stokes et al., 2003; Watanuki et al., 2005; Wang et al., 2006c; and sample 0519-6 in this study). However, the key difference between samples 0519-5 and -6 in this study, and therefore potentially between samples in other studies, may be differences in the mineral composition of the samples and hence the relative contribution from quartz to the [post-IR] OSL signal. The OSL IR depletion ratio supports this difference in the relative composition of the two samples (Fig. 3-3 and 3-5).
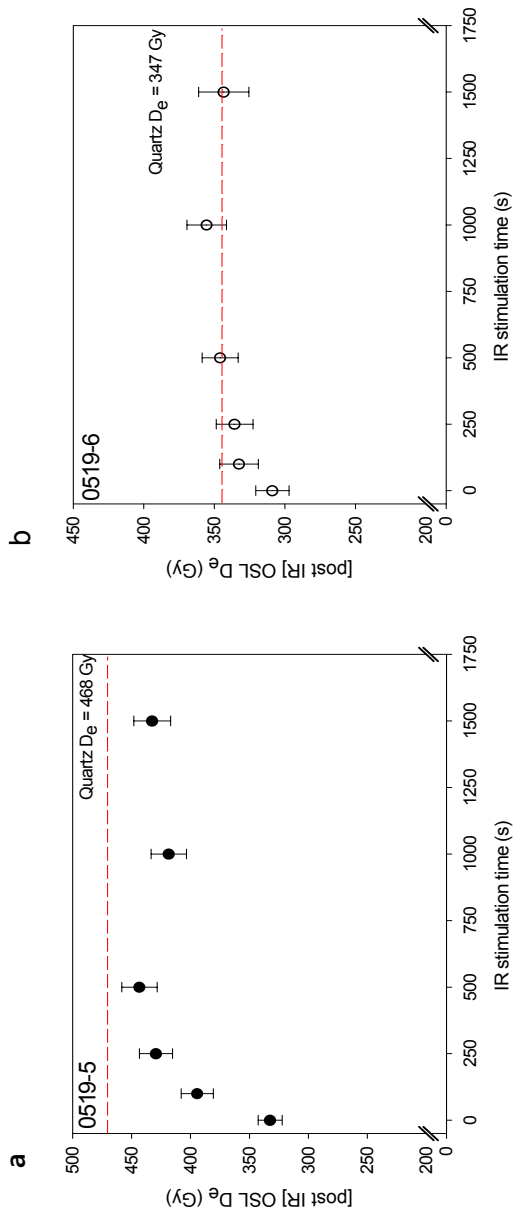
Fig. 3-6. Post-IR OSL D_e values for polymineral samples a) 0519-5 and b) 0519-6, determined for various IR stimulation times using a preheat of 220°C held for 10 s. The dashed line indicates the D_e value determined using quartz OSL at a preheat temperature of 200–240°C/10 s (n =6) for both samples; this quartz D_e value (Gy) is also shown.

3-4. Summary and conclusions

The different patterns in D_e values, decay curve shapes, and OSL IR depletion ratio with increased durations of IR exposure, all suggest that the [post-IR] OSL signal of sample 0519-6 has a higher proportion of quartz-derived signal compared to sample 0519-5. Thus, for sample 0519-5, a contaminating signal, possibly from feldspars, still contributes to the [post-IR] OSL signal even after what appears to be 'sufficient' IR stimulation (based on the establishment of a plateau in D_e values with increased IR-stimulation time). This gave rise to [post-IR] OSL D_e values that underestimated those from measurement of OSL from chemically-purified quartz. Thus, whilst use of a [post-IR] OSL measurement protocol will decrease the contribution of contaminants such as feldspar to the [post-IR] OSL signal, where the amount or intensity of IR- and blue light-responsive contaminants is high compared to quartz, the [post-IR] OSL signal could still contain a significant contribution from these contaminants and hence, may give rise to underestimated D_e values if this signal fades when measured using U-340 filters (eg. as shown by Roberts, 2007, for samples from North America containing volcaniclastic feldspars). Therefore, even where a plateau in D_e values with IR stimulation is established, use of the double SAR and [post-IR] OSL signal from polymineral samples does not always show agreement with quartz OSL D_e values.

The OSL IR depletion ratio test applied to polymineral samples appears to be an equally sensitive indicator of appropriate IR stimulation time as the D_e versus IR stimulation time plateau test of Wang et al. (2006c). Additionally, the OSL IR depletion ratio test gives an indication of the relative mineral composition of the samples by assessing the impact of IR stimulation, and hence also provides an

assessment of the likelihood of obtaining a quartz-dominated [post-IR] OSL signal. The polymineral sample with an OSL IR depletion ratio of ~0.9 after 500 s IR stimulation showed good agreement between the polymineral [post-IR] OSL D_e values and those from quartz. However, the polymineral sample with an OSL IR depletion ratio of ~0.7 after 500 s of IR stimulation gave lower D_e values than those from chemically isolated quartz grains.

For the Jeongokri samples in this study, use of higher preheat temperatures would assist in eroding the non-quartz component of the [post-IR] OSL signal from polyminerals. However, the strong preheat dependence of the polymineral [post-IR] OSL D_e values of sample 0519-5 means that it is impossible to determine which, if any, of the [post-IR] OSL D_e values obtained is correct for this sample; samples showing these characteristics therefore cannot be dated using the [post-IR] OSL signal.

All of the [post-IR] OSL D_e values for sample 0519-5 underestimate those obtained for quartz OSL. However, the quartz OSL data of samples 0519-5 and 0519-6 are not without their complications. This result shows that the double SAR method can be applied with differing degrees of success to adjacent samples from the same stratigraphic section, indicating that each individual sample must be examined carefully to assess the reliability of the [post-IR] OSL method in isolating a quartz-dominated signal. The double SAR method therefore does have limitations and cannot be applied ubiquitously, even after careful and rigorous study of one sample from a section. To avoid the uncertainties that may be associated with the source of the [post-IR] OSL signal, we suggest that quartz OSL dating using a range of preheat temperatures is the most suitable method for OSL dating of fine grain sediments.

CHAPTER 4. Comparing the OSL signals from the preheat plateau and dose recovery tests using quartz fine grains (4-11㎛) at Jeongokri, Korea.

Abstract

For the quartz fine grains, data from both natural D_e determinations and laboratory dose recovery tests are required to identify the appropriate preheat temperatures for dating, due to problems of thermal transfer. This phenomenon is particularly exaggerated for these samples due to the large D_e values ($\geq$350 Gy) and hence low slope of the dose–response curve. Together these preheat and dose recovery data show that the quartz OSL D_e values obtained using preheat temperatures between 200-240°C give the most consistent results and, as such, are the most appropriate for dating the samples from Jeongokri.

4-1. Introduction

The Single-Aliquot Regenerative-dose (SAR) procedure (Murray and Wintle, 2000) provides a method of D_e determination that includes a correction for sensitivity change of the OSL signal. The sensitivity change occurs during repeated cycles of irradiation, pre-heating and light exposure (Bøtter-Jensen et al., 2003). The best way to check the sensitivity change during the SAR measurement sequence is by the preheat plateau and dose recovery tests. The preheat plateau test is carried out in order to check the influence of different heating procedure and to determine the appropriate heating temperature. This test is also an indispensable step in checking how both charge transfer and sensitivity change are caused by preheating. The dose recovery test is a necessary step to check the ability of the SAR procedure to recover a known laboratory dose. In this study, there is an

apparent contradiction between the results of the preheat plateau test and the dose recovery test. While investigating the cause of this contradiction, an undesirable effect of charge transfer was observed.

There are several kinds of charge transfer. Thermal transfer is one type of charge transfer; pre-heating causes thermal transfer from thermally stable and light-insensitive traps to the main OSL traps during preheating (Spooner, 1994a). During the burial period, charge transfer may also occur, this charge transfer depends on the retention lifetime of electrons in the shallow traps (Aitken, 1998). Understanding of the charge transfer behaviour both during the burial period and in laboratory procedure is very important, since it can create significant problems in the dating of sediments. Many papers have been written about charge transfer, especially as a problem in the dating of young sediments (Rhodes and Bailey, 1997; Rhodes, 2000; Jain et al., 2002). However, the effects of charge transfer seem for fine-grained quartz having high natural dose (over 300 Gy) have not yet been fully explained.

In this paper, we estimated D_e values of chemically isolated fine-grained quartz of 4-11μm diameter at the Jeongokri archaeological site, Korea. The preheat plateau and dose recovery tests were applied as part of the SAR procedure for D_e estimation. We demonstrate the effects of charge transfer on the preheat plateau and dose recovery tests using TL measurements. Also, we discuss the suitability and limitations of the preheat plateau and dose recovery tests.

4-2. Methods

All experimental conditions and samples are same with those of Chapter 3. In this chapter, we used preheat plateau and dose recovery tests for compare the D_e

values. The D_e values were calculated using the chemically-purified quartz from samples 0519-5 and -6. Preheat plateau and dose recovery tests were conducted for preheat temperatures between 160 and 280°C at 20°C intervals, with the temperature being held for 10 s. For both techniques, the sample was held at 125°C during the 100 s stimulation with blue diodes, and a cut-heat temperature of 160°C was used following application of the test dose; the first 2 s of the OSL signal was used for dating, and the background was determined using the last 10 s of stimulation. In the dose recovery test, aliquots were bleached using blue-LED stimulation at room temperature for 1000 s, pausing for 10,000 s, and then blue-LED stimulation for a 1000 s before being given the known laboratory dose.

4-3. Results

4-3-1. Preheat plateau test

Fig. 4-1 shows the dose-response curves of samples 0519-5 and -6 for regeneration doses up to 600 Gy, fitted with an exponential-plus-linear component. The exponential component has a characteristic D_0 value in the range 80 to 104 Gy, where the fit is given by $I = I_0 + I_{max} (1-e^{-D/D_0}) + D \cdot g$. The values obtained are within the range of D_0 values obtained for the quartz fast component by OSL, summarised by Wintle and Murray (2006). All curves show continuous growth to 600 Gy, although the dose-response curve using a 280°C preheat shows a lower normalised OSL signal (L_x/T_x) than other preheats due to thermal depletion of the OSL signal. All of the SAR measurements give an acceptable OSL IR depletion ratio (over 0.95); for quartz-rich separates this test provides a check on purity and values approaching unity suggest that the OSL signal is derived from pure quartz. The recycling ratios, obtained by comparing the response to the lowest

regeneration dose (~36 Gy) applied at the beginning and at the end of the dose response curve measurements, are within 3% of unity. Signal recuperation is less than 3% of the natural signal. All errors (standard deviation) on D_e values are low, being less than 5%.

Figure 4-2 shows the D_e values obtained using the data shown in Figure 4-1, plotted against preheat temperature. For both samples, the D_e values obtained using low preheat temperatures of 160 and 180°C are much higher than those obtained using higher preheat temperatures (as much as 50% greater compared to mid-range temperatures). Consistent D_e values are obtained between preheat temperatures of 200-240°C (sample 0519-5) or 200-260°C (sample 0519-6) (Fig. 4-2), giving mean D_e values of 468 Gy and 347 Gy, respectively. The D_e values obtained for the high preheat temperature of 280°C are ~17 % lower for each sample. Both samples 0519-5 and -6 show similar patterns of D_e versus preheat temperature.

4-3-2. Dose recovery test

A dose recovery test was performed for both samples, using the same range of preheat temperatures and cut heat as used in the preheat plateau test discussed above. The test was performed using unheated aliquots of fine-grained quartz. The given laboratory doses to recover were approximately equivalent to the quartz D_e values in the mid-range of preheat temperatures (Fig. 4-2), being 452 Gy and 340 Gy for samples 0519-5 and -6, respectively. The dose-response curves observed in dose recovery test show continued growth up to 600 Gy, similar to that seen in Fig. 4-1 for the preheat plateau test. All aliquots in the dose recovery test had ideal recycling ratios and OSL IR depletion ratios which were close to unity (i.e. within ± 10%). Signal recuperation was less than 3% of the signal from the 'natural' (i.e. laboratory-given) dose.
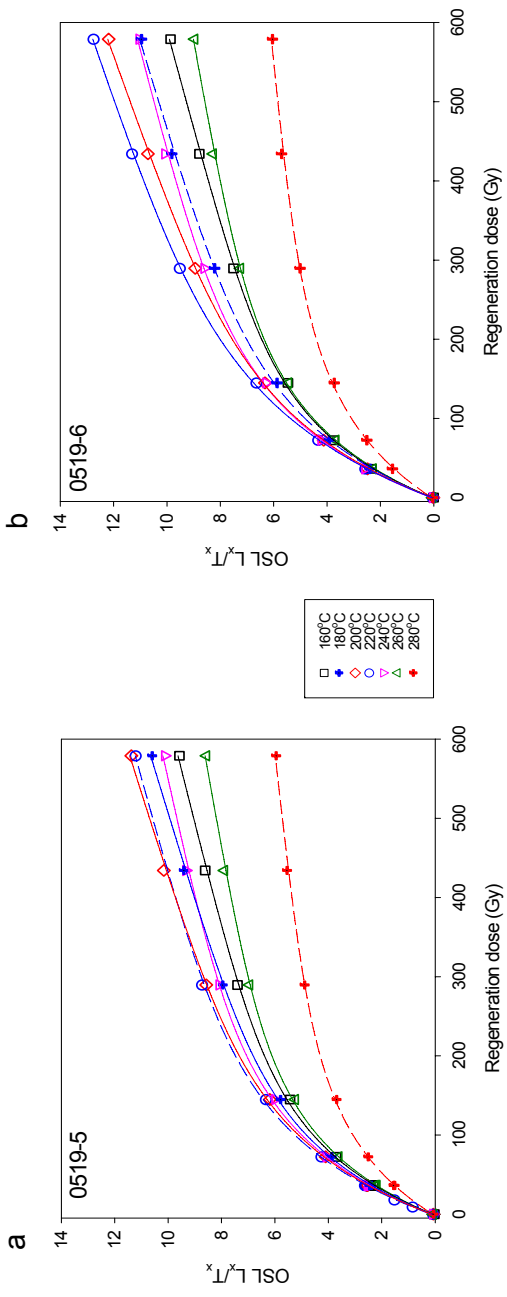
Fig. 4-1. Dose-response (L_x/T_x) curves up to 600 Gy for fine-grained quartz from samples a)0519-5 and b)0519-6, using different preheat temperatures from 160 to 280°C. Each data point shown is the mean of two aliquots.
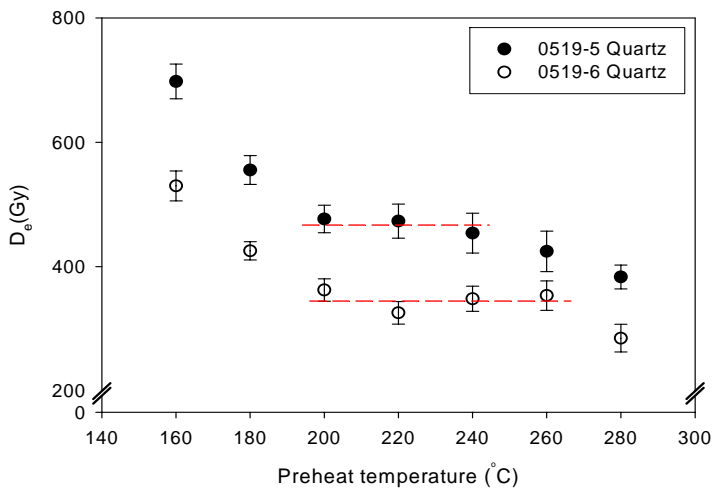
Fig. 4-2. Preheat plot showing the values of D_e versus preheat temperature for fine-grained quartz prepared from samples 0519-5 and -6. Each point shown is the mean of 2 aliquots, and the error shown is derived from combination of errors in quadrature.

As observed for the quartz aliquots used for the determination of natural D_e values (Fig. 4-2), the aliquots used in the dose recovery test gave highly reproducible results for both samples (see Fig. 4-3). However, for sample 0519-5 the pattern of values observed for the dose recovery test is different to that for the natural D_e values (Fig. 4-3a). The doses recovered at 160 and 180°C preheat temperatures are not notably higher than the doses recovered at higher preheat temperatures (Fig. 4-3a), giving rise to a longer plateau region (160-240°C preheat) for the dose recovery test compared to that observed for the preheat plateau test. Recovered dose values show good agreement with the given dose (within ±10%) for preheat temperatures between 160-240°C (Fig. 4-3b). At preheat temperatures of 260 and 280°C, the dose recovered underestimates the given dose by ~20 % for both samples.

4-4. Discussion

Erroneously high D_e values are observed only in the preheat plateau test when measuring the natural dose; these occur for 160 and 180°C preheat temperature (Fig. 4-2). Above 220°C preheat temperature, the D_e values decrease and show a plateau range. In contrast, the dose recovery test does not show these trends; instead, a long plateau, ranging from 160 to 240°C preheat temperature is obtained (Figs.4-3a and b).

Roberts (2006) observed similar patterns of quartz D_e values for loess from the North American midcontinent to those noted in this study in Figs. 4-2 and 4-3, observing a decrease (by as much as a factor of two) in natural D_e values with increasing preheat temperature from 160-300°C, whilst the dose recovery data did not show any trend with preheat. Roberts (2006) concluded that the region between
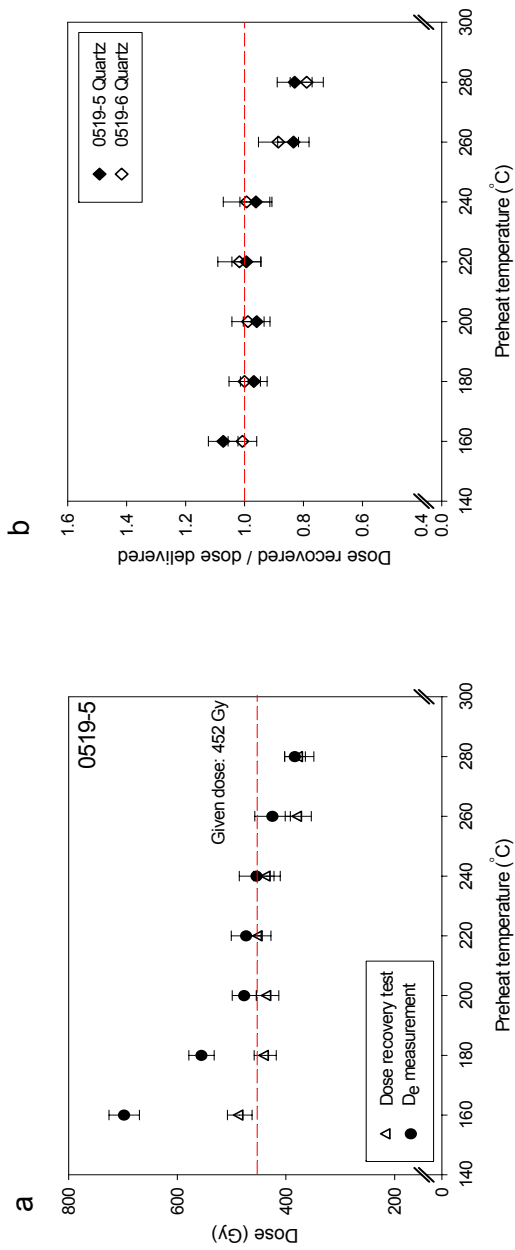
Fig. 4-3. D_e values obtained for the dose recovery test of fine-grained quartz sample 0519-5 compared with the natural D_e values obtained during the preheat plateau test. The dashed line indicates the laboratory dose delivered (452 Gy) in the dose recovery test. b) Dose recovery test results for fine-grained quartz samples 0519-5 and 6, showing the ratio of the measured ('recovered') dose versus the given ('delivered') dose. Each point is the mean of two aliquots and errors were calculated by combination in quadrature.

220 and 260°C was the appropriate one to select for D_e determination for the samples from North America. Roberts (2006) employed a modified SAR protocol that involved a cut-heat that tracks the preheat temperature by -20°C and found that samples could obtain a plateau of D_e values when using different preheat temperatures. Using the approach of Roberts (2006), we focused more on the major factors that cause these phenomena, in particular sensitivity change and charge transfer.

4-4-1. Sensitivity change

To monitor the sensitivity changes that occur through a SAR sequence, we investigated the quartz OSL signals obtained in the preheat plateau and dose recovery tests. The simplest way to monitor the sensitivity change is to make repeated measurements of OSL using the same conditions. The OSL response to the test dose (T_x) at the end of the main OSL measurement (L_x) is an appropriate monitor of the sensitivity change. In both preheat plateau and dose recovery tests, test dose ratios (T_x/T_n) can be used to monitor of sensitivity change, where T_n is the measurement related to the initial natural signal L_n. In the preheat plateau test obtained for two discs using the natural signal, both decreases and increases in ratios (T_x/T_n) are observed with repeated regeneration dose (Fig. 4-4a). Also, the ratios are higher for the higher preheat temperatures (160~240°C). In contrast, for 260 and 280°C preheat temperatures, the ratios decrease with repeated regeneration dose and are similar for both these preheat temperatures. These patterns observed in preheat plateau test are different with these observed in the dose recovery test (Fig. 4-4 b). In the dose recovery test, T_x/T_n ratios close to the ideal value of unity are observed for 220 and 240°C preheat temperatures. On the other hand, higher T_x/T_n ratios for low temperatures (<220°C) and lower T_x/T_n ratios for high

temperatures (260 and 280°C) are observed.

Though we do not know exactly whether these patterns of T_x/T_n ratio are related to different D_e value patterns or not, we believe that these sensitivity changes might not be the cause of the problem with the D_e values; this is because T_x/T_n ratios fluctuate regardless of the pattern of D_e values. Although the preheat plateau test has a very similar pattern of decreasing and increasing ratios of T_x/T_n for each preheat temperature, erroneously high D_e values were observed only for low preheat temperatures. On the other hand, the recycling ratios for all types of preheat plateau and dose recovery tests were close to unity, which means successful correction of sensitivity change during the SAR protocol. These results suggest that the observed sensitivity change couldn't play a significant role in the erroneously high D_e values and different D_e value patterns between preheat plateau and dose recovery tests.

Analysis of the OSL decay curve from quartz provides a valuable piece of information on the optical and thermal stability of the various OSL signal components. This information is fundamental to their suitability for dating (Bøtter-Jensen et al., 2003). When plotting OSL decay curves (normalized to the initial signal) for discs 0519-5 and 6, there is no difference in decay curve shape for each preheat temperature in both the preheat plateau and dose recovery tests (Fig. 4-5). Because the decay rates are very similar it is concluded that OSL signals are derived from same components regardless of preheat temperatures.

As simple method using different channels of OSL decay curve was carried out to investigate the effect of OSL components that make up the decay curves in Fig. 4-5. The rapid bleaching OSL component relates to a 325°C TL trap, and the initial part of the OSL decay curve represents it. Normally, the initial 5 channels (equivalent to 2s of stimulation time) of the 250 channels (100s) are used for OSL
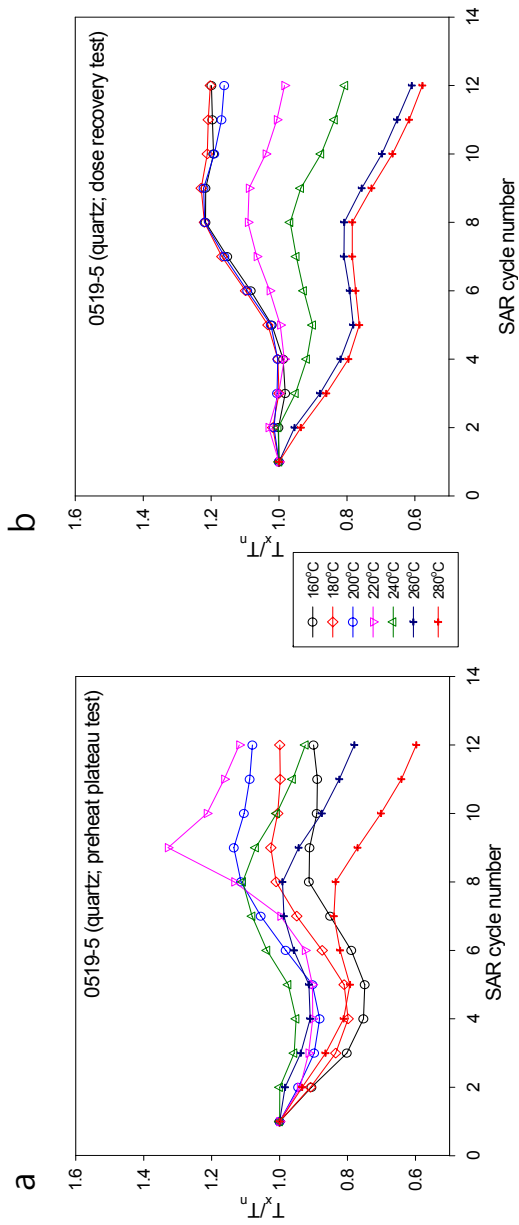
Fig. 4-4. The test dose ratios (T_x/T_n) used to monitor of sensitivity change in preheat plateau and dose recovery tests for preheat temperatures between 160-280°C.
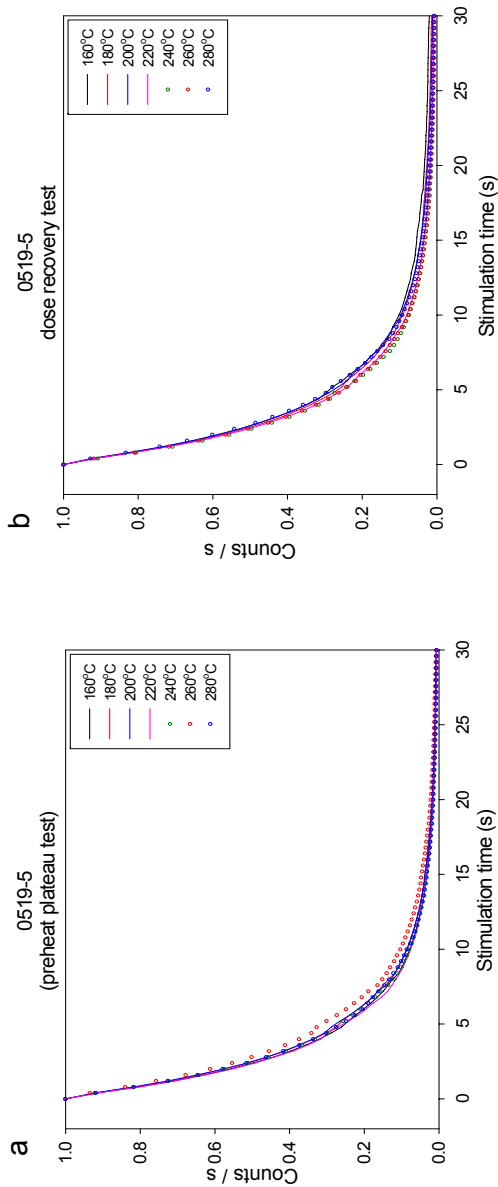
Fig. 4-5. Decay curves of natural dose in each preheat temperature (preheat plateau test-a), decay curves of given dose in each preheat temperature (dose recovery test-b).

signal integration, and the last 25 channels (10s) are subtracted as background. In this simple method of analysis, we used one channel for each integration. The D_e values obtained using each channel at each temperature are shown in Fig. 4-6. The D_e values obtained using channel 1 to 5 are not different from those of preheat plateau test. This indicates that the major part (five channels; 2s) of the OSL signal used for D_e estimation is mainly derived from the rapidly decaying OSL component. Therefore, the channels used for integration in the preheat plateau and dose recovery tests are suitable for D_e calculation. However, the D_e values obtained using channels 15 and 20 show relatively low D_e values, which suggest the presence of medium and/ or slow components.

As previously stated, tests have been undertaken on naturally irradiated quartz for the preheat plateau test and laboratory irradiated quartz after bleaching for the dose recovery test. Therefore, the high D_e values in the low preheat temperature part of the preheat plateau test and the different trend of D_e values between the preheat plateau and dose recovery tests might have originated from a discrepancy in the behaviour of the natural OSL and the laboratory-irradiated OSL signals. The SAR protocol normally uses the sensitivity-corrected signals for the natural dose (L_n/T_n) and the sensitivity-corrected signals for the laboratory regenerative dose (L_x/T_x). In the preheat plateau test, there is a different ratio for the natural dose (L_n/T_n) and the laboratory regenerative dose (L_x/T_x) at low preheat temperatures (less than 220°C). Roberts (2006) investigated the different quartz OSL signals in their study, using the L_n/T_n and L_x/T_x data for each preheat temperature between 160-280°C normalised to the L_n/T_n and L_x/T_x data for the mid-range preheat temperature 220°C. Examination of these data led Roberts (2006) to conclude that the region between 220 and 260°C was the appropriate one to select for D_e determination for the samples from North America. The same approach was taken

in this study for both Jeongokri samples; Fig. 4-7 shows these plots of L_n/T_n and L_x/T_x as a function of preheat temperature, normalised to the L_n/T_n and L_x/T_x data for the 220°C preheat, for sample 0519-5. For the natural D_e determinations (Fig. 4-7a), different patterns are observed for the natural dose (L_n/T_n, solid circles) and all laboratory regeneration doses (L_x/T_x, open circles) at low preheat temperatures (less than 220°C). The natural L_n/T_n ratios are consistent for preheat temperatures from 160-220°C; however, the regenerative L_x/T_x ratios are lower than the L_n/T_n ratios and gradually increase with increasing preheat temperature from 160-220°C (Fig. 4-7a). In contrast, for the dose recovery test, there is no difference between the L_n/T_n ratios for the given dose and the L_x/T_x ratios for the regenerative doses, demonstrating the same pattern of increase for both the laboratory-given dose and the regenerative doses with increasing preheat temperatures up to 220°C (Fig. 4-7b). In both experiments, the normalised L_n/T_n and L_x/T_x ratios rapidly decrease for preheat temperatures above 240°C.

4-4-2. Further consideration of preheat plateau and dose recovery tests

In the dose recovery test, all signals examined (L_n/T_n and L_x/T_x) have been the result of doses delivered within the laboratory; it therefore should come as little surprise that the pattern of normalised L_n/T_n and L_x/T_x values is the same for the 'given' and regenerative dose signals (Fig. 4-7b). For the natural D_e determination data, the different pattern observed for the normalised natural (L_n/T_n) and regenerative (L_x/T_x) dose signal ratios (Fig. 4-7a) may be due to charge transfer.

The pre-heat causes transfer of electrons from thermally stable and optically-insensitive traps to the OSL traps. During burial, the charge transfer process will have happened, to an extent that depends on the retention lifetime of electrons in the shallow traps, before the laboratory preheating. Also, during bleaching, some of
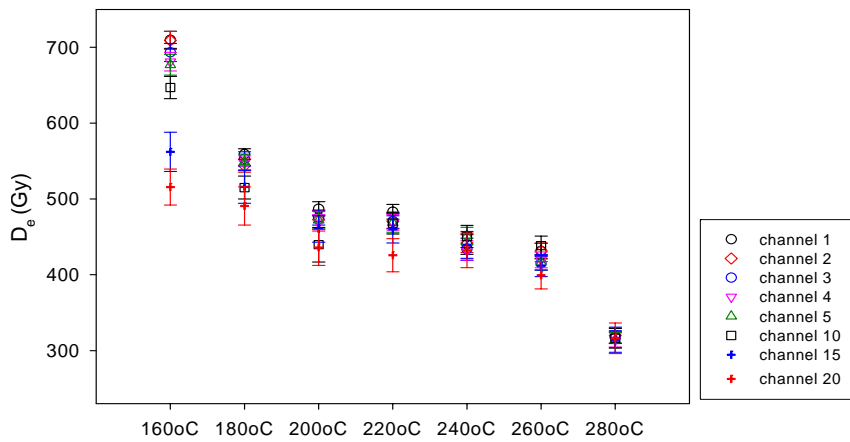
Fig. 4-6. The D_e values obtained using each channel at preheat each temperature. The D_e values obtained using channel 1 to 5 are not different from those of preheat plateau test. However, the D_e values obtained using channels 15 and 20 show relatively low D_e values.
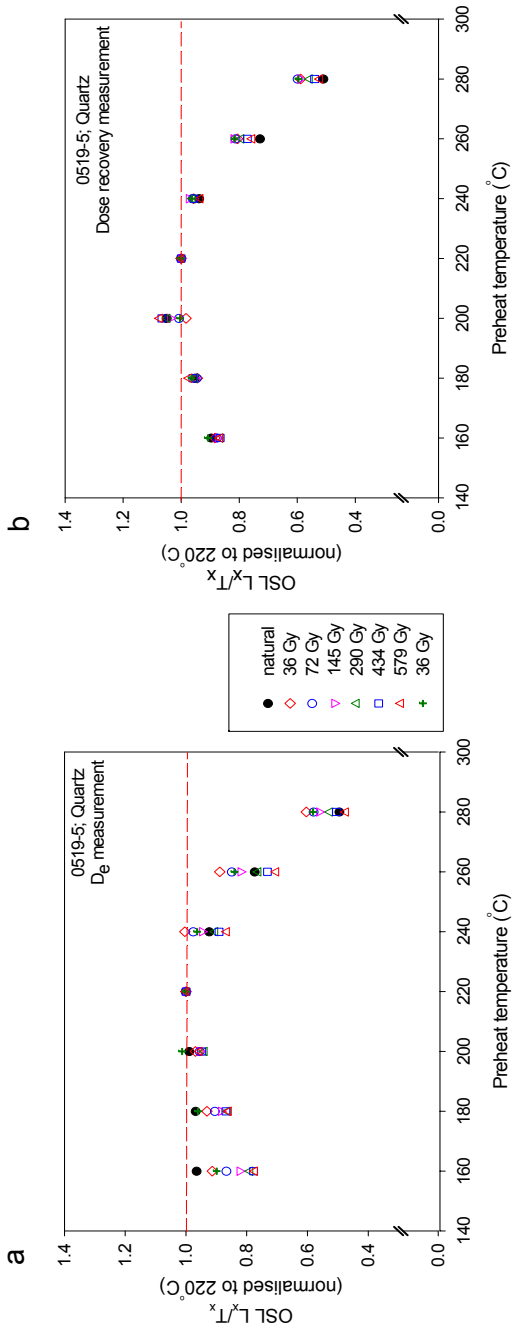
Fig. 4-7. L_n/T_n and L_x/T_x ratios for fine-grained quartz sample 0519-5 measured following preheats from 160 to 280°C held for 10 s, normalised to the L_n/T_n or L_x/T_x data collected using a 220°C preheat, for a) natural (filled circles) and regenerative dose signals, and b) laboratory-given (i.e. dose recovery) and regenerative dose signals. Each point shown is the mean of two aliquots.

electrons go to 'refuge traps'. Recuperation is a double effect with phototransfer (during bleaching) and thermal transfer (during preheating) (Aitken, 1998). These charge transfer can, in some cases, create significant problems in dating (Rhodes and Bailey, 1997; Aitken, 1998; Rhodes, 2000; Jain et al., 2002). Aitken (1998, p. 31) stated that if the laboratory preheat is insufficiently stringent, the transfer that occured during burial, preceding measurement of the natural OSL signal, is liable to be greater than that which occurs for a laboratory-induced OSL signal; this will give rise to an erroneously high D_e estimate. For natural doses, the extent of the charge transfer prior to laboratory preheating is dependent on the retention lifetime of electrons in the shallow traps (Aitken, 1998). In laboratory irradiated samples, at low preheat temperatures (e.g. below ~220°C or 240°C), this thermal transfer of trapped charge is only partially completed compared to the natural signal. These differences may have given rise to the different normalised L_n/T_n and L_x/T_x patterns (Fig. 4-7a) and hence to the erroneously high D_e values (Fig. 4-3a) observed in this study. Although there is only a small difference between the normalised L_n/T_n and L_x/T_x values at low preheat temperatures (Fig. 4-7a), it is significant enough to produce greatly increased D_e values for these samples because the dose response curve extends to very high regeneration doses (600 Gy). At such doses the dose response exhibits a very low slope because the exponential component is near saturation and the remaining growth is dominated by a linear component.

In this study, the effects of charge transfer for different preheat temperatures are also investigated using TL measurements obtained during the preheat plateau and dose recovery tests. In preheat plateau and dose recovery tests, the TL signal was observed during the pre-heating, ranging from 160 to 280°C in 20°C steps. In Fig. 4-8, TL glow-curves are shown as a plot of TL against temperature. In the case of the naturally irradiated sample, there is negligible TL below 220°C (Fig. 4-8a).

However, in the same sample which has received a laboratory dose, TL below 220°C shows much higher peak intensity.

These differences in the TL glow curve between the naturally-irradiated and laboratory-irradiated samples are caused by short electron-retention lifetime of the TL traps below 220°C. In naturally-irradiated samples, electrons decay naturally in the TL traps below 220°C during the burial period. In this process, some electrons may be transferred to the main OSL trap. In laboratory-irradiated samples, pre-heating prior to OSL measurement makes electrons to be transferred to the main OSL trap. However, low preheat temperatures (below 220°C) only partially complete the thermal transfer of electrons to the main OSL trap. This transfer is not enough to make the same amount of transfer as for the natural dose. This may have caused the erroneously high D_e values in this study. In theory, the efficiency of charge transfer during preheating should be same as that during burial. However, natural samples have a higher charge transfer effect than laboratory irradiated samples when low preheat temperatures are used. On the other hand, the dose recovery test shows high TL peaks from about 100°C for both the given dose and the regen dose (Fig. 4-8b). The dose recovery test was undertaken on quartz which had been laboratory irradiated after bleaching; therefore the amount of transferred charge for the given dose is same with that of the regen dose for the same preheat temperature.

This study demonstrates that the mismatch between the normalised laboratory-given regenerative dose (L_x/T_x) data and the normalised natural dose (L_n/T_n) data shown in Figure 4-7a can become a serious problem, giving rise to overestimation of D_e values (Fig. 4-3a). Significantly, in such cases the dose recovery test cannot be used to identify the preheat temperature range that yields the correct D_e values (Fig. 4-3a and b); instead, the data from natural D_e determinations conducted across

a range of preheat temperatures must be examined. For this study, both a plateau in D_e values (Fig. 4-2) and a match between the normalised regenerative dose (L_x/T_x) data and the normalised natural dose (L_n/T_n) data (Fig. 4-3a) are obtained in the preheat temperature range 200-240°C (holding for 10 s). In addition, a given laboratory dose could be recovered for preheat temperatures ≤ 240°C. The region 200-240°C is therefore selected as being appropriate for the determination of fine-grained quartz OSL D_e values for both samples (Fig. 4-2).

In both the preheat plateau and dose recovery tests, increasing values of L_x/T_x across the preheat range from 160 to 200°C suggests that there is significant thermal transfer of charge from a trap between 160 and 200°C into the OSL trap (c.f. Robert, 2006). Many studies just use a dose recovery test or a dose recovery test combined with preheat plateau test to select a suitable preheat temperature. With such studies it is difficult to find these problems. On the other hand, in many studies that used low preheat temperatures, problems of thermal transfer were not found, because these studies used very young age samples. In these young age samples, the TL traps below 220°C may not induce serious charge transfer during the burial period. Roberts (2006) demonstrated that for her younger loess samples (D_e approximately 50 Gy) the D_e values vary little with preheat plateau test and there is excellent dose recovery. Also, many other papers suggest that the thermal transfer is insignificant at low preheat temperatures and there exists a stable plateau range up to 260°C (Bailey et al., 2001; Murray and Clemmensen, 2001; Jain et al., 2002). These papers also used very young samples (D_e less than 10 Gy).

4-5. Summary

For Jeongokri fine-grained (4-11μm) quartz samples, insufficient thermal
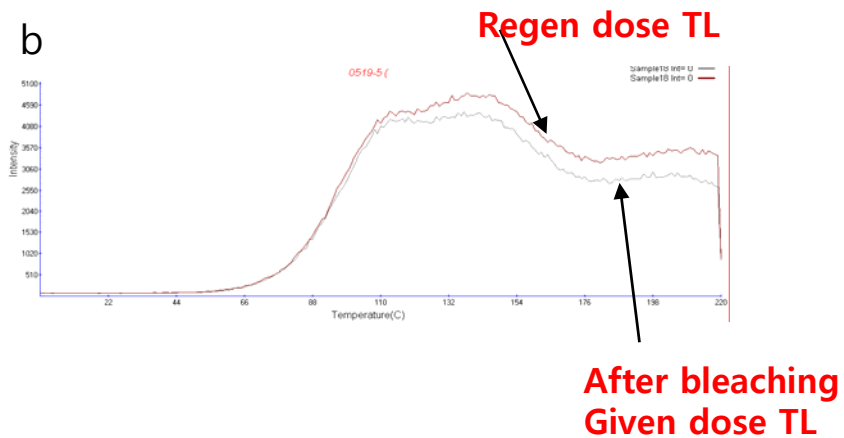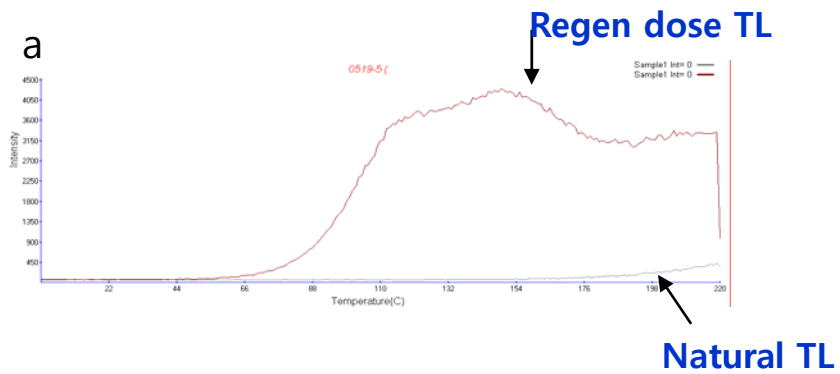
Fig. 4-8. TL measurements obtained during the preheat plateau (a) and dose recovery tests (b). TL glow-curves are shown as a plot of TL against temperature.

transfer may be responsible for the large apparent D_e values at low preheat temperatures; the phenomenon is particularly notable for these samples due to the high natural D_e values (in excess of ~ 350 Gy), and hence low slope of the dose response curves. This situation may also present problems for other old or high D_e value samples from other sites.

The dose recovery test as applied to unheated materials is useful, but it only confirms the appropriate laboratory procedures for artificial doses and is not sufficient to identify an appropriate preheat temperature for SAR dating measurements. Instead, a test examining D_e values versus preheat temperature is advocated, coupled with a comparison of the normalised L_n/T_n and L_x/T_x ratios to look for anomalies between the response to natural and laboratory doses. Together these preheat and dose recovery data show that the quartz OSL D_e values obtained using preheat temperatures between 200-240°C give the most consistent results and, as such, are the most appropriate for dating the samples from Jeongokri.

CHAPTER 5. Luminescence dating of Jeongokri fluvial sandy sediments

Abstract

In this study, we applied optically stimulated luminescence (OSL) dating to quartz grains from samples collected from the Jeongokri fluvial sediments to obtain the depositional ages of sediments containing these artifacts. Fluvial sediments, however, are not an ideal material for dating because of the potential for insufficient and/or varied exposure to daylight prior to burial, which may not have been sufficient to completely reset the OSL signal of all grains prior to deposition (Murray et al., 1995). OSL dating results from Jeongokri fluvial samples show stratigraphic inconsistency and large scattering in the OSL ages, ranging from 34 - 66 ka. Therefore, we carried out various experiments to resolve the observed inconsistency and scatter in the OSL ages. In this study, we present the most suitable method for OSL dating of the Jeongok fluvial sediments, and establish accurate chronologies for the Jeongok Paleolithic site.

5-1. Introduction

In this study, we applied OSL dating to quartz grains collected from the Jeongokri fluvial sandy sediments to investigate the reproducibility and accuracy of OSL dating. Used samples of this chapter were from the pit of the 2004 excavation at the Jeongokri site (Jeongok agricultural cooperative federation site; Fig. 5-1). The Jeongokri fluvial sediments are composed of dominant cross-bedding and horizontal-bedding units of coarse sand. We collected 7 samples along the same bedding plane of the cross-bedded unit. Also, we collected 4 samples from the lower and upper horizontal-bedded unit along the same bedding plane. We

expected that all samples from same bedding plane would show the same age results. However, initial OSL dating results from Jeongokri fluvial samples showed stratigraphic inconsistency in the ages. For samples collected from the same cross-bedded layer, ages ranged from 34 - 66 ka. It was unclear whether the wide range observed in the D_e values reflected sedimentary properties such as insufficient bleaching during transport, or different luminescence properties of the quartz and discrepancy in experimental suitability of the SAR procedure (Zhang et al., 2003).

This chapter describes the problems of luminescence dating from Jeongokri fluvial sediments and discusses the reproducibility of D_e distribution and the reliability of the OSL ages. Also, we carried out various experiments to resolve the observed inconsistency and scatter in OSL ages, including preheat plateau/dose recovery test. More detailed analysis of the OSL decay curve was measured by three exponential decaying components to investigate component defined behaviour. Finally, we suggest an alternative method to improve the reliability and reproducibility of OSL dating of Jeongokri fluvial sediments.

5-2. Sample description

The unconsolidated fluvial sediments overlie unconformably Quaternary Jeongokri basalt, and are divided into lower cross-bedded unit of nearly 3m thickness and about 2m of thick upper horizontal-bedded units. The JG-A series (7 samples) was collected along a single-bedding plane of the cross-bedded unit. The JG-HB series was collected from the lower part of the horizontal-bedded unit on the boundary between the cross-bedded unit and horizontal-bedded unit, and the JG-HT series was from the upper part of the horizontal-bedded unit (Fig. 5-1).

Accordingly, the expected OSL age order is JG-A (7 samples), JG-HB (2 samples) and JG-HT (2 samples) series in decreasing age.

5-3. Method

In this study, quartz grains (90-250 μm) were used after cleaning in 10% H_2O_2, 10% HCl and 40% HF. All OSL measurements were made using a Risø TL/OSL automatic reader. The stimulation light source was a blue-LED (470±30 nm) array. Photon detection was through 7 mm of Hoya U-340 filter. Equivalent doses (D_e) were measured using SAR protocol (Murray and Wintle, 2000). For our initial experiments, in the SAR protocol, a preheat temperature of 260°C for 10s and a cut-heat of 220°C for 0s were used. The temperature during blue light stimulation (40s) was held at 125°C in order to prevent retrapping of charges from the shallow trap corresponding to the 110°C TL peak (Murray and Wintle, 1998). The preheat plateau/dose recovery test was measured to determine the dependence of the D_e values on increasing preheat temperatures (220~295°C/10s with 15°C interval). First, samples were bleached at room temperature with blue LED for 1000s, left for 10,000s at room temperature and bleached again with blue LED for 1000s. The samples were then irradiated with a known given dose. We used given dose of the same order as the natural dose. Twenty-four aliquots for each sample were measured (three aliquots in each temperature). The D_e values with a recycling ratio within 10% and recuperation within 5% were used for age calculation.

5-4. Results and discussions

5-4-1. Initial SAR results

Our OSL ages are stratigraphically inconsistent and show large scatter, ranging from 34 - 66 ka. The investigated D_e values in each sample also show a relatively large scatter (130~250 Gy). These samples have a large number of rejected aliquots, a large error range and poor reproducibility. The mean equivalent dose (D_e), standard error and age calculation are listed in Table 5-1.

In the single bedding plane of the cross-bedded sediments (JG-A), the reproducibility of D_e measurement is poor, contrary to expectations. The cross-bedded sediments are typically found in moderate to high energy sedimentary environments. These environments could give rise to heterogeneous bleaching of the grains at deposition. However, there is no evidence for significant systematic effects of heterogeneous bleaching in ages older than about 20 ka, even from fluvial systems (Murray and Olley, 2002). Our initial OSL ages range from 34 - 66 ka. Therefore, we believe that for the studied sediments partial bleaching does not contribute significantly to the scatter of D_e values.

A wide range of D_e values can reflect the luminescence properties of the quartz (Packman et al., 2007). The luminescence properties related to the origin of the quartz. Porat et al. (2001) showed that the highest D_e values with the largest scatter were measured for grains from streams transporting colluvium on igneous and metamorphic rocks. In fluvial environment, sediments may be derived from various branch streams, which can result in a mixture of quartz from different origins. Therefore, source variation in fluvial sediments could affect the large D_e scatter. On the other hand, Ward et al. (2003) shows that fluvial samples demonstrating great D_e scatter exhibit significant pre-heat dependency. The OSL signal within quartz may be enhanced by thermal transfer during pre-heating.

The first step toward the solution of many questions and possibilities, in this study, preheat plateau/dose recovery test was used to investigate the dependence of
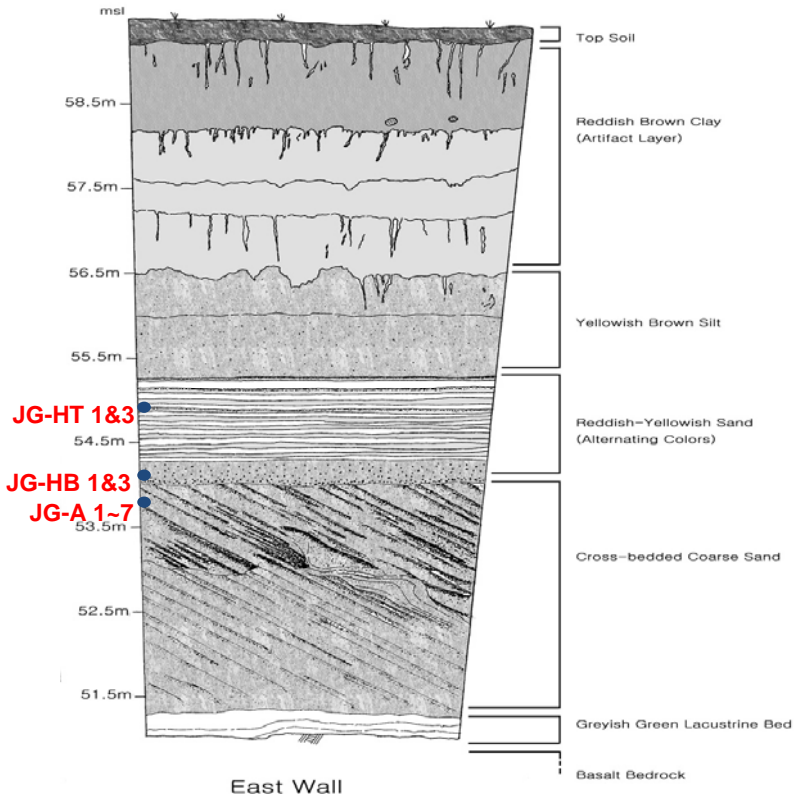
Fig. 5-1. Stratigraphy of JG site: 1) The JG-A series was collected along a single bedding plane of cross-bedded fluvial sediments. 2) The JG-HB series was collected from the lower part of the horizontal-bedded unit (border between cross-bedded unit and horizontal-bedded unit) and JG-HT series from the upper part of the horizontal-bedded unit.

Table 5-1.

sample. No	Quart size	Present water content (%)	Depth (m)	D_e values (Gy)	Dose rate (Gy/ka)	Age (ka)
JG-HT1	90-250$\mu\ell$	16.6	4.6	224.2±18.1	4.15 ± 0.1	54.0±4.5
JG-HT3	90-250$\mu\ell$	13.3	4.6	156.9±10.8	4.07 ± 0.1	38.6±2.8
JG-HB1	90-250$\mu\ell$	9.1	5.4	153.1±15.7	3.89 ± 0.09	39.4±4.1
JG-HB3	90-250$\mu\ell$	13.6	5.4	189.4±10.8	3.61 ± 0.09	52.5±3.3
JG-A1	90-250$\mu\ell$	14.8	6.5	250.1±26.2	3.76 ± 0.09	66.5±7.1
JG-A2	90-250$\mu\ell$	14.3	6.5	200.5±20.9	4.12 ± 0.1	48.7±5.2
JG-A3	90-250$\mu\ell$	17.1	6.5	207.8±50.4	3.82 ± 0.09	54.4±13.3
JG-A4	90-250$\mu\ell$	19.4	6.5	127.0±12.4	3.74 ± 0.09	33.9±3.4
JG-A5	90-250$\mu\ell$	19.3	6.5	168.6±21.2	3.65 ± 0.09	46.2±5.9
JG-A6	90-250$\mu\ell$	20.1	6.5	194.7±19.7	3.74 ± 0.09	52.1±5.4
JG-A7	90-250$\mu\ell$	12.2	6.5	196.8±12.1	4.06 ± 0.09	48.5±3.2

* The radionuclide concentrations of the samples were measured using low-level high resolution gamma spectrometry at Korea Basic Science Institute (KBSI), Korea.

* Conversion to dose rates used the data presented by Olley et al. (1996).

* All dose rates were modified using present water contents, and the attenuation factors given by Zimmerman (1971).

Cosmic ray contributions were calculated using the equations given in Prescott and Hutton (1994).

the equivalent dose on different preheat temperatures and to check the ability to recover the laboratory dose.

5-4-2. Preheat plateau/dose recovery test

The results from the preheat plateau/dose recovery test show that generally sample JG-A4 recovers a given dose well, but other samples were underestimated or overestimated and have large error ranges (Fig. 5-2). There are no discernable trends in recovered D_e values with increasing preheat temperature in each sample. This implies that each sample probably has a different behaviour to thermal treatment, even samples collected from the same bedding plane. The results of the preheat plateau/dose recovery test demonstrate no significant D_e dependence upon pre-heat temperatures, therefore preheat temperatures are not a main factor causing scatter of D_e values and large error ranges.

5-4-3. CW-OSL component separation

As mentioned in the previous section, the luminescence properties of the quartz could affect large D_e scatter. To investigate luminescence properties, an alternative approach is component separation. Especially, CW-OSL component separation takes less measurement time than LM-OSL and mathematical transformation is easily accomplished. The continuous wave-OSL (CW-OSL) decay curve can be described by the sum of three exponential decay components, termed fast, medium and slow, using first-order equations (Smith and Rhodes., 1994; Bailey et al., 1997). The fast component of CW-OSL decay curve corresponds to the 325°C TL peak and is the dominant signal in the initial part of the decay curve (Bailey et al., 1997). Accordingly, after component separation, using the fast component is useful for D_e estimation using the SAR procedure. CW-OSL component separation can also

distinguish mixed origins of quartz. Tsukamoto et al. (2003) shows that in tephric loess originating from a mixture of air-fall tephras and aeolian dusts from Chinese loess, the medium and slow components originate from volcanic quartz after CW-OSL deconvolution. In addition, many papers (e.g. Choi et al., 2003; Watanuki et al., 2005) suggest that experimental fitting of CW-OSL decay curves enables the successful separation of the "fast" component from the mixed signal and using only this "fast" component in D_e calculations resolves the stratigraphic inconsistency and produces reliable age results.

In this study, we used three components (fast, medium and slow) deconvolution of the CW-OSL decay curve. After deconvolution, only the fast component was used for D_e estimation. However, this method is inappropriate for determining the D_e of JG samples. Because, results in this experiment show that the growth curve shapes were irregular or impossible to fit well when only the fast component was used. Even though we could make a growth curve and then fitted well, the recovered D_e values were over or underestimated. Also, in preheat plateau/dose recovery test, the given dose was not recovered accurately when only the first component was used. These results imply that the first (fast) component used for D_e estimation was not derived from only fast component. To investigate these results further, additional analysis of the CW-OSL component separation was undertaken.

5-4-3-1. Detail in the CW-OSL decay curve

Separation of the CW-OSL decay curve into three exponential components (fast, medium and slow) was carried out using this equation:

$y = y_0 + Ae^{-b1x} + Be^{-b2x} + Ce^{-b3x}$

A, B and C are decay constants, and bn is the detrapping probability in each

component. In CW-OSL measurements, the decay constants for each component are determined by the stimulation light intensity and by the photoionization cross-section of components. Each component has a specific photoionization cross-section value (σ), which is proportional to the detrapping probability (b value). The first component (fast component) has the largest photoionization cross-section and the highest detrapping probability which means that this component is very sensitive to light and easy to empty trap. Traps with smaller photoionization cross-sections and lower detrapping probabilities yield the medium and slow components (Kuhns et al., 2000).

In this study, we compared b values of the first component (highest b value) in each JG samples after three components separation. The b values are proportional to the photoionization cross-section value (σ), although differ between OSL readers, because of the different stimulation light intensity in each OSL reader. In this study, after comparing b values of the standard quartz, we confirmed that the fast component has approximately 2-3 ranges of b value.

5-4-3-2. b value comparison in preheat plateau/dose recovery test

First, we used preheat plateau/dose recovery test data for separation of the CW-OSL decay curve and then compared the b values in each decay curve of the recovered given dose, regen dose and test dose at different preheat temperatures. As a result, we found b values decreased with increased preheat temperatures and regeneration cycles in the same sample (Fig. 5-3). Also, b values of the recovered given dose and regeneration dose at low temperatures (220-235°C) show a wide variation from 2 to 10 and above. However, at higher preheat temperatures (250-280°C), b values have low levels of 2-3 ranges, which would be expected for the fast OSL component. The b value represents a particular component of the OSL
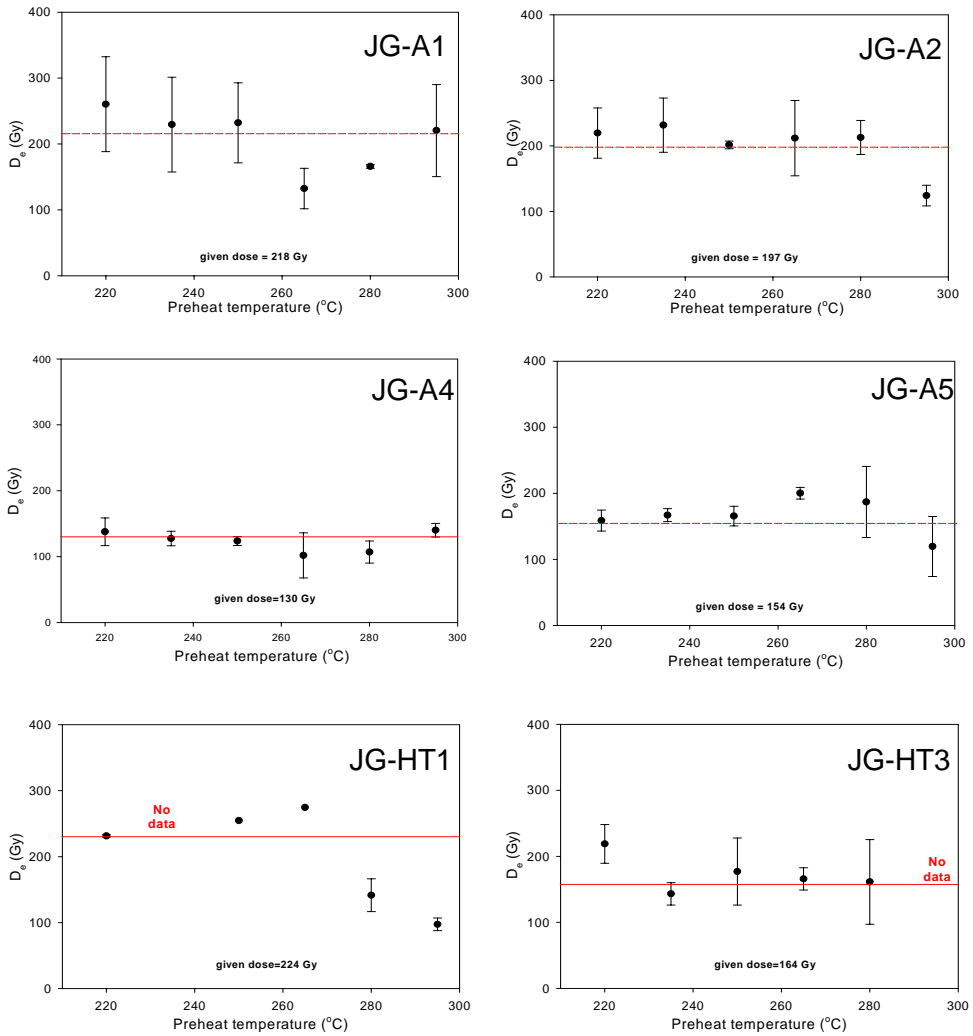
Fig. 5-2. The preheat plateau/dose recovery test results of JG samples show that generally sample JG-A4 recovers a given dose well, but other samples were underestimated or overestimated and have large error ranges.
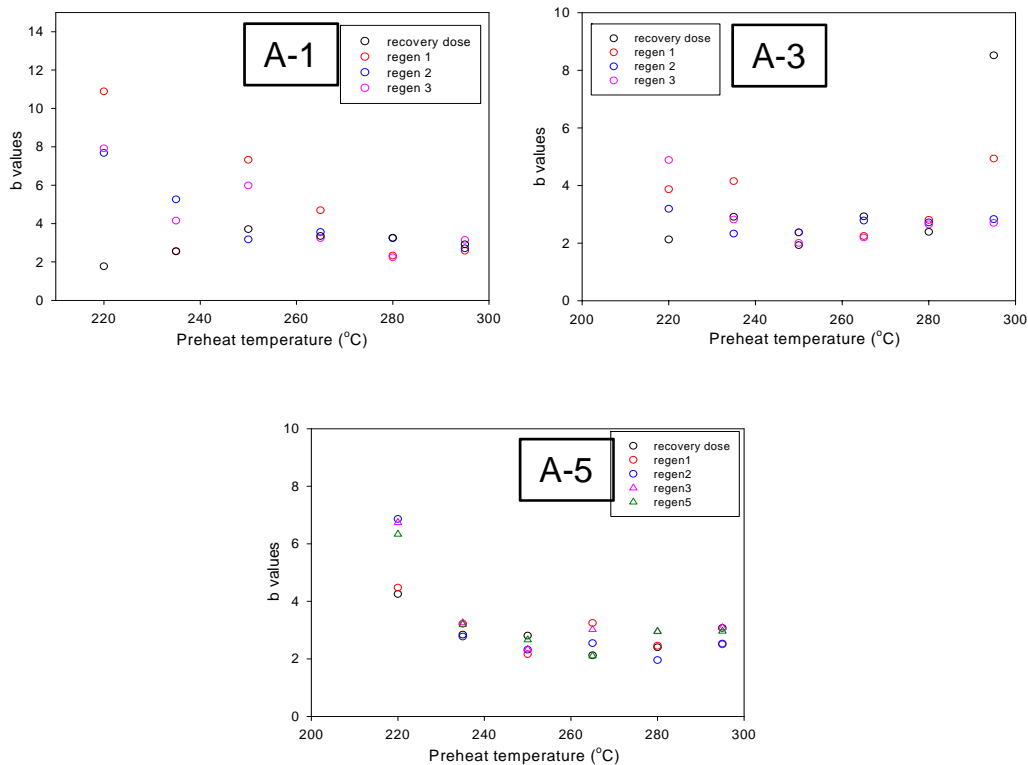
Fig. 5-3. b values of the first component of CW-OSL decay curves from preheat plateau/dose recovery test data. The b values were compared in each decay curve of the recovered given dose, regen dose and test dose at different preheat temperatures.

signal. Accordingly, different b values indicate that component distribution may vary according to each preheat temperature and regeneration dose. First component having higher b values of above 3 might be related to another component, such as the ultra-fast component. This component is dominant in low preheat temperatures (220-250°C). Also, this component increases with repeated regeneration doses. However, this component is thermally unstable and is removed with higher preheat temperatures (over 250°C).

5-4-3-3. b values of test dose

As mentioned above, the characteristics of component distribution will affect test dose more than regeneration dose because low cut-heat temperature (220°C) was used for test dose (c.f. Goble and Rittenour, 2006). These characteristics can be easily identified using CW-OSL component separation of the test dose.

Although the same cut-heat temperature (220°C) was used for all measurements, the b values showed a wide variation in each test dose (Fig. 5-4). In addition, b values of the test dose gradually increased with repeated regeneration cycles. One possible implication of this is that any luminescence sensitivity change may not be corrected by the SAR procedure due to the different proportion and distribution of components in each test dose. Uncorrected sensitivity change may create a large distribution of D_e values and error even for a well bleached sample. Accordingly, we need more accurate sensitivity correction and complete removal of the unstable first component.

5-4-4. LM-OSL

A more detailed analysis of the OSL component separation from sedimentary quartz can be performed in LM-OSL curves more than CW-OSL decay curves. We

applied LM-OSL to JG samples and standard quartz (WIDG 8). In LM-OSL data, large variation of brightness in three samples (JG-A1, A6 and HT1) was apparent. The first peak position was similar. In general four or five components were fitted. The first peak shows 1.28-2.23 of b values and $1.82-2.95*10^{-17}$ of the photoionization-cross section ranges. The WIDG 8 sample which has been used as a standard quartz in this study shows 2.08 of b value and $2.7*10^{-17}$ of the photoionization-cross section range. If we use preheat temperature of $160°C/10s$, we can get another first peak such as an ultra-fast component (c.f. Jain et al., 2003; Singarayer and Bailey, 2003). This component shows 63.1 of b value and $7.86*10^{-16}$ of the photoionization-cross section range. However, in over $160°C$ preheat, we couldn't find this peak. In this experiment, we expected same b value and the photoionization cross-section value between CW-OSL and LM-OSL in the first peak. However, despite successful fitting of the LM-OSL curves, b value and the photoionization cross-section values are not consistent (c.f. Kuhns et al., 2000). Also, unlike results of the CW-OSL component separation, ultra-fast component did not exist over $160°C$ preheat temperatures. This indicates that ultra-fast component in CW-OSL is derived from thermally unstable and sensitized fast component. Also, CW-OSL curve fitting do not necessarily mean contributions from only three components, and several components may be overlapping to produce the observed signals (Kuhns et al., 2000). These results require further research.

5-4-5. An alternative method to isolate the cause of the problems

The high preheat and cut-heat temperatures are probably essential to completely remove of the unstable ultrafast component. Choi et al. (2003) proposes applying a $220°C$ cut-heat after the test-dose to improve the accuracy of the D_e

estimation of the preheat plateau test. However, in this study, despite a high cut-heat temperature of 220°C, it was not enough to remove the unstable first component. Jain et al. (2003) suggested that the ultra-fast component could be removed completely by heating to 260°C. However, Packman et al. (2007) report that the ultra-fast component remains after using preheat of 240°C. They suggest that for complete removal of ultra fast component, 300°C preheat is necessary. Goble and Rittenour (2006) also shows that the ultrafast component is still present at 260°C /10s preheat, and 300°C preheat for at least 20s can fully remove the ultrafast component. However, a higher preheat temperature to 300°C would cause thermal depletion of the fast component. Therefore, we attempted an alternative approach to remove the unstable first component.

For our OSL analyses, we used the initial luminescence signal (0-0.8s; initial 5 channels) in the CW-OSL decay curve (total 40s; 250 channels) for D_e estimation and age determination. This signal range principally originates from the fast component. However, when we used the SAR protocol, we identified that the first two of the 250 channels had a great effect on the variation of b values. The decay curve, which had a high b value of 4-11 shows a large interval (rapid decrease) between the first and second channels. On the other hand, the decay curve, which had a low b value (2-3) shows a small interval between the first and second channels, as well as between the second and third channels (Fig. 5-5). Especially, these distinctive features were dominant in test dose. It implies that first two channels could be contributed from another component, such as an ultra-fast component, and changes in the relative proportions of the components may yield erroneous D_e values.

To eliminate the effect of this component on D_e estimation, we used 0.48-1.12s initial luminescence signals instead of 0.0-0.8s for D_e estimation of preheat
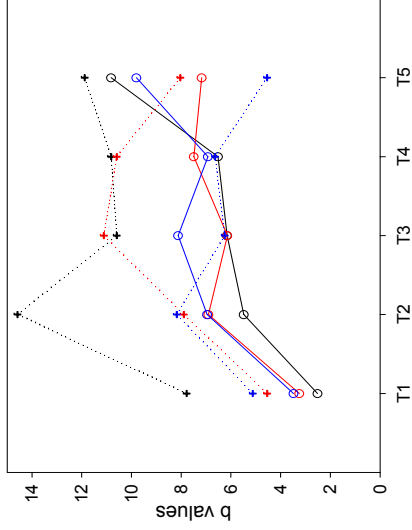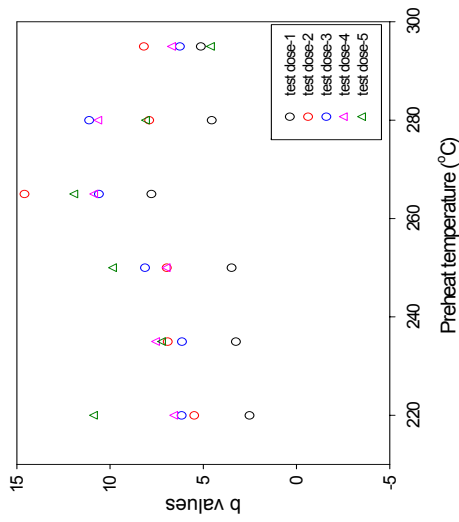
Fig. 5-4. b values comparison in each test dose (JG-A5). b values showed a wide variation in each test dose and gradually increased with repeated regeneration cycles.
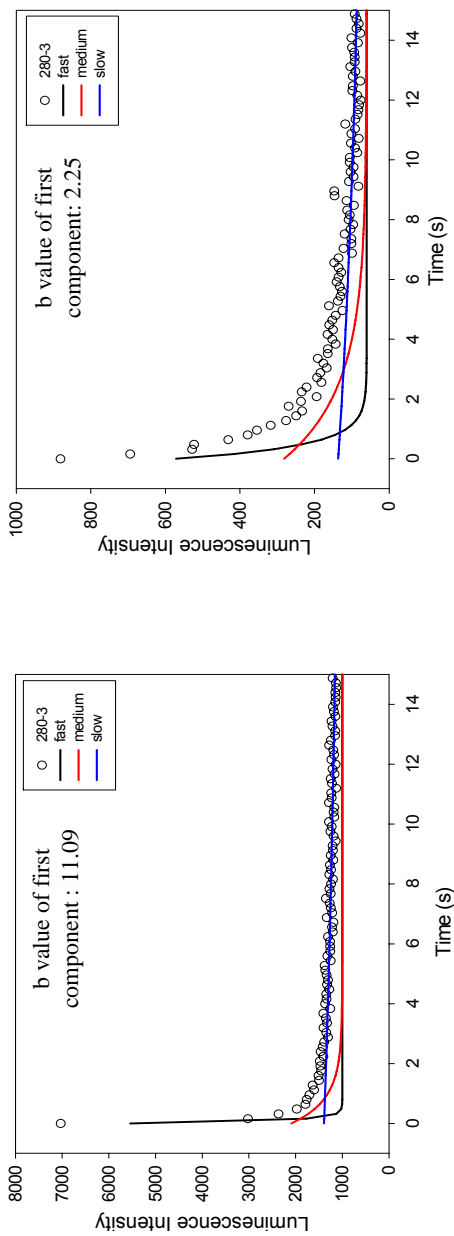
Fig. 5-5. The CW-OSL decay curve (total 40s; 250 channels) was used for D_e estimation. a) decay curve having high b value of 11 shows a large interval (rapid decrease) between the first and second channels, b) decay curve having low b value (2-3) shows a small interval between the first and second channels.

plateau/dose recovery test. As a result, we obtained consistent b values (2-3), more reliable D_e values and small error ranges in the D_e values. Fig. 5-6 shows consistent recovery dose with given dose and considerably reduced error ranges from the preheat plateau/dose recovery test after removal of first two channels. In radial plot we confirmed the improved reproducibility of D_e values as well as graph of preheat plateau/dose recovery test (Fig. 5-7).

5-4-6. Application to OSL ages of the Jeongokri (JG series) sediments

Our OSL dating of the Jeongok (JG series) samples resulted in a wide variety of ages with large errors, which were nor stratigraphically consistent. It was necessary to reject a relatively large number of aliquots to obtain D_e estimates, and the samples showed significant sensitivity change with poor reproducibility.

In the preheat plateau/dose recovery test, it was possible to improve the reproducibility and reliability of D_e estimation using an alternative method. In this study, D_e calculation used the 0.48-1.12s luminescence signal instead of 0.0-0.8s. From this, there was a considerable improvement in age consistency of JG samples. The ages also show a reduced error range and age dispersion (Fig. 5-8). Therefore, OSL dating using the 0.48~1.12s signal provides a possible solution to the problems in stratigraphic consistency and reproducibility. However, a few samples (JG-A4, A5 and HT1) still show underestimated age results than average value of same bedding samples and age inversion. As a result, the OSL age range still shows large age distribution pattern. JG-A series collected from cross-bedded sediments have an age range of 33~55ka. Also, JG-HB series and JG-HT series collected from horizontal-bedded sediment have an age range of 32~45 ka.

5-4-7. The credibility of the D_e estimation by changing channel number

A similar method was suggested by Packman et al. (2007). They used the 0.32-0.64s initial signal instead of 0.0-0.32s (known as the "later-light" method), and showed that this method is likely to provide greater accuracy in the D_e estimation. However, in the same study, they also show that this method produces a higher D_e for the dose recovery experiment. In this study, a few samples (JG-A4, A5 and HT1) still show inconsistent D_e values and age inversion.

These problems are possibly derived from not only the removal of unstable first component, but also of the fast component. However, if we remove more than 2 initial channels (0.36s), the b value becomes lower than 2 and D_e errors increase. This implies that removal more than 2 initial channels (0.36s) might be affected by depletion of fast component or addition of medium and slow component signal. Therefore, the removal of the first 0~0.36s channels is sufficient for the removal of the initial unstable luminescence signal.

The low luminescence intensity of decay curve is another possible cause of these problems. In this case, after removal of the first two channels, the remaining signal is very low such as a background level. In this case, accurate D_e measurement is quite difficult. Samples JG-A4, A5 and HT1 show very dim luminescence characteristics. Particularly, in these samples, the luminescence signal of test dose after removal of the first two channels shows very low luminescence intensity. Therefore, this problem could seriously affect in D_e measurement. The luminescence properties of quartz grains could be influenced by quartz origin. Also, they can be influenced by the frequency of weathering, bleaching and number of deposition cycles (Richardson, 1994). In fluvial environment, sediments may be derived from a variety of different sources, which may have experienced different weathering or deposition cycles. This study has

shown that not all Jeongokri sediments are suitable for OSL dating due to these reasons. Further detailed work, such as a systematic and comparative investigation of the OSL properties of quartz, is required to solve these problems.
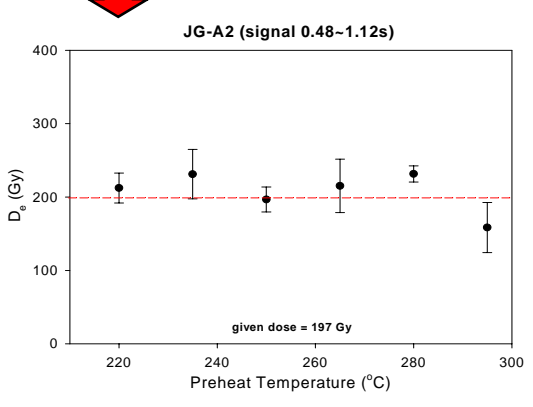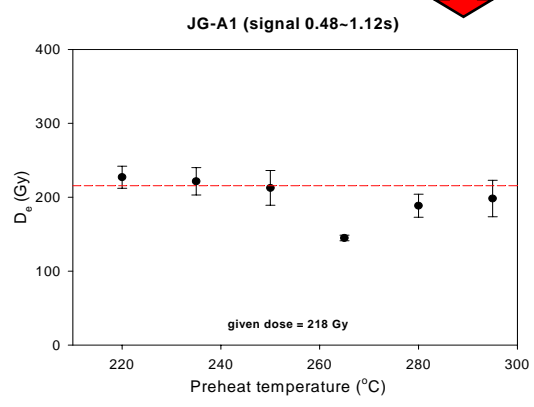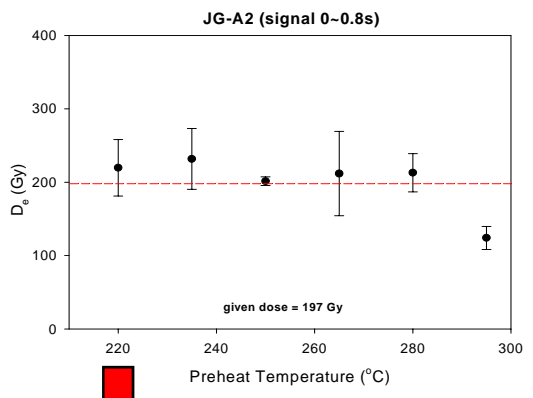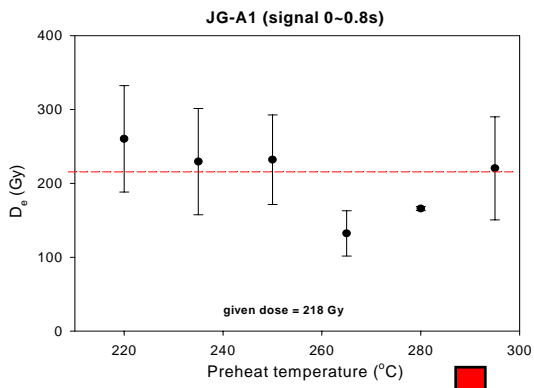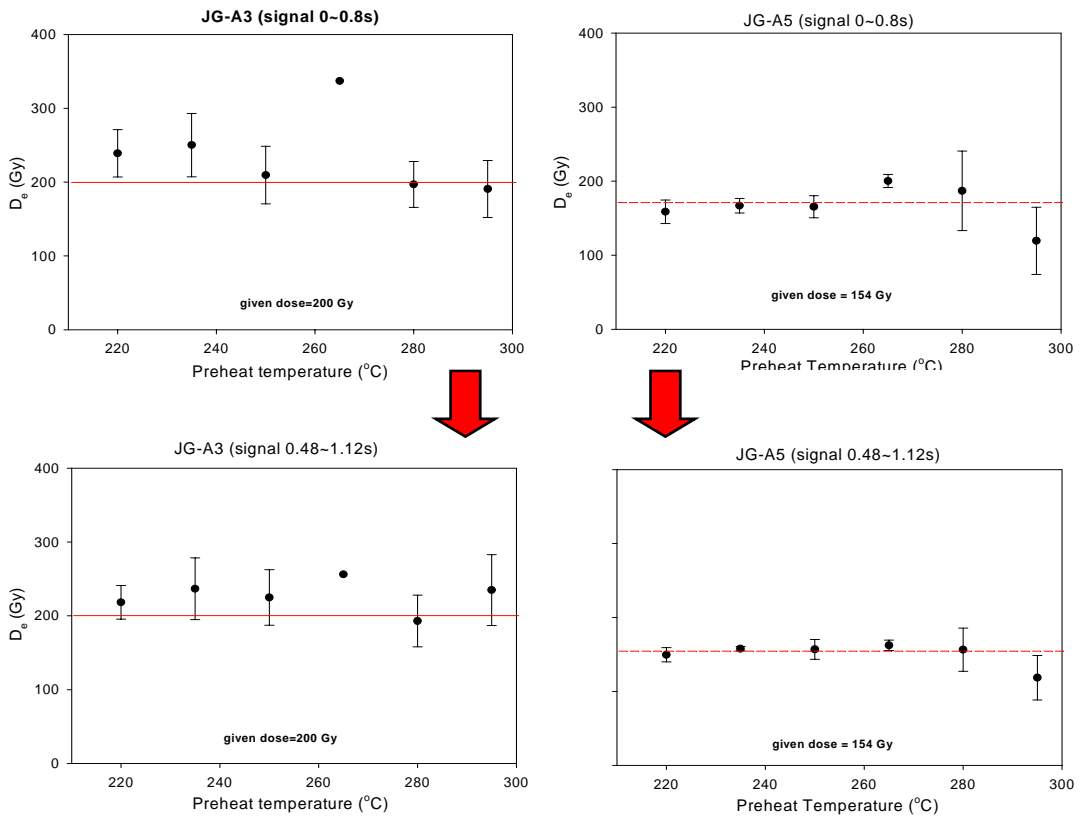
Fig. 5-6. D_e estimation using 0.48-1.12s of initial luminescence signals instead of 0.0-0.8s from preheat plateau/dose recovery test shows consistent recovery dose with given dose and considerably reduced error ranges after removal of first two channels.
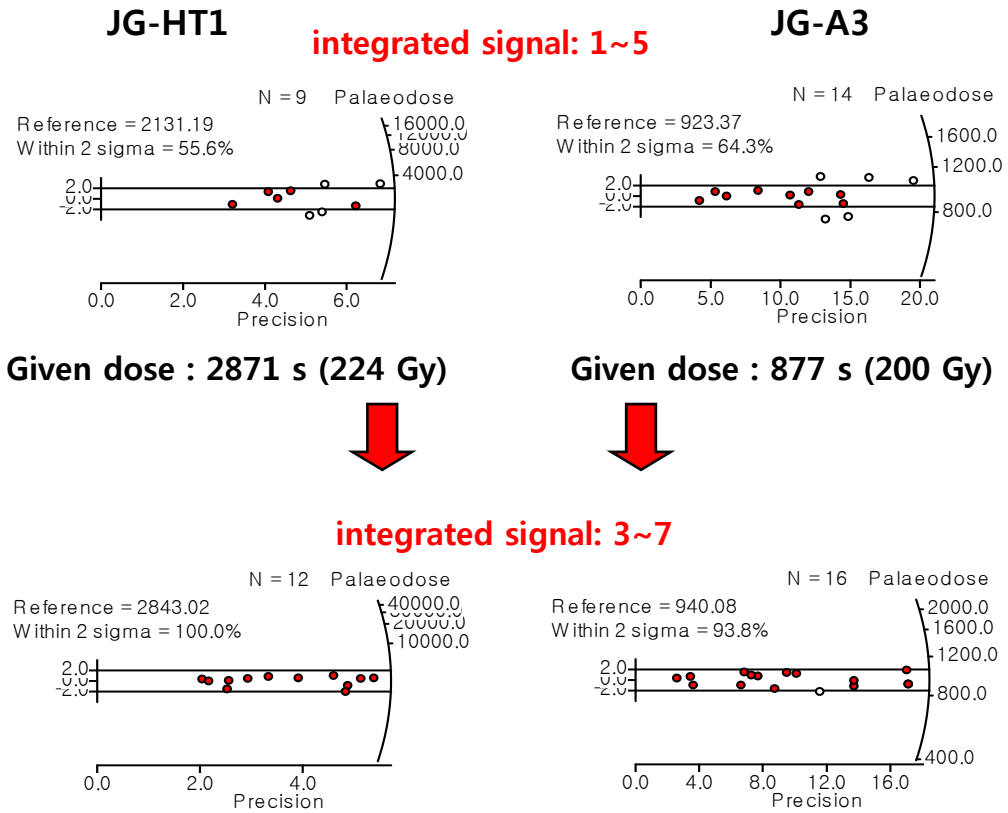
Fig. 5-7. Radial plot showed the improved reproducibility of D_e values as well as graph of preheat plateau/dose recovery test.
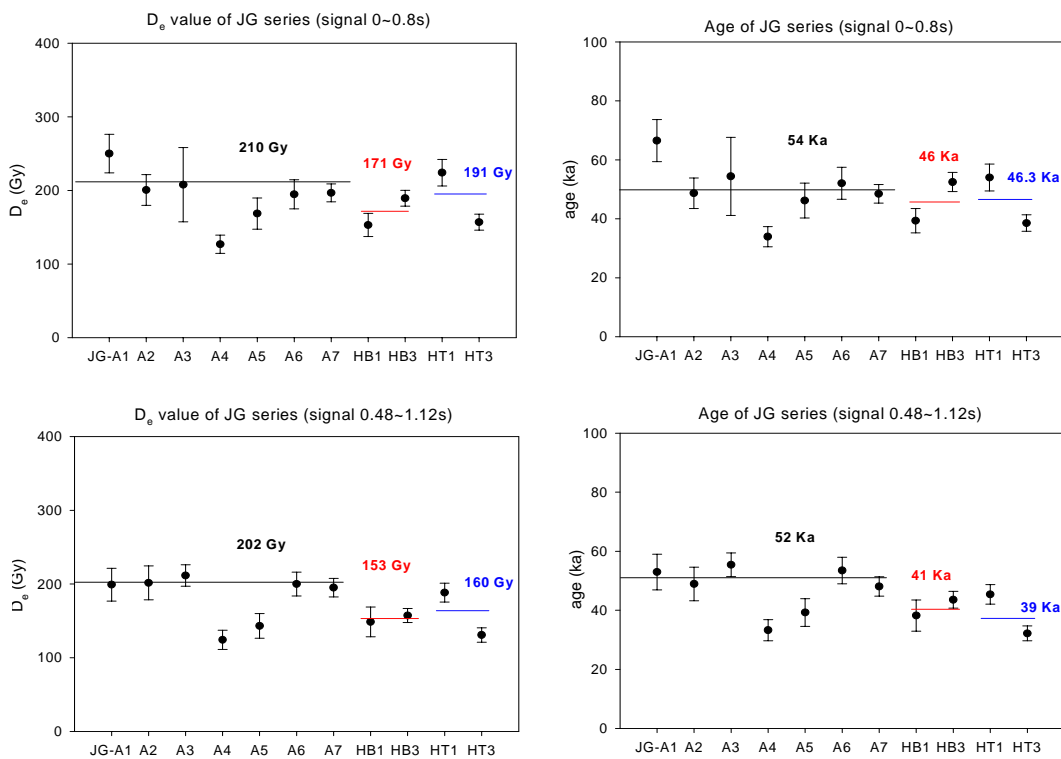
Fig. 5-8. Considerable improvement in D_e values and ages of JG samples were showed using the 0.48-1.12s luminescence signal instead of 0.0-0.8s. The OSL dating using the 0.48~1.12s signal provides a possible solution to the problems in stratigraphic consistency and reproducibility.

CHAPTER 6. Dose dependence of thermally transferred optically stimulated luminescence signals in quartz

Abstract

The thermally transferred optically stimulated luminescence (TT-OSL) responses of chemically purified fine-grained quartz from seven loess-like samples from Korea are presented. In particular, the experimental procedures used to separate the dose-dependent (recuperated OSL, ReOSL) and dose independent parts of the signal were explored. The OSL signals used to monitor the sensitivity changes that take place during the measurement sequences used to determine the equivalent dose were investigated. A single aliquot procedure was used for the TT-OSL measurements and resulted in linear growth of the ReOSL with dose up to at least 2 kGy. For this suite of samples, a standardised growth curve (SGC) was constructed for the ReOSL, tested with dose recovery experiments, and was used to obtain D_e values for the seven samples.

6-1. Introduction

In order to extend the age range of luminescence dating of sedimentary quartz grains, a thermally transferred optically stimulated luminescence (TT-OSL) signal has been investigated (Wang et al., 2006a). A multiple aliquot procedure was put forward by Wang et al. (2006b) and tested on samples of loess taken at Luochuan on the Chinese Loess Plateau. Included in the test were four samples from the Brunhes/Matuyama magnetic reversal boundary, thus having an age of ~ 780 ka (Coe et al., 2004). Subsequently, a single aliquot regenerative dose (SAR) procedure has been proposed (Wang et al., 2007). This procedure is based on

repeating the measurement protocol established for the multiple aliquot procedures. Tsukamoto et al. (2008) tested this SAR protocol on loess from another site in China and wind blown sands from a cave on the southern coast of South Africa. They found a build up of signal during the SAR protocol and reduced its effect by inserting an additional optical stimulation at the end of each measurement cycle. Tsukamoto et al. (2008) confirmed that the TT-OSL signals from samples from both sites continued to grow with dose, well above the dose levels at which the usually observed fast component of the OSL signal saturates (Wintle and Murray, 2006). They also demonstrated that the TT-OSL signal was reduced by light exposure many orders of magnitude more slowly than the fast OSL signal.

A TT-OSL signal is observed when a sample is optically stimulated in the laboratory after it has previously had the OSL signal zeroed using the same light source and then been heated for a few seconds at a temperature that does not empty the trap related to the fast component of the OSL signal (e.g. 10 s at 260°C). In their empirical study, Wang et al. (2006a) concluded that the TT-OSL signal has two components, the recuperated OSL (ReOSL) and basic transferred OSL (BT-OSL), as proposed by Aitken (1998). The latter could not be zeroed using the laboratory light source and was considered to be dose independent. Similar non-dose-dependent TT-OSL signals were reported by Li and Li (2006) and by Li et al. (2006). In contrast, the ReOSL signal was dose dependent and it was shown to have sufficient thermal stability to date back as far as 780 ka (Wang et al., 2006b).

Further studies on the ReOSL signal have been carried out by Adamiec et al. (2008) in order to elucidate the source of the electrons that give rise to the ReOSL signal. The source appears to be a thermally stable, light sensitive trap, but one that is far less light sensitive than the fast and medium component traps that are observed in measurements of the OSL signal. The mechanism has been the subject

of numerical modelling (e.g. Pagonis et al., 2008) which has reproduced a variety of the behaviours observed in empirical studies. The initial optical bleach in the laboratory (Step 3, Table 6-1) does not affect the electrons in the TT-OSL source trap, but heating at 260°C for 10 s (Step 4, Table 6-1) is able to eject some electrons into the conduction band from where they can be captured by the fast OSL trap. In their measurement sequence, Wang et al. (2006b) proposed a measurement sequence to separate the two components (ReOSL and BT-OSL) by heating the sample for 10 s at 300°C (Step 9, Table 6-1) in the middle of each measurement cycle. This step was aimed at removing any electrons that were remaining in the source trap. Ahead of this annealing step, the TT-OSL contains both components, whereas after the step, the signal relates only to the BT-OSL component.

In this chapter, we use quartz from a set of samples from Jeongokri to investigate the contribution of the BT-OSL signal to the TT-OSL signal and to find out whether the annealing step is achieving its goal. In addition, as the SAR procedure for ReOSL contains many steps, and for older samples the repeated irradiation needed to construct a dose response curve becomes very time consuming, we have investigated whether it is possible to construct a standardised growth curve as has been proposed for the dose response of the fast component of the OSL signal (Roberts and Duller, 2004; Burbidge et al., 2006) and used for dating loess (Lai, 2006; Lai et al., 2007; Stevens et al., 2007), thus reducing the instrument time required. Finally, for the suite of samples from Korea, we have compared the equivalent dose values obtained using the fast component OSL signal that contains a saturated exponential component and a linear component with the equivalent dose values obtained using the TT-OSL signal.

6-2. Equipment and samples

Luminescence signals were measured with two Risø automated systems. All of the measurements involving only the fast component OSL signal were made on a TL/OSL-DA-10 system, while all the measurements involving TT-OSL used a TL/OSL-DA-20. The two systems were equipped with blue light emitting diodes (LEDs) for optical stimulation (Bøtter-Jensen et al., 2003), delivering 16.9 mW.cm^{-2} and 50 mW.cm^{-2} respectively. Luminescence emission was detected with EMI-9635Q photomultiplier tubes filtered with 7.5 mm of Hoya U-340 colour glass filter. All preheating and TL measurements were made at 5°C/s. The measurement protocol followed that in Table 6-1; it is a recuperated SAR (ReSAR) protocol from Tsukamoto et al. (2008), similar to that of Wang et al. (2007). All optical stimulation was made at 125°C, except for the 100 s optical stimulation at 280°C at the end of each measurement cycle. All optical stimulations were for 100 s, except the first in each cycle (step 3, Table 6-1) where it was for 300 s in order to remove the electrons from the fast and medium OSL traps.

The seven samples were collected from fine grained, loess-like sediments at Jeongokri, South Korea; laboratory number E55S20IV, samples 2-7 and 9. No independent age control was available as the initial aim of the study had been to provide a chronology. The samples were chemically treated with sodium pyrophosphate to disperse and remove clays, H_2O_2 and HCl to remove organic matter and carbonates, and settled in a dilute sodium oxalate solution to obtain the 4-11 μm grain size fraction. Quartz grains were separated from the samples using hydrofluorosilicic acid etching for two weeks to remove the feldspars (Roberts, 2007). The grains were mounted out of suspension in acetone onto 9.8 mm diameter aluminium discs, with 1 mg being deposited on each disc.

6-3. TT-OSL signals

A typical OSL and TT-OSL signal obtained for sample E55S20IV-5 (later shown to have received a dose in nature of ~ 700 Gy) is shown in Fig. 6-1. The signals are very similar to those shown by Wang et al. (2006a) for a sample of Chinese loess that had received a dose of ~ 400 Gy. Both the OSL and TT-OSL signals appear to be dominated by the fast component. Adamiec et al. (2008) demonstrated the similarity by fitting the signals using single exponential decays. This suggests that the electrons are captured in the same trap either as a result of ionising radiation (in the case of OSL) or thermal ejection from a deep trap (in the case of TT-OSL). The TT-OSL signal is an order of magnitude greater than the end of the OSL signal immediately prior to the preheat (10 s at 260°C) and soon drops to a similar level (Fig. 6-1).

The ReSAR protocol in Table 6-1 was applied to two discs for all seven samples in order to obtain the dose response curve of the ReOSL signal for each sample and permit calculation of the equivalent dose (D_e). In this protocol, the thermally-transferred OSL signals (L_{TT-OSL} and L_{BT-OSL}) are measured in Steps 5 and 12 (Table 6-1). The luminescence sensitivity is measured in response to a test dose of 15 Gy (Steps 6 and 13, Table 6-1) and the signals used are the OSL responses to the test dose (T_{TT-OSL} and T_{BT-OSL}) (Steps 8 and 15, Table 6-1). It should be noted that the test dose used in this study was three times larger than that used by Tsukamoto et al. (2008). In their development of a SAR protocol, Wang et al. (2007) concluded that for dating the best results were obtained when the test dose was chosen to be about 10% of the expected unknown dose. For the sample under study here, this would imply a test dose of ~70 Gy. However, the use of an optical stimulation at 280°C at the end of each cycle (Step 16, Table 6-1) will prevent

Step		Signal measured
1.	Regeneration dose (D_i)	
2.	Preheat at $260°$ C for 10 s	
3.	Optical stimulation at $125°$ C for 300 s	
4.	Preheat at $260°$ C for 10 s	
5.	Optical stimulation at $125°$ C for 100 s	$L_{TT\text{-}OSL}$
6.	Test dose ($D_t = 15$ Gy)	
7.	Preheat at $220°$ C for 10 s	
8.	Optical stimulation at $125°$ C for 100 s	$T_{TT\text{-}OSL}$
9.	Anneal at $300°$ C for 10 s	
10.	Optical stimulation at $125°$ C for 100 s	
11.	Preheat at $260°$ C for 10 s	
12.	Optical stimulation at $125°$ C for 100 s	$L_{BT\text{-}OSL}$
13.	Test dose ($D_t = 15$ Gy)	
14.	Preheat at $220°$ C for 10 s	
15.	Optical stimulation at $125°$ C for 100 s	$T_{BT\text{-}OSL}$
16.	Optical stimulation at $280°$ C for 100 s	
17.	Return to Step 1	

Table 6-1. Single aliquot regenerative dose (SAR) procedure for construction of the dose response curve for the thermally transferred OSL signal (from Tsukamoto et al., 2008).

accumulation of charge through the SAR protocol, as suggested by Tsukamoto et al. (2008).

For both TT-OSL and OSL measurements the signal used is from the first 1.25 s of the decay curves of the type shown in Fig. 6-1. The dose response curves for the sensitivity-corrected TT-OSL signal ($L_{TT\text{-}OSL}/T_{TT\text{-}OSL}$) and the sensitivity-corrected ReOSL signal ($L_{TT\text{-}OSL}/T_{TT\text{-}OSL} - L_{BT\text{-}OSL}/T_{BT\text{-}OSL}$) are shown in Fig. 6-2 for one disc of sample E55S20IV-5. As also shown by Wang et al. (2006a, 2007) and by Tsukamoto et al. (2008), the ReOSL signal continues to grow with dose well beyond 2 kGy. From Fig. 6-2, it can also be seen that the ReOSL signal makes up most of the TT-OSL signal. The sensitivity-corrected BT-OSL signal ($L_{BT\text{-}OSL}/T_{BT\text{-}OSL}$) is also shown, and unexpectedly it also increases with dose. BT-OSL has previously been described as being independent of dose and not reset by optical stimulation (Wang et al., 2006b). The results in Fig. 6-2 show the BT-OSL signal does grow with dose, a result which is consistent with the data of Wang et al. (2006b, Figs. 4e and A1e), though they did not comment explicitly upon this. D_e values can be obtained for each of the signals for this one aliquot; values of 704.9±15.0, 702.2±18.0 and 697.0±25.1 Gy were obtained for the TT-OSL, ReOSL and BT-OSL signals, respectively (Table 6-2a, column headed "Conventional").

The TT-OSL and BT-OSL signals used to construct the dose response curves shown in Fig. 6-2 were calculated by integrating the first five channels of optical stimulation (a total of 1.25 s) and then subtracting a background based upon the average from the last 10 s (390-400 s on Fig. 6-1). Fig. 6-1 shows that this background level, presumably dominated by slow components in the OSL signal (e.g. Singarayer and Bailey, 2003), continues to drop throughout the period of optical stimulation. The TT-OSL signal shown in Fig. 6-1 was obtained from the natural dose of this aliquot (~700 Gy). At lower doses, the relative importance of
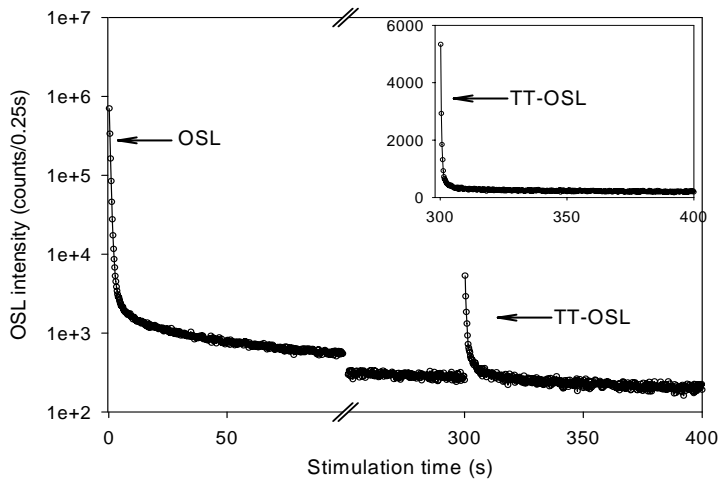
Fig. 6-1. The natural OSL decay curve for an aliquot of sample E55S20IV-5 measured for 300 s at a temperature of 125°C. The aliquot was then heated to 260°C for 10 s and the TT-OSL decay curve measured for 100 s. Note the break in scale on the x-axis. Inset shows the TT-OSL signal on a linear scale. Data points shown every 0.25 s.
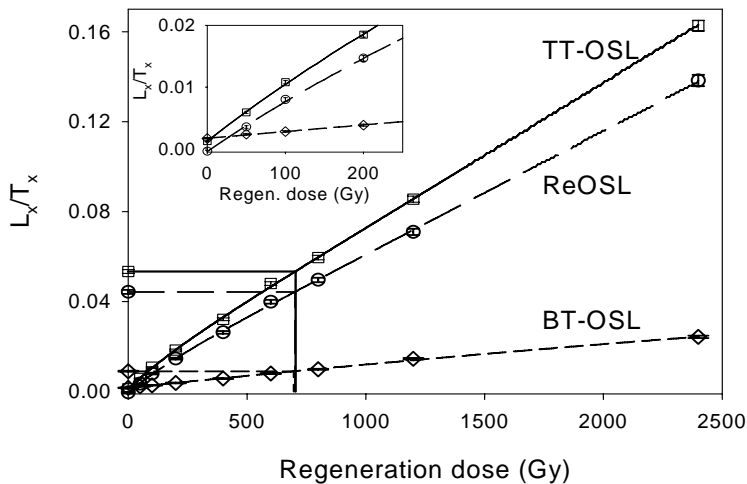
Fig. 6-2. ReSAR dose response curves constructed using the sensitivity-corrected TT-OSL, BT-OSL and ReOSL from an aliquot of sample E55S20IV-5. The D_e calculated for this aliquot using each signal is listed in Table 6-2a. The inset shows the same data set up to a maximum dose of 200 Gy. The values of L_x/T_x shown here were obtained by subtracting the last 10 s of the measured TT-OSL and BT-OSL signals as the background. This gave D_e values of 704.9 ± 15.0 Gy for the TT-OSL, 697.0 ± 25.1 Gy for the BT-OSL and 702.2 ± 18.0 Gy for the ReOSL.

the background subtraction is likely to increase. The D_e values obtained are given in the first column of Table 6-2a. The recycling ratios obtained for a 200 Gy regeneration dose are given in the first column of Table 6-2b.

As well as this conventional method of estimating the background to be subtracted, two alternative methods have been assessed. The first uses the background from the last 10 s of the previous OSL measurement (290-300 s on Fig. 6-1). The second method, described by Adamiec et al. (2008) and indicated in Fig. 2 of Wang et al. (2006a), is to fit a straight line to the last 80 s of the TT-OSL decay curve (320-400 s on Fig. 6-1) and to extrapolate this to the interval used for signal integration (300-301.25 s on Fig. 6-1) to calculate the background. These different methods were applied to the data used to construct dose response curves and D_e values obtained using the resulting TT-OSL, ReOSL and BT-OSL signals are given in Table 6-2a. No systematic differences are seen in the D_e values obtained using the different methods of background subtraction. This is probably because in each case the measured background is derived from the slow component of the OSL signal.

In the sequence of measurements used to construct Fig. 6-2, following measurement of the natural signal, regeneration doses are given with the dose increasing with each cycle, starting with a dose of 0 Gy. The sequence also included repeat measurements for doses of 0 Gy and 200 Gy at the end, with the latter allowing a recycling ratio to be calculated using the data for the 200 Gy measurement (Table 6-2b). For all signals, and using all methods of calculating the background, the recycling ratio is greater than 1. The ReOSL consistently has the lowest recycling ratio (~1.25) of the three signals. In spite of these recycling ratios being significantly different from unity, and despite them being very different for the various signals, the D_e values obtained are consistent with each other within

96

errors (Table 6-2a).

For these samples we do not see any distinct advantage in one method of background subtraction compared with another. Thus for the remainder of the paper we have used the conventional method of taking the average of the last 10 s of the TT-OSL measurement for the background.

The dose dependence of the BT-OSL, as shown in Fig. 6-2, and the similarity of the D_e value obtained using its natural signal to that calculated for ReOSL suggest that, as measured, the BT-OSL signal contains a significant portion (~20% or more) of the ReOSL signal, i.e. the 10 s anneal at 300°C does not result in all the electrons in the source trap being released as had been proposed by Wang et al. (2006b) and this is explored in the following section.

6-4. Characterisation of the BT-OSL signal

Both Wang et al. (2006a, Fig. 3b) and Tsukamoto et al. (2008, Fig. 3b) showed that repeating the cycle of TT-OSL measurement twenty times, to obtain L_{TT-OSL}/T_{TT-OSL}, reduced this ratio to an almost constant level. The identical procedure was applied to an aliquot of E55S20IV-5 (Fig. 6-3a). Tsukamoto et al. (2008, Fig. 3e) also showed that the BT-OSL level (measured after the 10 s anneal at 300°C) reached a similar level to that obtained at the end of the 18 cycles without the annealing step. Fig. 6-3b obtained for another aliquot of E55S20IV-5 also shows that a similar sensitivity-corrected TT-OSL is reached after annealing as is found after more than 18 cycles of thermal transfer (Fig. 6-3a). Additionally, in Fig. 6-3b when the TT-OSL measurement cycle is repeated (without any additional annealing) a constant level is maintained over 10 cycles. This level would be expected to be the sensitivity-corrected BT-OSL. One difference between the data shown in Fig.

(a) D_e (Gy)   Method of calculating the background contribution

Signal	Conventional (last 10 s)	Previous signal (last 10 s)	Extrapolation (last 80 s)
TT-OSL	704.9±15.0	702.8±13.1	696.0±13.1
ReOSL	702.2±18.0	698.1±16.7	689.9±15.2
BT-OSL	697.0±25.1	696.5±26.0	700.2±25.5

(b) Recycling ratio   Method of calculating the background contribution

Signal	Conventional (last 10 s)	Previous signal (last 10 s)	Extrapolation (last 80 s)
TT-OSL	1.38±0.04	1.38±0.04	1.32±0.04
ReOSL	1.26±0.05	1.25±0.06	1.20±0.05
BT-OSL	1.83±0.11	1.83±0.11	1.87±0.12

Table 6-2. (a) Comparison of D_e values (Gy) obtained for the data shown in Fig. 6-2 using different signals, and using different methods for calculating the background for the TT-OSL and BT-OSL signals. (b) Comparison of recycling ratios for a 200 Gy regeneration dose for the different signals and background subtraction methods used in (a).

6-3a and that shown by Tsukamoto et al. (2008) is that a constant TT-OSL level was not achieved, even after 18 cycles.

The lack of a constant value in Fig. 6-3a may be taken as casting doubt on the selection of 300°C for the annealing temperature that is applied in order to transfer the electrons remaining in the source trap as proposed by Wang et al. (2006a). It should be noted that for their measurements Wang et al. (2006a) used equipment manufactured by Daybreak (Inc.), rather than Risø as used in this study. If the temperature attained in Step 9 (Table 6-1) was not sufficiently high, it would result in the signal measured as BT-OSL (Step 12, Table 6-1) being derived from electrons from the ReOSL source trap; this would result in dose dependence of the BT-OSL signal, as seen in Fig. 6-2. The dose dependence of the BT-OSL signal can also be seen when the ratio of BT-OSL/TT-OSL obtained during the construction of a dose response curve (of the type shown in Fig. 6-2) is plotted as a function of the regeneration dose (Fig. 6-4a). In this example, the ratio decreases with dose until a constant ratio is seen for doses above ~ 500 Gy. This is interpreted as showing the increasing effect of a dose-independent part of the BT-OSL signal on the ratio at low doses; at doses above 500 Gy the effect appears negligible and the BT-OSL increases linearly along with the TT-OSL, yielding a constant ratio (Fig. 6-4a).

In order to investigate the possibility that 300°C is inadequate as an annealing temperature (Step 9, Table 6-1) to enable the release of all electrons from the ReOSL source trap, the ReSAR measurement sequence in Table 6-1 was repeated, but using annealing temperatures of 310°C and 320°C (Step 9, Table 6-1) as shown in Fig. 6-4b and 6-4c, respectively. The same pattern in the ratio of BT-OSL divided by TT-OSL as a function of regeneration dose is observed for all three temperatures; but when the value obtained for a dose of 1200 Gy is plotted as a function of the annealing temperature, a decrease in the BT-OSL/TT-OSL ratio is

a

1. Preheat 260°C for 10 s
2. OSL at 125°C for 300 s
3. Preheat at 260°C for 10 s
4. TT-OSL at 125°C for 100 s, L_{TT-OSL}
5. Test dose 15 Gy
6. Preheat 220°C for 10 s
7. Test dose OSL at 125°C for 100 s, T_{TT-OSL}
8. Back to 3

Optical wash (280°C blue 100 s)

b

1 –7 as Fig.3a
8. Anneal at 300°C for 10 s
9. OSL at 125°C for 100 s
10. Preheat at 260°C for 10 s
11. TT-OSL at 125°C for 100 s, L_{TT-OSL}
12. Test dose 15 Gy
13. Preheat 220°C for 10 s
14. Test dose OSL, T_{TT-OSL}
15. Back to 10

(after 300°C annealing)

Optical wash (280°C blue 100 s)

Fig. 6-3. Sensitivity-corrected TT-OSL as a function of cycle for single aliquots of E55S20IV-5 (a) for repeated cycles of thermal transfer, with preheating to 260°C for 10 s. After the first 19 cycles the aliquot was exposed to blue diodes in the Risø reader for 100 s while holding the sample at 280°C. After this, a further 10 cycles of thermal transfer were undertaken. (b) For a second aliquot annealed at 300°C for 10 s after measurement of the natural TT-OSL signal. Twelve cycles of thermal transfer were then undertaken, followed by an optical wash at 280°C, and then further thermal transfer and optical washes.
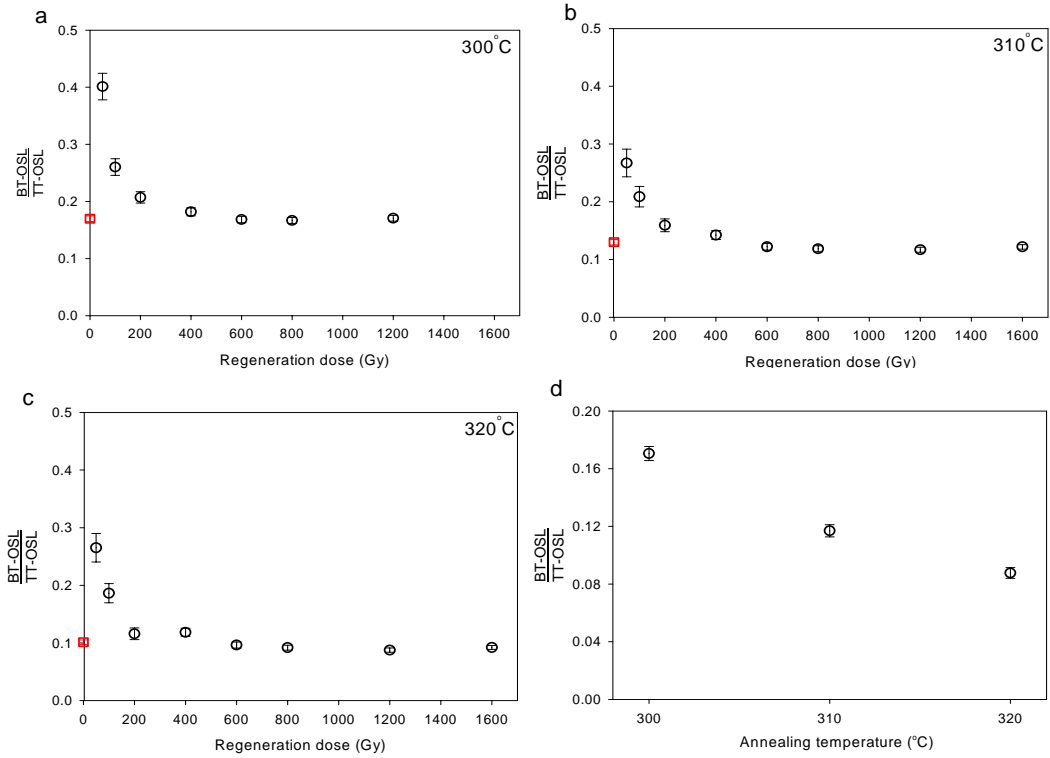
Fig. 6-4. Ratio of the sensitivity-corrected BT-OSL (L_{BT-OSL}/T_{BT-OSL}) and TT-OSL (L_{TT-OSL}/T_{TT-OSL}) from aliquots of E55S20IV-5 as a function of regeneration dose, for different annealing temperatures in Step 9 of Table 6-1: (a) 300℃, (b) 310℃ and (c) 320℃. The square symbol indicates data from measurement of the natural. (d) Ratio of BT-OSL/TT-OSL as a function of annealing temperature for a dose of 1200 Gy with data points taken from a, b and c.

seen as the temperature is increased (Fig. 6-4d). It can be seen that the value does not reach zero, and from this it is concluded that there is nothing special about the selection of any particular temperature for this step in the ReSAR measurement protocol, although the contribution to BT-OSL of electrons from the ReOSL source trap is less for an annealing temperature of 320°C. Higher temperatures cannot be employed as they would cause thermal eviction of electrons from the OSL trap. The dose response curves for the sensitivity-corrected ReOSL obtained for these three aliquots are shown in Fig. 6-5. For the laboratory irradiated response, the sensitivity-corrected ReOSL increases with annealing temperature because the magnitude of the BT-OSL signal that is subtracted decreases, but the natural values are almost unaffected by the changing annealing temperature. For annealing temperatures of 300 and 310°C similar values of D_e are obtained, while for annealing at 320°C the D_e is ~150 Gy lower. The data points obtained after annealing at 320°C show more scatter around the dose response curve than do the data for the lower annealing temperatures. For subsequent experiments, an annealing temperature of 300°C was used as this is consistent with previous studies (Wang et al., 2007; Tsukamoto et al., 2008).

6-5. Estimating the contribution of the dose-independent BT-OSL signal

The results described above (Figs. 6-4a, b and c) have demonstrated that, after annealing to 300, 310 or 320°C, the signal that is designated as BT-OSL in Table 6-1 is not independent of dose. If this signal consists of both a proportion of the dose-dependent ReOSL signal and a dose-independent, BT-OSL signal, is it possible to estimate the magnitude of the latter? A number of approaches can be used to estimate the maximum magnitude of the signal. Firstly, in the inset to Fig. 6-2, the

lowest sensitivity-corrected BT-OSL (L_x/T_x) is 0.0017±0.0001 as measured for the cycle in which the first zero regeneration dose is measured. Secondly, in Fig. 6-3a repeated cycles of thermal transfer are able to reduce the sensitivity-corrected TT-OSL to a level of 0.0092±0.0003 as measured after 18 cycles, while in Fig. 6-3b annealing to 300°C reduces the signal to 0.0084±0.0003. Thirdly, the experiments in Figs. 6-3a and b were extended by inserting a step where the aliquot was optically stimulated using blue LEDs for 100 s while holding the sample at 280°C; this is termed an 'optical wash'. This step is used at the end of each regeneration cycle (Step 16, Table 6-1) to remove any remaining charge from optically sensitive traps. In Figs. 6-3a and 3b this optical wash caused the sensitivity-corrected TT-OSL measured in the next cycle to fall to values of 0.0015±0.0002 and 0.0017±0.0002 respectively. In both cases, subsequent cycles of thermal transfer see the TT-OSL signal increase (Figs. 6-3a and 3b). The cause of this increase in subsequent cycles is not clear, but the two smallest values measured (0.0015±0.0002 and 0.0017±0.0002) demonstrate that the dose-independent BT-OSL signal must be equal to, or smaller, than this.

A further indication of the magnitude of the dose independent BT-OSL signal can be found by undertaking a bleaching experiment using a powerful light source (SOL2) with a wide wavelength range (Fig. 6.5 in Aitken, 1998). Eighteen aliquots of sample E55S20IV-5 were bleached in a SOL2 solar simulator for periods from one minute to one week. The remaining TT-OSL and BT-OSL signals (after annealing at 300°C) were measured using the procedure in Table 6-1 and the sensitivity-corrected TT-OSL ($L_{TT\text{-}OSL}/T_{TT\text{-}OSL}$) and BT-OSL ($L_{BT\text{-}OSL}/T_{BT\text{-}OSL}$) are shown in Fig. 6-6. The TT-OSL decreases in a manner similar to the drop in ReOSL previously observed by Tsukamoto et al. (2008, Fig. 6a and b). Fig. 6-6 also shows that the BT-OSL signal decreases, albeit more slowly than the TT-OSL,
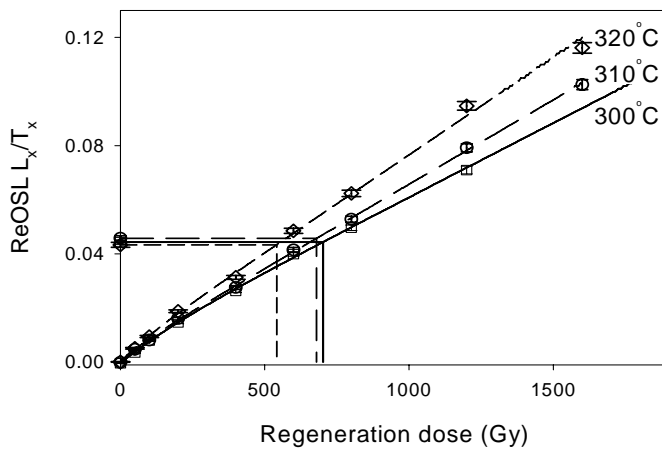
Fig. 6-5. ReOSL dose response curves for aliquots of E55S20IV-5 obtained using annealing temperatures of 300, 310 and 320°C in Step 9 of Table 6-1. The same experimental data were used for Fig. 6-4a–c.

with the sensitivity-corrected BT-OSL reaching a value of 0.0041±0.0004 after one week. In comparison, the OSL signal (Step 3, Table 6-1) dropped to less than 2% of its initial value after one minute in the SOL2 (not shown). For longer SOL2 exposure times, the subsequent drop in this OSL signal was very similar to that observed for the TT-OSL (Step 5, Table 6-1); this is unsurprising since both measurements were made following a preheat at 260°C for 10 s which would have resulted in thermal transfer.

All three methods provide a maximum value for the dose-independent BT-OSL. Two methods give very similar values of 0.0017 for the ratio of (L_{BT-OSL}/T_{BT-OSL}), implying that for sample E55S20IV-5 the BT-OSL is negligible (~3%) compared with the sensitivity-corrected TT-OSL value from the natural (~0.05; Fig. 6-2). Subtracting the signal measured following annealing at 300°C, i.e. that termed BT-OSL, appears to have no significant impact upon the form of the growth curve (Fig. 6-2) or the D_e value obtained (Table 6-2a). The implication of this is that it may not be necessary to make a separate measurement of the BT-OSL. However, for consistency with previously published work (e.g. Tsukamoto et al., 2008), for the remainder of this paper the BT-OSL signal measured following annealing at 300°C has been subtracted to calculate ReOSL, as originally proposed by Wang et al. (2006a).

6-6. Constructing dose response curves for ReOSL

Dose response curves for sensitivity-corrected ReOSL, such as that shown for an aliquot of E55S20IV-5 shown in Fig. 6-2, were constructed for two aliquots of each of the seven samples collected at the site. In this way, two values of D_e were obtained for each sample. However, in OSL dating it is usual to obtain D_e values
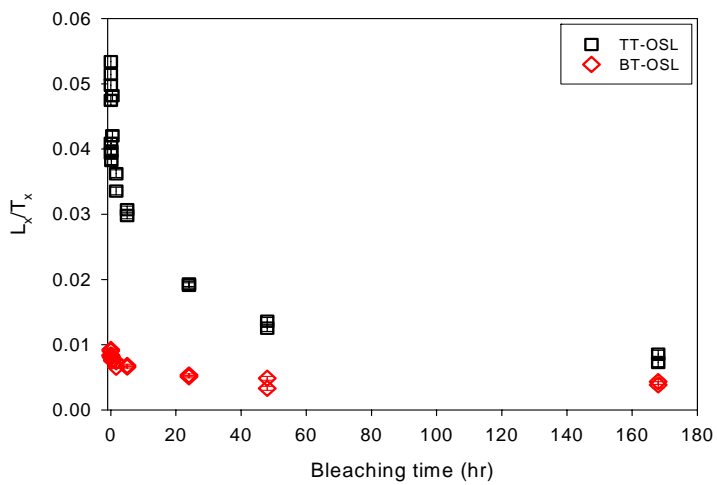
Fig. 6-6. The sensitivity-corrected TT-OSL ($L_{TT\text{-}OSL}/T_{TT\text{-}OSL}$) and BT-OSL ($L_{BT\text{-}OSL}/T_{BT\text{-}OSL}$) remaining in 18 aliquots of sample E55S20IV-5 after SOL2 exposures ranging from 0 to 168 h (1week).

for a minimum of ten discs. In order to construct dose response curves the samples require very long irradiations, with doses of several hundreds of Gy, taking 24 hours for each aliquot of these samples.

In order to reduce the instrument time needed for dating this suite of seven samples, we investigated whether it was possible to construct a standardised growth curve (SGC) for the ReOSL signal, as has been previously carried out for the fast component of the OSL signal (e.g. Roberts and Duller, 2004; Burbidge et al., 2006; Lai, 2006; Lai et al., 2007; Stevens et al., 2007). The ReSAR data points (L_x/T_x) obtained for the laboratory irradiation of discs from all seven samples were multiplied by the test dose (15 Gy) and plotted as a function of the regeneration dose (Fig. 6-7a). The data points for each dose point agree well, independently of from which sample they were taken; this enables the construction of a SGC for this suite of samples (Fig. 6-7b).

For an additional eight discs of each of the seven samples, a short version (3 cycles) of the ReSAR protocol was applied, in which measurements for only the natural (N), zero dose (0 Gy) and 400 Gy regeneration dose were performed. The value for the natural ReOSL ($L_{TT-OSL}/T_{TT-OSL} - L_{BT-OSL}/T_{BT-OSL}$) for each of these 56 discs was projected onto the SGC (Fig. 6-7b) and the D_e value determined, with errors calculated using a Monte Carlo approach (Duller, 2007). This gives rise to eight independent D_e values for each sample. These are shown as solid circles for sample E55S20IV-2 and E55S20IV-4 in Figs. 6-8b and 8d, respectively.

The set of measurements (N, 0, 400 Gy) was chosen following the work of Burbidge et al. (2006) who had suggested that, when using a SGC approach, the validity of the SGC for each aliquot could be assessed by including the measurement of one regeneration dose, in this case 400 Gy. Applying the ReOSL value from the 400 Gy regeneration point to the SGC curve should yield an average

calculated dose of 400 Gy. Fig. 6-8a shows that for sample E55S20IV-2, the dose calculated for this regeneration point using the SGC (closed circles) is systematically greater than 400 Gy, though the mean (419±8 Gy) is just within two standard deviations of the expected value. However, for E55S20IV-4 (Fig. 6-8c) the value is only 298±17 Gy. For the remaining samples the value for this 400 Gy regeneration dose obtained using the SGC varied between the extremes shown in Fig. 6-8a and c. This finding casts doubt on the ReSAR protocol as it was used to construct the SGC.

A second set of measurements was made on 3 aliquots for each sample. An even shorter version (2 cycles) of the ReSAR procedure was applied, but one in which only the natural and a 400 Gy regeneration dose were measured; i.e. no zero dose point was measured. For these three aliquots the doses calculated by applying the ReOSL value measured following the 400 Gy regeneration dose to the SGC in Fig. 6-7b are now much closer to the expected values (Figs. 6-8a and c, shown as open squares). Greater consistency with the given dose of 400 Gy was found across all seven samples. It is not known why the calculated dose obtained using the ReOSL signal obtained from a 400 Gy regeneration point differs depending upon whether it was measured immediately following the zero dose (N, 0, 400 Gy) or not (N, 400 Gy). The same effect presumably led to the poor recycling values obtained in Table 6-2b where the signal generated by a 200 Gy regeneration dose was different depending upon whether a zero dose regeneration measurement had been made or not.

6-7. Monitoring sensitivity change using OSL

One source of the problems related to recovery of known doses could be that
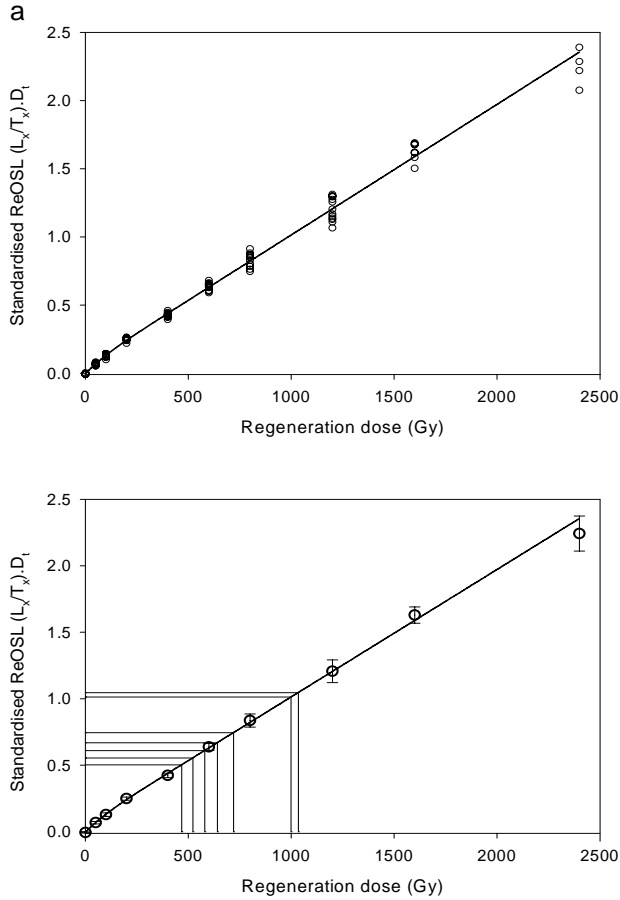
Fig. 6-7. (a) ReOSL dose response data for one aliquot of E55S20IV-2 and two aliquots from each of the six other samples that were used to define the standardised growth curve (SGC). (b) SGC from the average ReOSL value from data shown in (a). For each of the seven samples, the mean natural ReOSL value for the eleven aliquots measured using the shortened ReSAR procedures is shown, indicating the D_e value obtained by interpolating the value onto the SGC.
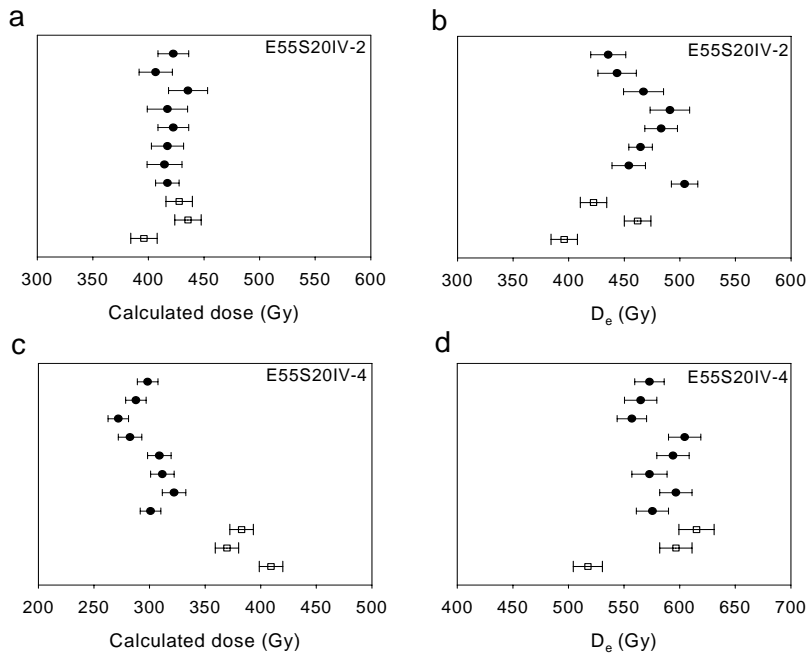
Fig. 6-8. (a and c) Calculated dose values obtained for a given dose of 400 Gy (for samples E55S20IV-2 and E55S20IV-4 respectively). (b and d) D_e values obtained using the SGC (for samples E55S20IV-2 and E55S20IV-4 respectively). Filled circles obtained using the short ReSAR sequence: N, 0, 400 Gy. Open squares obtained using the even shorter ReSAR sequence: N, 400 Gy.

the OSL signals used to correct for sensitivity changes (T_{TT-OSL} and T_{BT-OSL}, measured in Steps 8 and 15 in Table 6-1) are incorrectly registering the sensitivity. This has been investigated for sample E55S20IV-5.

First, it was investigated by carrying out repeated measurement cycles using a fixed dose, given after the first cycle had been used to measure the natural signals. This test was carried out using a regeneration dose of 400 Gy and a test dose of 15 Gy. This study, which was carried out ahead of the construction of the dose response curve, showed that the sensitivity-corrected ReOSL changed little for the three cycles measured after the natural measurement (Fig. 6-9a). A cycle using zero dose was then carried out, followed by a further three cycles with a dose of 400 Gy. These gave three ReOSL values that were very similar to the first three (Fig. 6-9a). A ReOSL value close to zero (-0.0005±0.0002) was obtained for the zero dose cycle. When the test dose OSL signal (T_{TT-OSL}) is plotted as a function of the TT-OSL signal (L_{TT-OSL}) (Fig. 6-9b), it is seen that the sensitivity decreased by about 40% over the course of the eight measurement cycles. The data points for the 400 Gy regeneration dose were consistent with a linear relationship between T_{TT-OSL} and L_{TT-OSL}. The proportionality of L and T is the major criterion put forward for SAR dating (Wintle and Murray, 2006). There is thus no a priori reason that the ReSAR protocol will not work and give the correct values of D_e for this sample. However, it should be noted that the value of T_{TT-OSL} for the 400 Gy dose in cycle 6 (Fig. 6-9a) was higher than for the zero dose measured in cycle 5 and the best fit line does not pass exactly through the origin for the 400 Gy data points.

The OSL sensitivities (T_x) following both TT-OSL and BT-OSL measurements during this set of measurements made with a repeated 400 Gy dose can be normalised to the value of T_{TT-OSL} for the first cycle (the natural, T_n). When plotted as a function of cycle they show a monotonic change with cycle prior to the zero
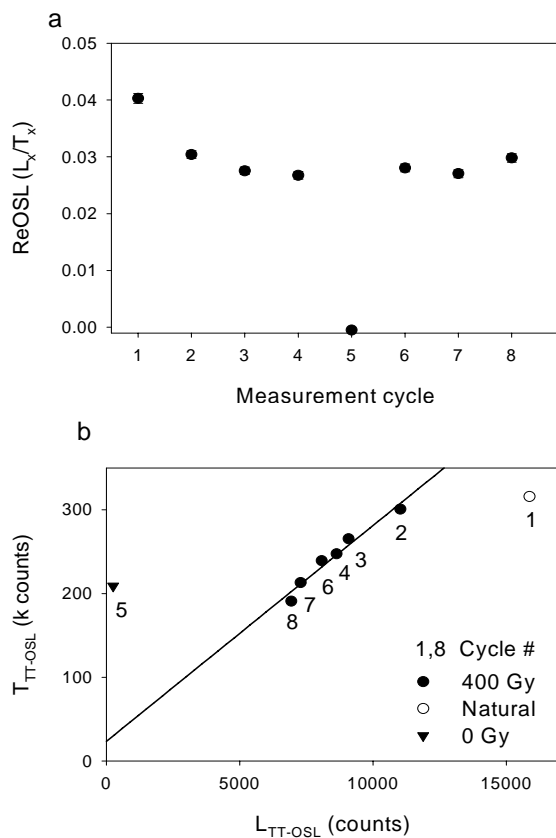
Fig. 6-9. (a) ReOSL measured for repeated regeneration cycles for an aliquot of E55S20IV-5. The first cycle measured the natural signal, and for the other cycles the regeneration doses were 400 Gy (cycles 2–4 and 6–8) and 0 Gy (cycle 5). (b) The $T_{TT\text{-}OSL}$ signal from each cycle as a function of the $L_{TT\text{-}OSL}$ signal. The line of best fit is shown for the 6 cycles with a regeneration dose of 400 Gy.

dose measurement (cycle 5) (Fig. 6-10a). The rise in T_{TT-OSL} after the zero dose is clearly seen for cycle 6.

The T_{TT-OSL} measurements obtained during the experiments that gave rise to the results in Figs. 6-3a and 3b are shown in Fig. 6-10b. From these it can be seen that sharp decreases in sensitivity are brought about by heating at 280°C for 100 s during the optical wash (cycles 12 and 20 in the open circle data set and cycle 19 in the closed circle data set) and by heating at 300°C for 10 s in the attempt to isolate the BT-OSL signal (step 1 in the open circle data set).

Secondly, the sensitivity was monitored using OSL during the construction of the ReSAR response curve shown in Fig. 6-2. In each cycle it was monitored twice, once before and once after the 300°C annealing in that cycle (T_{TT-OSL} and T_{BT-OSL}, respectively). Between each cycle there was an optical wash at 280°C. These values of T_{TT-OSL} and T_{BT-OSL} are shown for each cycle in Fig. 6-10c. Once again it can be seen that the 300°C annealing for 10 s within the cycle and the 280°C optical wash between cycles resulted in sensitivity decreases. For all three data sets it can be seen that T_{BT-OSL} is always lower than T_{TT-OSL} measured in the same cycle.

To attempt to understand the inability to recover a dose for sample E55S20IV-4 using the first short version of the ReSAR protocol (filled circles, Fig. 6-8c), the change in sensitivity (T_x/T_n) is plotted in Fig. 6-11a. The T_{TT-OSL} signal measured for the 400 Gy dose point is seen to have increased relative to the previous cycle (Fig. 6-11a). This would cause underestimation of the 400 Gy responses for both TT-OSL and ReOSL. This would result in underestimation of the dose recovered from the SGC (filled circles in Fig. 6-8c). However, the T_{TT-OSL} measurements for the second short protocol (N, 400 Gy) do not show any change in T_{TT-OSL} for the 400 Gy dose (Fig. 6-11b). This type of behaviour results in the recovery of the 400 Gy dose from the SGC (open squares in Figs. 6-8a and c). We do not understand
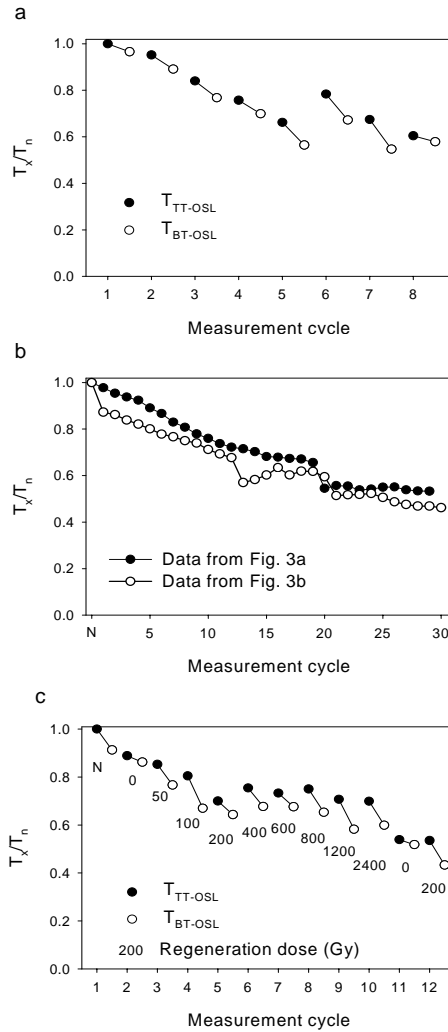
Fig. 6-10. Sensitivity (T_x/T_n) measured through various experimental procedures for aliquots of sample E55S20IV-5. (a) T_{TT-OSL} and T_{BT-OSL} from the experiment shown in Fig. 6-9a. (b) T_{TT-OSL} from Figs. 6-3a and b. (c) T_{TT-OSL} and T_{BT-OSL} from the ReSAR data shown in Fig. 6-2.
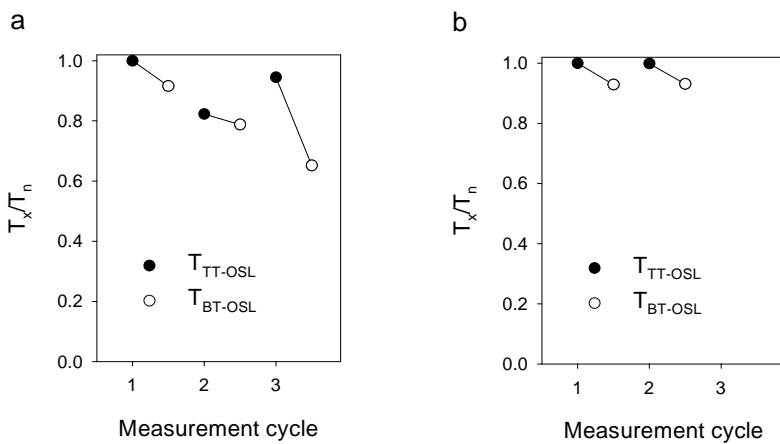
Fig. 6-11. Sensitivity (T_x/T_n) for T_{TT-OSL} and T_{BT-OSL} for two aliquots of E55S20IV-4 measured to determine the D_e using the SGC. (a) Short ReSAR sequence (N, 0 Gy, 400 Gy), (b) Shorter ReSAR sequence (N, 400 Gy).

the mechanism that led to the difference observed, but it appeared systematically for all aliquots in Fig. 6-8.

It is thus concluded that for testing the applicability of the SGC for D_e determination, two ReSAR cycles should be performed on each aliquot, one being for the natural and one for a 400 Gy dose. This is a more appropriate diagnostic test than the use of the other approach using three cycles (N, 0 and 400 Gy). For the same reason, the recycling ratio as was first used in this study (Table 6-2b) is likely to be a poor assessment of whether this ReSAR protocol is appropriate for each aliquot.

6-8. Testing the SGC for ReOSL

In the sequences described above, the sensitivity-corrected ReOSL for the natural dose was the first measurement made; both for the eight discs analysed using the short sequence, and the three aliquots analysed using the shorter sequence (no zero dose measurement). Values of D_e can be obtained for these eleven discs based solely upon this value of ReOSL for the natural dose using the SGC curve shown in Fig. 6-7b. For each sample, it is now possible to compare the two ReSAR D_e values obtained using the full dose response curve with the eleven D_e values obtained from the SGC given in Fig. 6-7b (only nine D_e values were available for E55S20IV-9). This comparison is shown in Fig. 6-12, where it is seen that there is excellent correspondence between the D_e values obtained using both methods up to 1.1 kGy. This confirms our proposal that it is possible to use a SGC for ReOSL, in the same way that it was used for OSL D_e determination. The measurements necessary to calculate a D_e using the SGC approach took 4 hours per aliquot for these samples compared with 24 hours per aliquot for a complete dose response

116
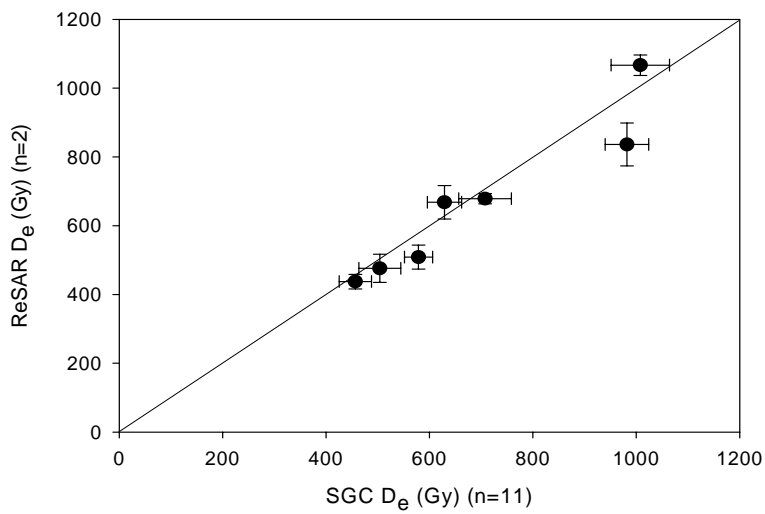
Fig. 6-12. Mean of two D_e values obtained for each of seven samples using the ReSAR procedure with 10 dose points, plotted as a function of the mean of eleven D_e values obtained for these seven samples using the natural ReOSL measurements and the SGC.

curve (e.g. Fig. 6-2).

6-9. Comparison of ReOSL and OSL dose response curves

Having established that it is possible to use a SGC for ReOSL measurements to obtain reproducible values of D_e giving doses up to 1.1 kGy, it is interesting to compare the ReOSL data with that obtained using OSL measurements. Dose response curves obtained using the SAR procedure for one aliquot from two samples (E55S20IV-5 and E55S20IV-9) are shown in Figs. 6-13a and 13b, respectively. The SAR protocol used a preheat of 260°C for 10 s and a cut-heat of 160°C (Murray and Wintle, 2000). Both OSL dose response curves (Figs. 6-13a and 13b) are best fitted by a function which is the combination of a linear and a saturating exponential function. D_e values of 650±24 Gy and 705±29 Gy were obtained for these aliquots of E55S20IV-5 and E55S20IV-9, respectively. These values are obtained in a dose range where the exponential component is saturated. For these two aliquots, the characteristic values of D_0 obtained when fitting the saturating exponential component ($1\text{-}exp^{-D/D0}$) were 95±5 Gy and 101±6 Gy, respectively. These values are very similar to the values summarised by Wintle and Murray (2006).

This type of behaviour is not uncommon in sedimentary quartz and apparently appropriate OSL ages are obtained from D_e values obtained in this way (e.g. Pawley et al., 2008). However, it should be pointed out that when the fast component was isolated, either using LM-OSL measurements (Singarayer and Bailey, 2003) or from pseudo-LM-OSL curves (Singarayer and Bailey, 2004), the dose response curve could be represented by only a single saturating exponential function. It is for this signal that the SAR protocol was developed and tested

(Wintle and Murray, 2006). Murray and Funder (2003) obtained an OSL dose response curve that could be fitted by a single saturating exponential function for their known age (130 ka) sands from the Danish coast, but they obtained an age underestimation of ~10%. Murray et al. (2007) investigated another sandy deposit of the same age taken from the Sula River in northern Russia. The dose response curve was best fitted by a function that was the sum of two saturating exponential components. Using the D_e values (ranging from 87 to 180 Gy), obtained for the parts of the dose response curve where one of the components was saturated, resulted in a ~14% age underestimation. In an investigation of older samples (ages ~ 200 ka) from the Seyda River in northern Russia, Murray et al. (2008) fitted their OSL data with the sum of an exponential and a linear component. The D_e values for these samples were obtained further up the linear part of the dose response curve (~ 400 Gy). The OSL ages obtained were in agreement with independent age control provided by stratigraphic information and uranium-series ages on peat, thus implying that the SAR protocol is appropriate for the linear portion of the OSL dose response curve.

In Figs. 6-13c and 13d, typical dose response curves are shown for the ReOSL measurements made on separate aliquots of the same two samples as shown in Figs. 6-13a and b. As in Fig. 6-2, the ReOSL responses are effectively linear for doses from about 50 Gy up to at least 1.6 kGy, and D_e values of 634±15 Gy and 1045±26 Gy were obtained for the aliquots shown in Figs. 6-13c and d, respectively. Thus, the values obtained for E55S20IV-5 are quite similar for both OSL and ReOSL (650±24 Gy and 634±15 Gy), whereas those for E55S20IV-9 (705±29 Gy and 1045±26 Gy) are substantially different. This implies that some D_e values obtained using the OSL signal where the dose response curve is in the linear portion of the dose response curve are reliable (e.g. Figs. 6-13a, c), as implied by Murray et al.

(2008), but that others which appear to be on the same part of the dose response curve are not (e.g. Figs. 6-13 b, d). From the OSL data alone there appears to be no indication whether the D_e value is accurate or not.

The ability to recover a dose with both the OSL and ReOSL signals was tested by means of a dose recovery test. Since no modern analogue sample was available, the dose to be recovered was given to aliquots that had been bleached in the laboratory, by the blue light source in the case of the OSL measurements and using the SOL2 solar simulator in the case of the ReOSL measurements. For the OSL dose recovery experiment, two blue light stimulations were carried out for 1,000 s at room temperature (RT), separated by a storage time of 10,000 s at RT. The SOL2 bleaching was for 7 days so that the TT-OSL signal reached a low level, as shown in Fig. 6-6. The temperature of the sample during bleaching did not get above 50°C. Several different doses were given, ranging from 0 Gy to 1.0 kGy. The short protocol was used to obtain the D_e, i.e. measuring the ReOSL and then applying this to the SGC in Fig. 6-7. Fig. 6-14a shows the doses recovered using OSL measurements and the SAR protocol for samples E55S20IV-5 and E55S20IV-9 as a function of the known dose given after bleaching. The doses obtained using OSL show a systematic underestimation of ~ 10% for doses above 600 Gy where the OSL signal is in the linear portion of the response. The behaviour of the ReOSL dose recovery data is more complex (Fig. 6-14b). As shown in Fig. 6-6, after one week in the SOL2 the ReOSL signal does not reach zero, and the dose measured for the two samples was 48±3 Gy (E55S20IV-2) and 50±7 Gy (E55S20IV-5). Assuming that the given doses are added on to this unbleached dose, the diagonal line shown on Fig. 6-14b indicates the doses that would be expected to be recovered. Data for E55S20IV-2 and -5 lie close to this line, demonstrating that the dose can be recovered accurately.
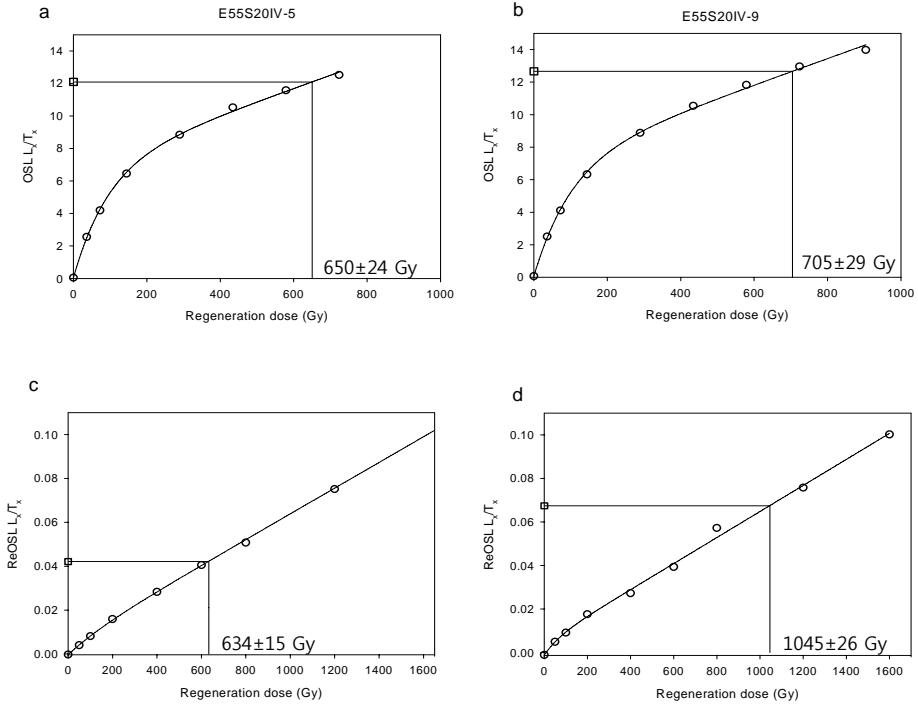
Fig. 6-13. (a and b) OSL dose response curves for representative aliquots of samples E55S20IV-5 and E55S20IV-9; (c and d) ReOSL dose response curves for representative aliquots of the same two samples. The same preheat temperature of 260°C was used for all measurements. For each aliquot one regeneration dose (~50 Gy for the OSL data, and ~200 Gy for the ReOSL data) was repeated to assess recycling, and this data point is shown by a triangle on each figure.
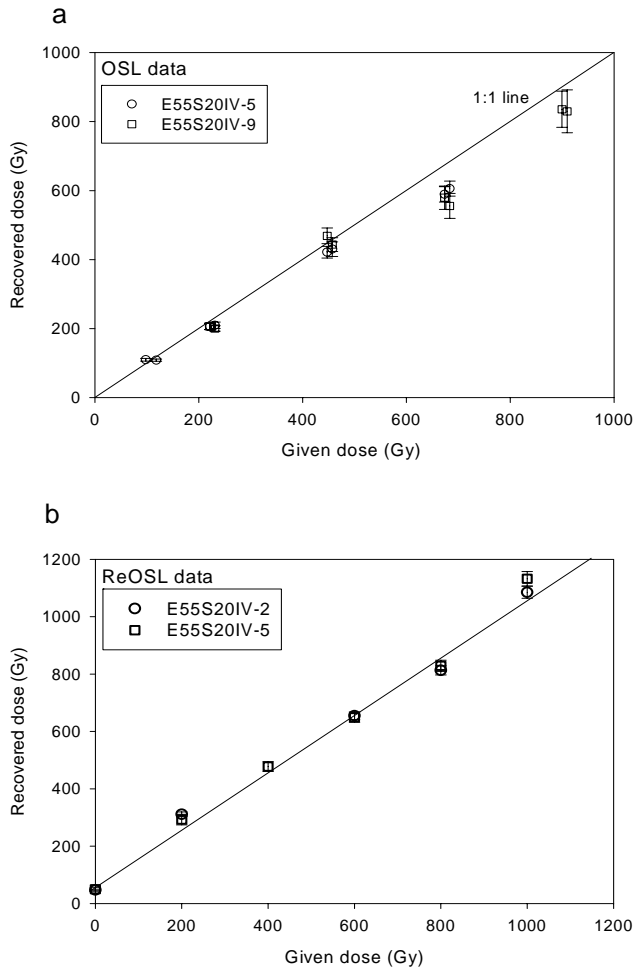
Fig. 6-14. Dose recovery data for OSL and ReOSL over a range of given doses, each for a different aliquot. (a) OSL obtained using the SAR protocol showing the 1:1 line. (b) ReOSL using the SGC in Fig. 6-7b. The line shown is for a one to one relationship offset by 50 Gy, based on the D_e determined for the two aliquots not given any dose.

D_e values were obtained using the SAR protocol for the OSL (as exemplified in Figs. 6-13a and 13b) for nine aliquots on each of the seven samples. D_e values were obtained using the ReSAR protocol of Table 6-1 for the ReOSL (as exemplified in Figs. 6-13c and 13d) for two aliquots of each of the seven samples. In addition, the SGC approach was used to determine a further eleven D_e values for each sample, giving a total of 13 D_e values based upon ReOSL. No correction has been made for any residual signal that may have remained at deposition. Although doses of 48±3 Gy and 50±7 Gy were measured after bleaching in the SOL2 for 7 days, it is not clear whether this value would be obtained from a recently deposited sample. No modern analogue is available for these samples. However, Tsukamoto et al. (2008) showed that, for Chinese loess, a laboratory bleaching exercise using the identical SOL2 for 7 days gave a residual of 52.2±2.6 Gy, but a modern analogue yielded a dose of 15.9±2.3 Gy. Wang et al. (2006b) had measured a value of 10.0±2.1 Gy from the same modern analogue using ReOSL. It is not clear whether the SOL2 is reproducing the effects of sunlight in the natural environment in bleaching the traps responsible for ReOSL. The OSL and ReOSL D_e values are shown in Fig. 6-15, where it can be seen that there is good agreement for the values obtained in the range from 400 Gy to ~650 Gy, but that for larger doses OSL underestimates the D_e when compared with ReOSL.

6-10. Conclusions

The fine-grained quartz from this suite of samples from Jeongokri (E55S20IV pit) exhibited TT-OSL characteristics that are very similar to those previously described for Chinese loess (Wang et al., 2006 a, b; Tsukamoto et al., 2008). Replicate measurements of the TT-OSL signal showed the same pattern of depletion (Fig 6-

3a) and annealing at 300°C reduced the TT-OSL to a similar level (Fig. 6-3b). However, the BT-OSL signal that remained following this annealing at 300°C was dose-dependent, and yielded D_e values that were similar to those derived from the ReOSL signal (Fig. 6-2, Table 6-2a). Increasing the annealing temperature decreased the magnitude of the BT-OSL signal, but was unable to isolate a dose-independent signal (Fig. 6-4). We conclude that the electrons giving rise to the dose-dependent BT-OSL signal are derived from the same traps as those providing electrons for the ReOSL as calculated in this study. The magnitude of the dose-independent BT-OSL signal was estimated using a variety of approaches, and these suggested that it is much smaller than that measured following annealing at 300°C (Fig. 6-3b). Further work is required to refine methods for accurately assessing the BT-OSL so that a more appropriate value can be used in the calculation of ReOSL.

Sensitivity was monitored using OSL and the pattern of change observed during the ReOSL measurements used to construct the dose response curve is complex (Fig. 6-10c). Sensitivity was consistently lower during measurements of BT-OSL than TT-OSL within a cycle. Fig. 6-9 showed that the sensitivity correction is appropriate, but recycling ratios exceeding 1.2 were commonly observed when remeasuring the signal from a 200 Gy dose (e.g. Table 6-2b). In spite of the very different recycling ratios for the TT-OSL, ReOSL and BT-OSL signals when using the 200 Gy dose, the values of D_e obtained using all three signals were consistent (Table 6-2a), suggesting that the recycling ratio is a poor indicator of the quality of the data.

Comparison of the ReSAR dose response curves for the seven samples measured in this study revealed very similar patterns of growth (Fig. 6-7a) and this made it possible to define a standardised growth curve (SGC) for the ReOSL signal (Fig. 6-7b). This allowed rapid measurement of D_e values for further aliquots,
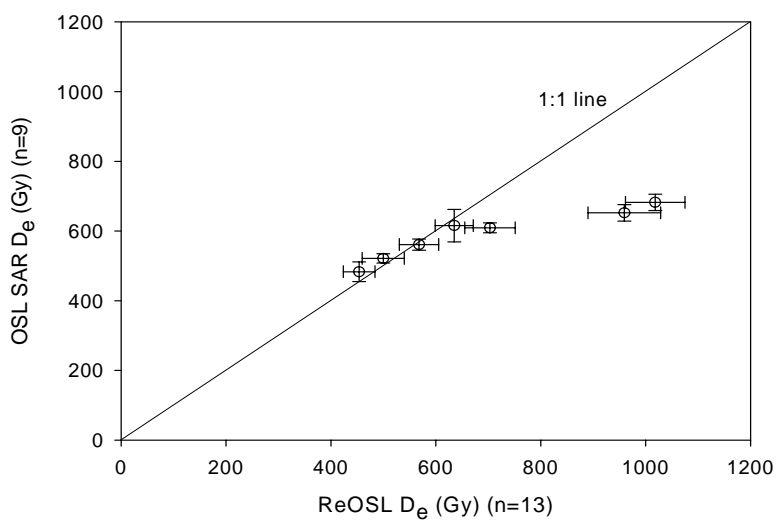
Fig. 6-15. For the seven samples D_e values obtained using SAR OSL as a function of D_e obtained using two full ReSAR analyses and eleven D_e values obtained using the SGC in Fig. 6-7b.

requiring only the natural signals to be measured.

For these seven samples from Korea, a comparison of the D_e values obtained using both ReOSL and OSL (Fig. 6-15) showed that for values between 400 Gy (the lowest D_e value for this suite of samples) and 650 Gy the two signals yielded consistent results. For doses exceeding ~650 Gy, the ReOSL D_e values became progressively larger than those for OSL. The dose at which OSL D_e values became inaccurate is difficult to define. Comparison of the two OSL dose response curves in Fig. 6-13 showed very little difference, yet one gives D_e values consistent with the ReOSL whilst the other underestimated the D_e by 50%. This raises a significant concern over whether OSL D_e values that are reliant upon growth of the linear component beyond the saturating exponential signal are accurate.

CHAPTER 7. Re-evaluation of the chronology of the palaeolithic site at Jeongokri, Korea, using OSL and TT-OSL signals from quartz

Abstract

Seven samples were collected from sediments at the Palaeolithic site of Jeongokri, Korea, known for the first discovery of Acheulian-like handaxes in East Asia. Optically stimulated luminescence (OSL) ages obtained from chemically purified quartz from the upper five samples are in stratigraphic order, but the ages of the lower samples are not. The OSL signal of the oldest samples occurs well above the saturation level of the exponential part of the dose response curve; however, the OSL signal has an additional component that grows linearly at high doses, making it possible to calculate a D_e value and thus an age. However the reliability of calculating D_e using this linear component is not clear. In contrast, the thermally transferred OSL (TT-OSL) signal grows linearly with dose up to at least 1600 Gy, thus permitting its use for dating. The TT-OSL ages are in agreement with those from the OSL for the four uppermost samples, but give older ages for the lower three samples. Ages obtained using TT-OSL are in stratigraphic order and indicate that the oldest artefacts have an age of ~195 ka.

7-1. Introduction

In this study, we have dated fine-grained sediments (E55S20IV) containing archaeological remains from Jeongokri using luminescence measurements on 4-11 μm quartz. The optically stimulated luminescence (OSL) signal from quartz has been widely applied to dating sediments, but saturation of the OSL signal limits the age range that can be measured. Recently, a thermally transferred optically

stimulated luminescence (TT-OSL) signal has been investigated for extending the age range. Wang et al. (2006a and b) have investigated a TT-OSL signal for quartz from Chinese loess and they separated the recuperated OSL (ReOSL) from the basic transferred OSL (BT-OSL). They were able to date Chinese loess up to 780 ka using the ReOSL signal. Also, good agreement was observed between the ReOSL ages and OSL ages for Chinese loess from 15 to 130 ka. In this study, we measured both OSL and TT-OSL signals to determine the age of the sediments at Jeongokri, and compared OSL with TT-OSL ages.

7-2. Previous geochronological studies

At the main excavation site at Jeongokri, the thickest sedimentary sequence is found at an excavation unit of E55S20IV, where ~7 m of unconsolidated fine-grained sediments overlie the Jeongok Basalt (Fig. 7-1). The majority of these sediments are silt and clay. Shin et al. (2004) interpreted the upper 4 m of sediment as a loess-palaeosol sequence although poorly supported, and the lower 3 m as fluvial or lacustrine sediments. Glass shards have been reported from two horizons, 10-45 cm and 100-110 cm below the surface and identified as AT and K-Tz tephra (Yi et al., 1998; Danhara et al., 2002), with ages of 25.1 ± 0.3 C^{14} ka BP (Miyairi et al., 2004) and 90-95 ka, respectively (Machida and Arai, 1992; Machida, 1999). However, only two shards of the K-Tz tephra were recovered (Danhara et al., 2002) making it difficult to be confident in the identification of the tephra, and thus we have not used its age to compare with the results obtained in this study.

7-2-1. Previous luminescence measurements

OSL and isothermal TL (ITL) methods have been applied to directly date

sediments from site E55S20IV and the results were reported by Shin et al. (2004) and Choi et al. (2006). Four samples from the upper 3 m of the section were measured, but none bracketed the archaeological horizon. Limited technical details are available about the OSL, but Choi et al. (2006) reported that the samples were close to saturation and relied upon a linear component that grew at higher doses. This is consistent with measurements undertaken on samples in this study, but work by Kim et al. (2009a) has shown that D_e values relying upon this linear component in the OSL may yield age underestimates. This has also been observed by other authors (e.g. Murray and Funder, 2003; Murray et al., 2007) and it has been recommended by Wintle (2008) that D_e values should not be calculated if they are greater than twice the value of D0, the dose characterising the rate of increase of signal within the saturating exponential (Wintle and Murray, 2006). ITL measurements at 310°C were made on the same samples, and these gave ages that were in stratigraphic order (Choi et al., 2006). However, it has been reported that ITL procedures may give incorrect results (e.g. Buylaert et al., 2006) due to the inability to assess the extent of sensitivity changes during the course of the first ITL measurement. Due to the difficulties in evaluating the reliability of both OSL and ITL ages presented previously on samples from this site, TT-OSL ages have been obtained in this study to provide a revised luminescence chronology.

7-3. Sample preparation and dosimetry

In this study, a 6m long core was collected adjacent to pit E55S20IV. From this core, as described in Chapter 7, seven samples were collected from the upper 5 m of unconsolidated fine grained sediments (laboratory number E55S20IV, samples 2-7 and 9; Fig. 7-1). The uppermost five samples (2-6) are clayey silts, and

correspond to the loess/palaeosol units of Shin et al. (2004). Samples 7 and 9 are sandy silts of fluvio-lacustrine origin (Shin et al., 2004). At this particular excavation unit, the archaeological horizon is composed of stratigraphic units VI to XI (Fig. 7-1), with the oldest and the highest concentration of archaeological materials being found in the uppermost part of unit XI. Sample E55S20IV-4 would provide a younger age limit for the archaeological materials and sample E55S20IV-7 an older age limit.

The detailed preparation of samples is introduced in CHAPTER 7. Kim et al. (2009b) demonstrates that chemical separation of quartz is essential to obtain accurate D_e values, and that even after optimising the length of the IR exposure, [post-IR] OSL measurements still underestimate the D_e due to a contribution from feldspars. All the measurements reported here were undertaken on this chemically purified quartz.

No in situ dosimetry was carried out as the samples were taken from a core. Instead, the radionuclide concentrations of the sediment were measured using low-level high resolution gamma spectrometry at the Korea Basic Science Institute (KBSI). Conversion to dose rates used the data presented by Olley et al. (1996) and the water content was estimated from measurements of the water content when collected and the saturation water content (Table 7-1). Detail illustration of the dosimetry calculation is in Appendix.

7-4. Results

7-4-1. Quartz OSL

A typical dose response curve derived using the single aliquot regenerative dose (SAR) procedure applied to chemically-purified quartz grains of 4-11 µm
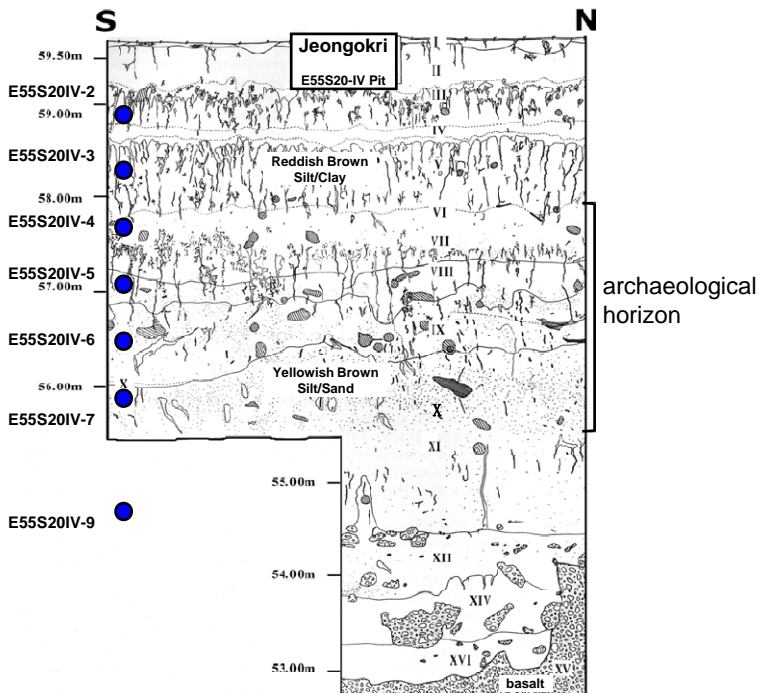
Fig. 7-1. (a) The location of Jeongokri, (b) a schematic geological section illustrating the major units discussed in the text (from Bae, 1989), and (c) the position of the archaeological area relative to the Hantan river.

diameter is shown in Fig. 7-2a. This was constructed using the initial signal from OSL measurements following a preheat of 220°C for 10 s after the main dose and a cut-heat of 160°C after the test dose (14 Gy). Measurements using preheats at 200, 220 and 240°C yielded consistent D_e values. The sensitivity-corrected OSL data for nine aliquots of this sample are shown in Fig 7-2a, demonstrating the excellent reproducibility of the OSL data. The dose response is typical of all seven samples from E55S20IV and is best fitted with a combination of an exponential component that has a D0 value of ~ 100 Gy (Kim et al., 2009a) and a linear component. The luminescence characteristics of the material are suitable for SAR as all the aliquots have recycling ratios within 3% of unity, IR-OSL depletion ratios consistent with unity (Duller, 2003), and recuperation of signal that is less than 3% of the natural signal.

The OSL D_e values increase with depth from 483±9 Gy for the uppermost sample to a value of 682±8 Gy for the lowermost (Table 7-1). OSL ages calculated from D_e values for the five uppermost samples are in stratigraphic order; however, because the dose rates at the base of the section are greater than for the overlying sediment (Table 7-1), the OSL ages calculated for the two lowest samples are younger than the ages for the overlying sediment (Fig. 7-3). Since D0 for these samples is ~100 Gy and all of the D_e values are well over 200 Gy, the ages may be suspect (c.f. Wintle, 2008).

7-4-2. Quartz TT-OSL

Thermally transferred OSL (TT-OSL) is a signal that has a much higher value of D0 than the fast component of the OSL signal from quartz (Wang et al., 2006a). The TT-OSL protocol proposed by Tsukamoto et al. (2008, Table 2-C), similar to that of Wang et al. (2007), has been applied to the same seven samples. Aliquots of

prepared quartz were first preheated at 260°C for 10 s and then the same preheat was used to generate the TT-OSL. The dose response curve obtained using the sensitivity-corrected ReOSL signal is shown in Fig. 7-2b. The dose response curves show linear growth with dose up to at least 1600 Gy and a similar degree of reproducibility was observed as for the OSL signal. This behaviour permitted the development of a standardized growth curve (SGC; Roberts and Duller, 2004) for the TT-OSL method (Kim et al., 2009a). Two aliquots of each sample were used to obtain their SAR dose response in the range from zero to between 1600 and 2500 Gy, and the data from these aliquots combined to generate an SGC (Kim et al., 2009b). For each sample an additional 9 aliquots had just their natural ReOSL signal measured and D_e was interpolated using the SGC. This gave a total of 11 D_e values for each sample and the average of these values are given in Table 7-1. D_e values obtained using TT-OSL are similar to those from OSL for the four uppermost samples (Table 7-1), giving similar ages to those obtained using OSL (Fig. 7-3). For the three lowermost samples, the TT-OSL D_e values are significantly higher than those from OSL, and progressively increase down section, up to 1018±17 Gy. Unlike the OSL results, the ages derived from the TT-OSL D_e values are in stratigraphic order, though the ages of the three lowermost samples are indistinguishable within the quoted uncertainties.

7-5. Discussion

The OSL characteristics of the quartz from Jeongokri are well suited for application of the SAR protocol, and the material is extremely reproducible. However, the D_e values for these samples are beyond the limit suggested by Wintle (2008) for reliable application of the method. It is only possible to obtain D_e values

Lab. No	Depth (m)	Water Content (%) †	Alpha dose (Gy/ka)*‡	Beta dose (Gy/ka) ‡	Gamma dose (Gy/ka) ‡	Cosmic dose (Gy/ka) ‡	Dose rate (Gy/ka)	D_e (Gy)		Age (ka)	
								OSL	TT-OSL	OSL	TT-OSL
E55S20IV-2	0.9	21±5	0.49±0.25	1.78±0.12	1.23±0.07	0.19±0.01	3.695±0.284	483±9	454±8	131±10	123±9
E55S20IV-3	1.5	21±5	0.51±0.26	1.96±0.13	1.31±0.08	0.17±0.01	3.954±0.297	522±4	500±11	132±10	126±10
E55S20IV-4	2.1	20±5	0.55±0.28	2.04±0.13	1.39±0.08	0.16±0.01	4.148±0.318	561±5	568±10	135±11	137±11
E55S20IV-5	2.7	22±5	0.55±0.28	1.96±0.12	1.34±0.08	0.15±0.01	4.002±0.312	616±16	635±10	154±13	159±12
E55S20IV-6	3.3	25±5	0.56±0.28	1.83±0.11	1.35±0.08	0.14±0.01	3.870±0.312	609±5	703±13	157±13	182±15
E55S20IV-7	3.9	26±5	0.71±0.36	2.27±0.14	1.70±0.10	0.13±0.01	4.803±0.394	652±8	959±19	136±11	200±16
E55S20IV-9	5.1	35±5	0.86±0.44	2.42±0.14	1.98±0.10	0.11±0.01	5.369±0.467	682±8	1018±17	127±11	190±17

† The water content is expressed as the weight of water divided by the weight of dry sediment.

* Alpha dose rate was calculated using an a-value of 0.04 ± 0.02 (Rees-Jones 1995).

‡ Alpha, beta, gamma and cosmic dose rates are rounded to two decimal places, but calculation of the total dose rate was carried out prior to rounding.

Table 7-1. Dose rate information, equivalent dose values and ages for sediments from Jeongokri using OSL and TT-OSL.

for these samples by using the part of the dose response curve that is based upon the growth of a linear component. Previous work using this linear growth has been equivocal, with some studies obtaining apparently reliable ages (e.g. Murray et al., 2008), while others underestimate the age (e.g. Murray and Funder, 2003; Murray et al., 2007).

The TT-OSL signal from the same quartz is also very reproducible and, using the protocol of Tsukamoto et al. (2008), Kim et al. (2009a) have shown that given laboratory doses up to 1000 Gy can be recovered. D_e values and ages obtained using the TT-OSL are in agreement with those from OSL for the youngest samples, but for the three oldest samples ages based on TT-OSL become progressively larger than those based on OSL. The TT-OSL ages are thought to be more accurate than the OSL because they are not affected by signal saturation in this age range, and because they are in stratigraphic order, unlike the OSL. One disadvantage of TT-OSL compared with OSL is the speed with which the signal is removed by exposure to daylight at deposition. The OSL signal from quartz is reduced to a negligible level within minutes of exposure to daylight, but Tsukamoto et al. (2008) have shown that the equivalent reduction in the TT-OSL will take many tens of hours. The agreement of the OSL and TT-OSL ages in the upper part of the section supports the supposition that both signals were adequately reset at deposition. At the base of the section the TT-OSL ages are greater than the OSL. It is conceivable that these TT-OSL ages may overestimate the true age if the TT-OSL signal was not sufficiently zeroed at deposition. Since the sediments are fine-grained, it is difficult to test such a possibility, but any overestimation of age must be limited since the sediments cannot be younger than 157±13 ka, the oldest age obtained using OSL. The excellent stratigraphic consistency in the TT-OSL, and recent reports that the TT-OSL signal in natural environments can be reduced to very low levels (e.g.
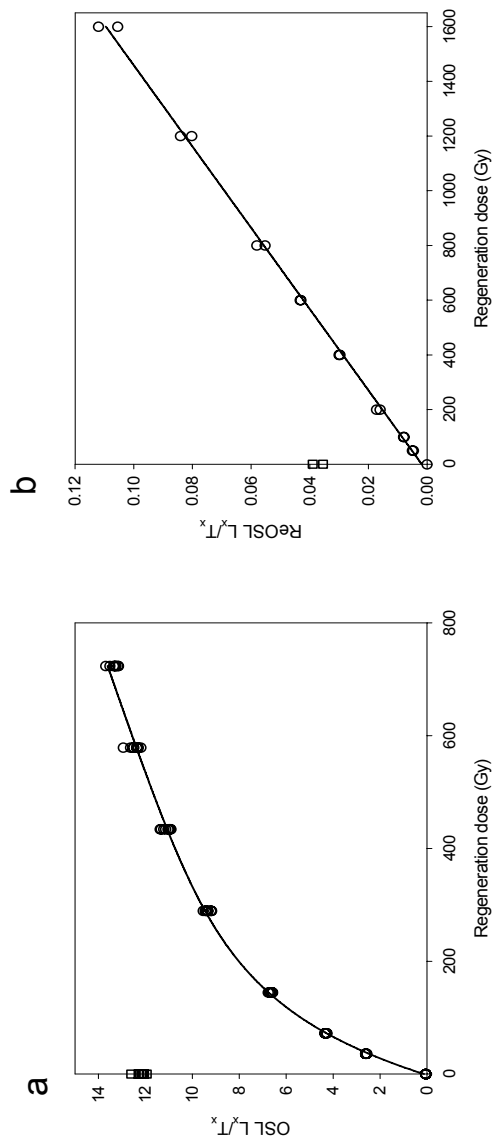
Fig. 7-2. Stratigraphy of excavation pit E55S20IV showing the units as defined by Bae et al. (2001). The sample interval for the core used in this study is 60 cm for the six uppermost samples (E55S20IV-2-7) with 120 cm between samples E55S20IV-7 and -9.
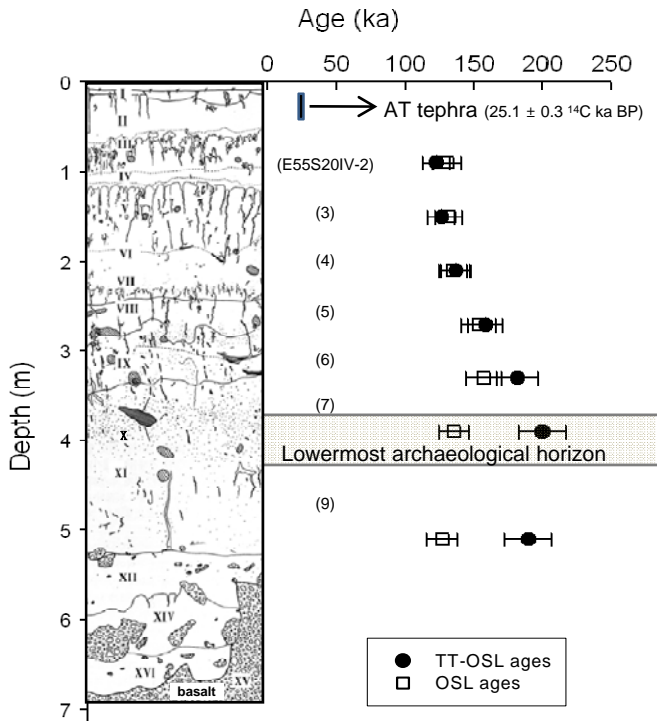
Fig. 7-3. SAR dose response curves for sample E55S20IV-4 using (a) the OSL signals measured from nine different aliquots and (b) the TT-OSL signals from a typical aliquot of the same sample. Preheat temperatures were either 200, 220 or 240°C for 10 s for OSL, and 260°C for 10 s for TT-OSL.

Porat et al., 2009), lead us to conclude that the TT-OSL ages are not affected by incomplete bleaching. The TT-OSL ages (Fig. 7-3) show that the 5 uppermost samples record their formation from 182±15 ka to 123±9 ka, broadly corresponding to oxygen isotope stage (OIS) 6. The TT-OSL ages are in stratigraphic order and suggest a complete record of sedimentation for stratigraphic units IX to III. However, the presence of the AT tephra (25.1 ± 0.3 14C ka BP) at a depth of 10-45 cm (Yi et al., 1998) suggests that limited sediment record is preserved during the last glacial/interglacial cycle. The lower two samples in the fluvial (or lacustrine) sediments (E55S20IV-7 and -9) give very similar ages, with a weighted mean value of 195±12 ka, and provide an upper limit for the age of the archaeological material. The lower limit provided by sample E55S20IV-4 is 137±11 ka, as given by the TT-OSL age (Table 7-1). Thus, at this particular pit, artifacts appear to have been deposited for about 60,000 years. The TT-OSL ages constrain the age of the sediments in which the earliest artefacts are found to between 182±15 ka and 195±12 ka.

7-6. Conclusions

In this study, OSL ages for sediments from the Jeongokri Paleolithic site, Korea are stratigraphically consistent up to 150 ka. However, for older samples, the OSL ages are not in stratigraphic order. In contrast, ages based on measurements of TT-OSL are in stratigraphic order throughout the sequence. Re-evaluation of the age of the Jeongokri archaeological site in this study shows that the ages of the unconsolidated sediments above the Jeongok Basalt range from 200±16 ka to 123±9 ka. The earliest hominin occupation, found at a depth of 4 m below the ground surface, is constrained by ages between 182±15 ka and 195±12 ka.

CHAPTER 8. Geochemical characteristics of Jeongokri sediment as indicators of provenance

8-1. Introduction

East Asia during the Quaternary has been affected by monsoonal activity. The East Asian Monsoon transports eolian dust from dry areas of the north-western Asia to East Asia by winter monsoon blown. Chinese Loess Plateau has been made from East Asian monsoon effect, which contains the longest documented, nearly continuous record of terrestrial sequence for the past 2.5 Myr and beyond (Liu et al., 1985; Kukla et al., 1988; Kukla and An, 1989; Rutter et al., 1990; Liu and Ding, 1998). Chinese Loess Plateau is composed of the repeated loess-paleosol sequences, corresponding to the glacial and the interglacial periods. Therefore, Loess-paleosol sequences are thought to be a direct monitor of the East Asian monsoon system (Liu et al., 1985; An, 2000).

The monsoonal activity had an influence on paleoenvironments of the Korean Peninsula during the Quaternary Period. Loess-paleosol sequences are expected to be distributed in Korea, because the Korean Peninsula is located in the path of monsoonal wind. Many previous studies suggested that red-yellow soils in the western areas of Korea were loess deposits and were supplied mostly from the Chinese loess terrain and deserts in northwest China (Park, 1987; Lee and Yi, 2002; Naruse et al., 2003; Shin et al., 2004; Park et al., 2007; Yoon et al., 2007; Yu et al., 2008). Based on this premise, many studies tried to correlate the stratigraphy of Quaternary sediment of Korea with that of the loess-paleosol sequence of the Chinese Loess Plateau. However, most terrestrial records in Korea are relatively short (less than 8m) and/or discontinuous. Although geological and chronological

approaches have been tried to identify sediment provenance of Quaternary sequence in the Korean Peninsula, the published results are not enough for understanding them. For these reasons, more detailed provenance study is essential for stratigraphic correlation between the Korean Quaternary sequence and Chinese Loess Plateau.

The study area is Jeongokri site, which is one of the most well-known archaeological sites and one of the areas having the thickest Quaternary sequence in the Korean Peninsula. Although many studies have been done to estimate age of the Jeongokri site, the chronological framework is still under debate. Kim et al. (2009c) re-evaluated the chronology of Jeongokri archaeological site (E55S20IV pit) using luminescence dating. Based on this age-dating result, this study aims to elucidate provenance of Jeongokri sediments by their geochemical properties such as major, trace, and rare earth elements (REEs) composition. The geochemistry of Jeongokri sediments provides evidence to understand sediment provenance because it reflects the signature of parent material. Especially, rare earth elements and trace elements compositions of Jeongokri sediments are paid more attention because of their immobile behavior. In this study, geochemical characteristics of Jeongokri sediments are compared with those of probable sources to interpret the provenance. The identification of provenance for Quaternary Jeongokri sediments may provide valuable information of Quaternary sedimentary environments of the Korean Peninsula.

8-2. Samples and analytical methods

Sixty-two samples were collected from a 7 m-long core in this pit for major, trace, and rare earth elements analysis. Samples were taken at 5 cm intervals for

140

grain-size analysis and 5-10 cm intervals for geochemical analysis. Dry sieving was used for grain-size distribution of grains larger than 63μm (sand and gravel). The fine grain sediments smaller than 63μm were determined by using Micrometrics Sedigraph 5100. Mineralogy was analyzed for forty-three samples by using a X-ray diffractometer (XRD, Panalytical expert-pro)). Major element compositions were determined by a Phillips PW2404 X-ray fluorescence spectrometer. Trace and rare earth element concentrations were determined by Inductively Coupled Plasma Mass Spectrometer (Elan 6100) and Inductively Coupled Plasma Atomic Emission Spectrometer (138 Ultrace). All major, trace, and REE elements were analyzed at the Korea Basic Science Institute.

8-3. Chronological framework

The chronological information on the studied core sediments was described in Chapter 7. OSL and TT-OSL ages for four uppermost samples are in agreement within error ranges, however, lower three samples show significantly lower OSL ages than those of TT-OSL because of saturation of luminescence traps. Accordingly, in this study, used are average ages of OSL and TT-OSL ages for the upper four samples and only TT-OSL ages for the lower three samples. Seven ages of an E55S20IV core sediments show that the four uppermost samples (E55S20IV-2, -3, -4 and -5) record their deposition from 157±12 ka to 127±9 ka. The lower three samples (E55S20IV-7, -8 and -9) yield ages between 182±15 ka and 200±16 ka (Fig. 7-3; Kim et al., 2009). The presence of the AT tephra at a depth of 10-45 cm represents 25.1 ± 0.3 14C ka BP (Yi et al., 1998; Miyairi et al., 2004).
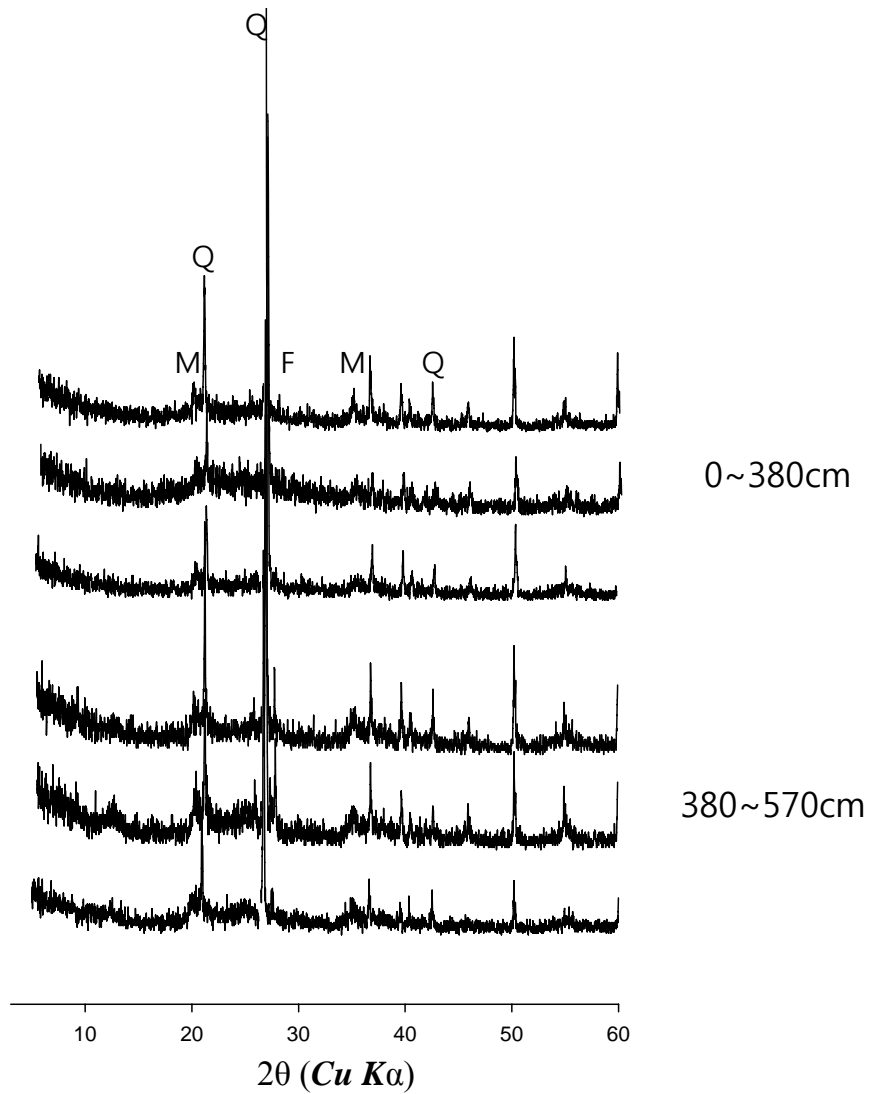
Fig. 8-1. The mineralogy of bulk sediments was obtained from X-ray diffraction analysis.
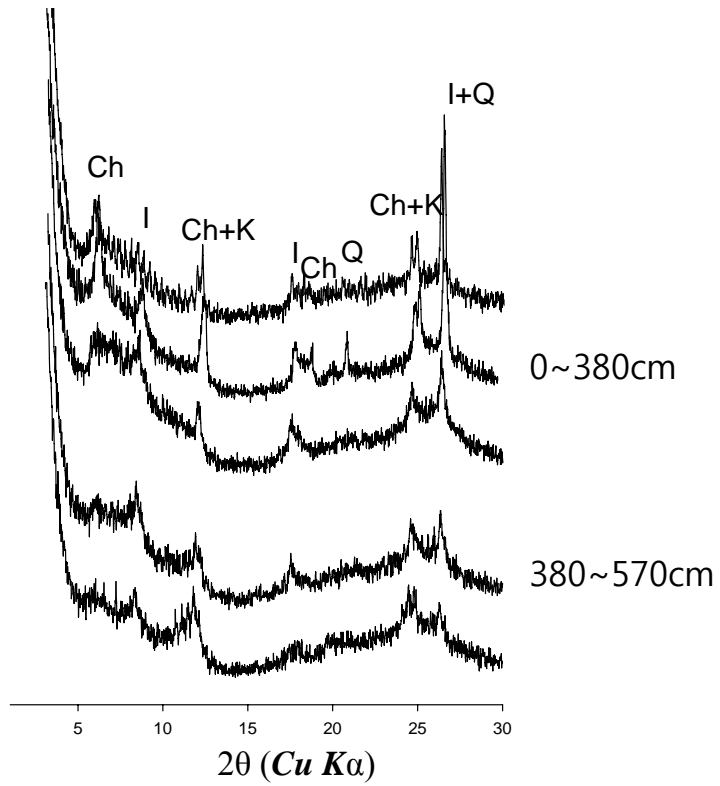
Fig. 8-2. The <2μm fraction is composed of a wide variety of clay minerals: illite, chlorite, and kaolinite

8-4. Results

8-4-1. Mineralogy

　　In the mineralogy of bulk sediments (Fig. 8-1), quartz and mica are dominant minerals in Jeongokri sediments. Feldspar is rarely observed in the upper interval (above than 380 cm depth). However, feldspar is remarkably observed in the lower interval below 380 cm. Calcite peak is not observed throughout the sequence. The <2μm fraction is composed of a wide variety of clay minerals: illite, chlorite, and kaolinite (Fig. 8-2).

8-4-2. Grain-size distribution

　　Fig. 8-3 shows that variations of clay, silt and sand contents, and mean size. Also shown are sorting and skewness. Sediment consists of 40-60 % clay, 20-40 % silt, and 0-20 % sand. Fig. 8-4 shows a classification of Jeongokri sediment. All sediments plot in clay and silty clay fields. The vertical variation of grain size distribution is mainly divided into two distinguished intervals. First, the upper-middle part of the core (~380 cm from surface) is mainly composed of silty clay and clay with less than 2 % sand. Sand-sized grains are increased up to 20 % in the lower part of the core (380~570 cm). The mean grain size of core sediments ranges from 7.3 ø to 9.2 ø and averages 8.5 ø. The upper-middle part of core sediments containing silty clay and clay has consistent mean size values (8.0-9.0 ø). However, in the lower part, sediments having high contents of sand-sized grains show low values of mean size (less than 8.0 ø). The upper-middle part of the core (~380 cm from surface) is poorly sorted (1.0-2.0 ø). The lower part of the core (380~565 cm) is very poorly sorted (2.0-4.0 ø) due to the intercalation of sand fraction. All skewness show negative values. Middle part of the core having the highest clay

144
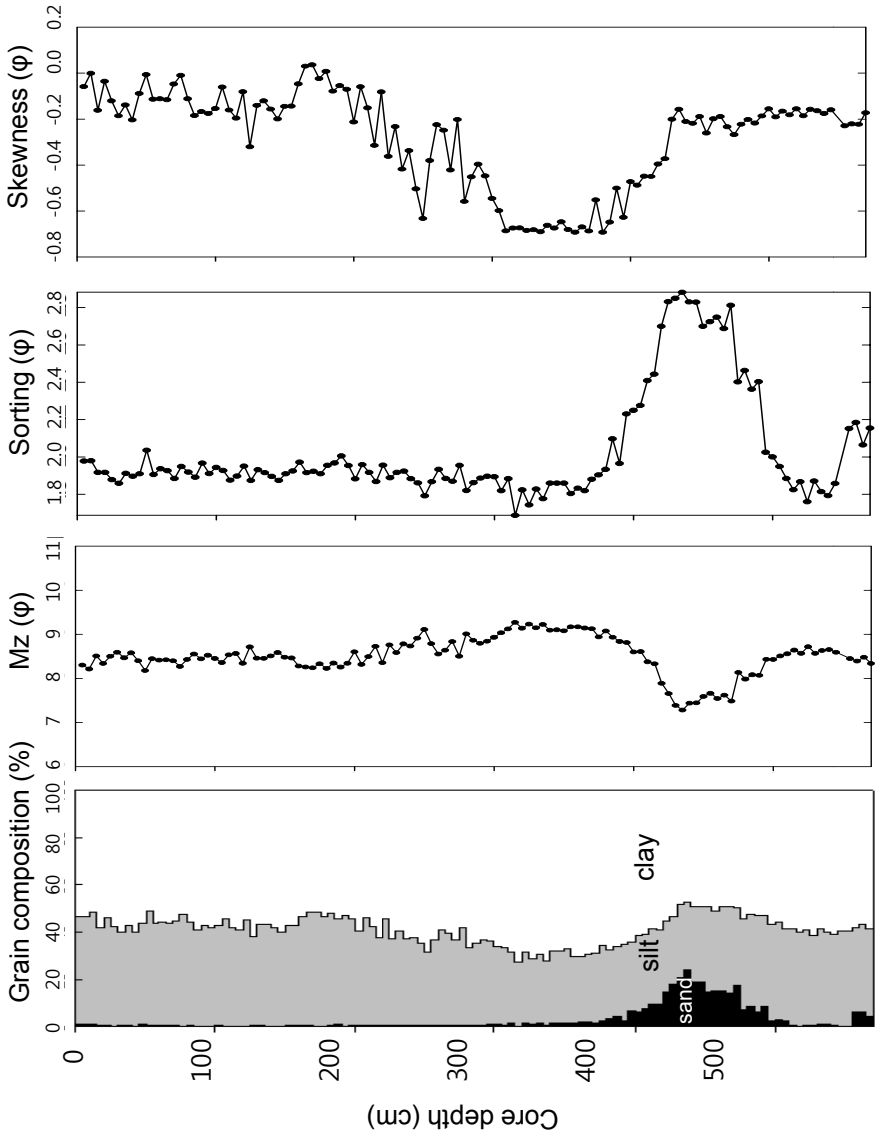
Fig. 8-3. Fig. 8-3 shows that variations of clay, silt and sand contents, and mean size. Also shown are sorting and skewness. Sediment consists of 40-60% clay, 20-40% silt, and 0-20% sand.

145
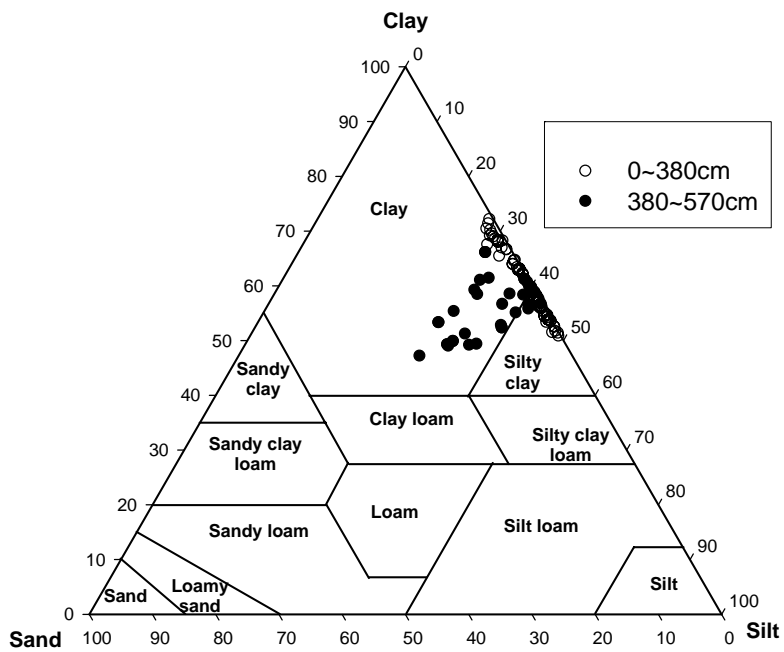
Fig. 8-4. A classification of Jeongokri sediment. All sediments plot in clay and silty clay fields.

contents shows the lowest values of skewness.

8-4-3. Major elements

Major element compositions are presented in Table 8-1. In the sequence, generally SiO_2 concentration decreases and Al_2O_3 content increases with increasing depth. Based on major element abundances, the upper part of the core (~380 cm from surface) can be distinguished from the lower part (380~570 cm) by higher contents of TiO_2, SiO_2, Na_2O and MgO. On the other hand, the lower part is relatively enriched in Al_2O_3 and K_2O. Overall, CaO shows a negligible content less than 0.4 wt% (Fig. 8-5).

8-4-4. Trace and Rare Earth elements

Concentrations of trace elements of Jeongokri sediments are shown in Table 8-2. Fig. 8-6 shows variations of Ba, Cr, Sc, Sr, Zn, Zr, and V contents (ppm). Ba, Cr, Zn and Zr concentrations are fluctuated below depth of 280 cm from surface. Zr and Ba concentrations increase downcore from 280 cm, and decrease from 500 cm. On the other hand, V concentrations gently decrease downcore from 280cm, and show negligibly low values to the bottom part.

Th/Yb, La/Th and Th/Sc ratios are also fluctuated in the lower part of the core (380-570cm) (Fig. 8-7). In this study, the average Th/Yb, La/Th and Th/Sc ratios in the upper part of the core (~380cm) are 5.96, 2.72 and 1.01, respectively. The average Th/Yb, La/Th and Th/Sc ratios in the lower part of the core (380~570cm) are 8.48, 2.23 and 2.58, respectively.

REE distribution patterns are shown in Fig. 8-8. All REE patterns are remarkably similar in shape, with enriched LREE and depleted and flat HREE profiles. These patterns resemble to that of average UCC (upper continental crust;

148
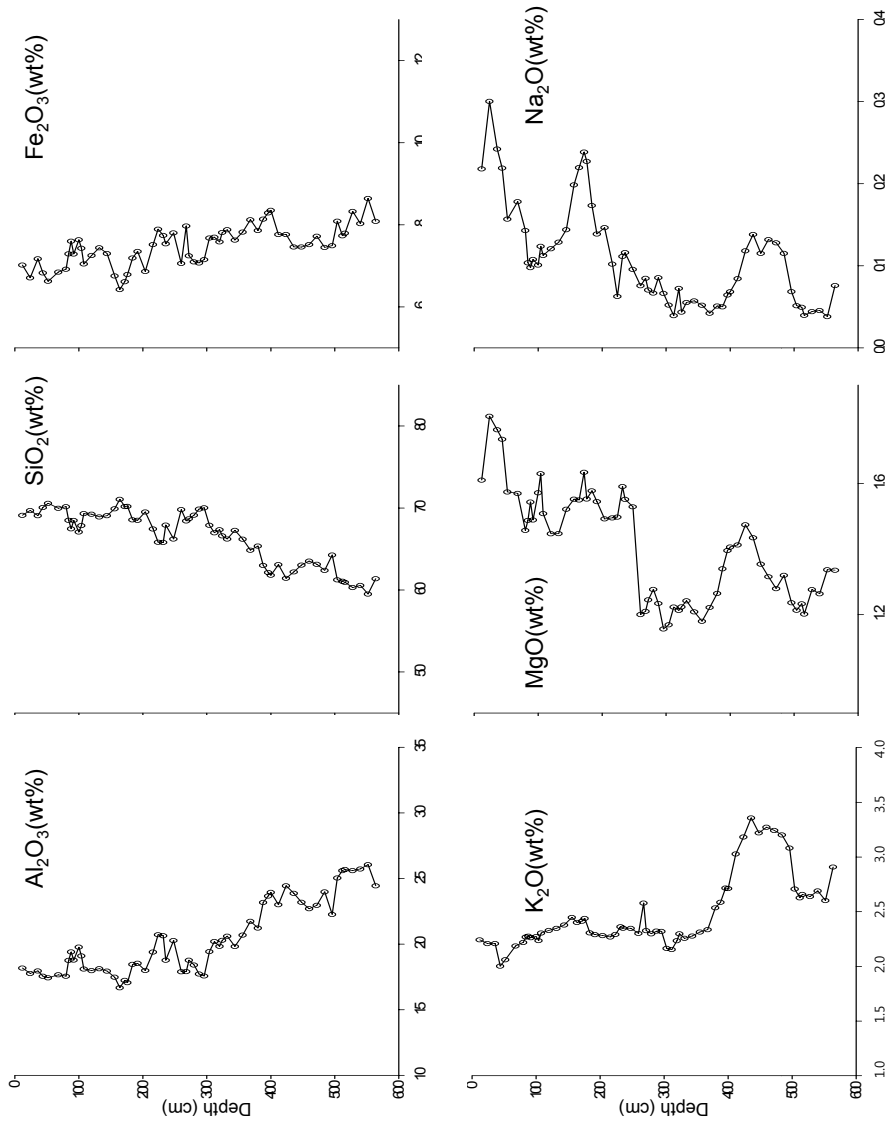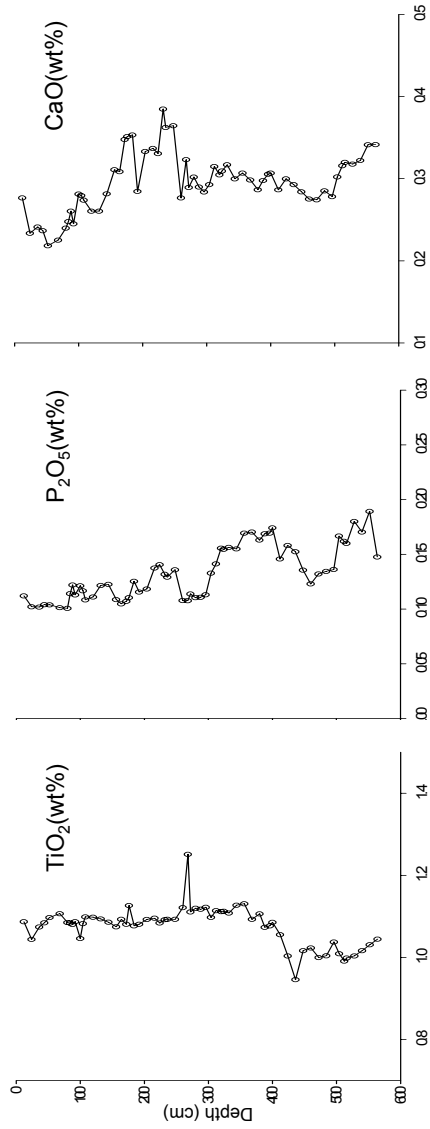
Fig. 8-5. Vertical variations of major elements of pit E55S20IV sediments, in the Jeongokri.

Taylor and McLennan, 1981). Total REE abundances in the lower part are higher than those of the upper part. Moreover, REE patterns show significant negative Eu anomalies (Eu/Eu*=0.57-0.74). Ce anomaly varies with depth (0.75~1.60).

8-5. Discussion

8-5-1. Geochemical variation of sediment and its implication

Geochemical variation of sediment is primarily controlled by source rock composition, and weathering processes play a minor role. Weathering is closely related with climate. Grain size effect on concentration of elements has to be considered because of close relationship between grain size and geochemical composition. The major-element abundances may reflect the composition of source rock. However, in some cases, their proportions may be modified by weathering processes that affect the source rocks and by post-depositional changes that affect the sediments (Boles and Franks, 1979; Nesbitt et al., 1996; McLennan, 2001; Spalletti et al., 2008). On the contrary, trace and rare earth elements are extremely insoluble and considered least susceptible to fractionation by exogenic processes including weathering, transportation, and diagenesis (Taylor and McLennan, 1985). Therefore, these elements can be transferred from source rock to sediment without significant fractionation (Balashov et al., 1964; Nesbitt, 1979; Davies, 1980).

In major element concentration of Jeongokri sediments, the upper and lower parts are well distinguished by 380 cm boundary horizon. Relatively enriched Al_2O_3 and K_2O in the lower part (380-570 cm) can be ascribed to input of feldspar, which is supported by XRD analysis. High SiO_2 concentrations in the upper part (~380 cm) are associated with increasing quartz contents. Generally, Al_2O_3 is enriched in silt- and clay-sized sediments, and depleted in sand-sized sediments,
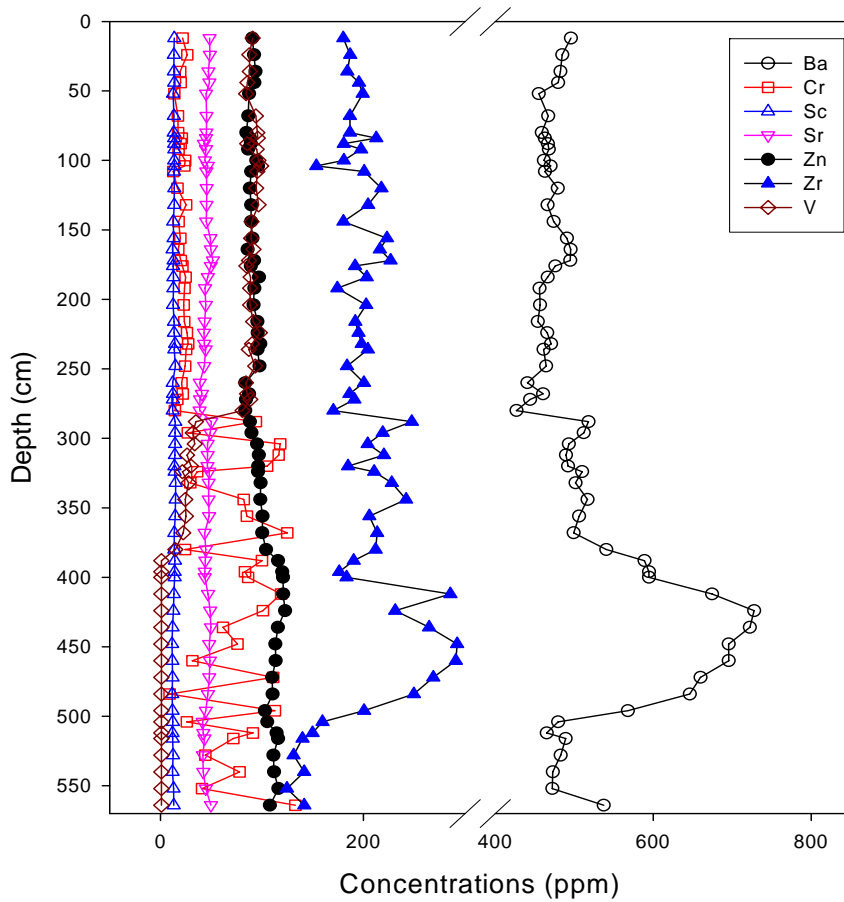
Fig. 8-6. Vertical variations of Ba, Cr, Sc, Sr, Zn, Zr, and V contents (ppm). These elements concentration are fluctuated below depth of 280 cm sediments. Most trace element concentrations increase downcore from 280 cm, and decrease from 500 cm.
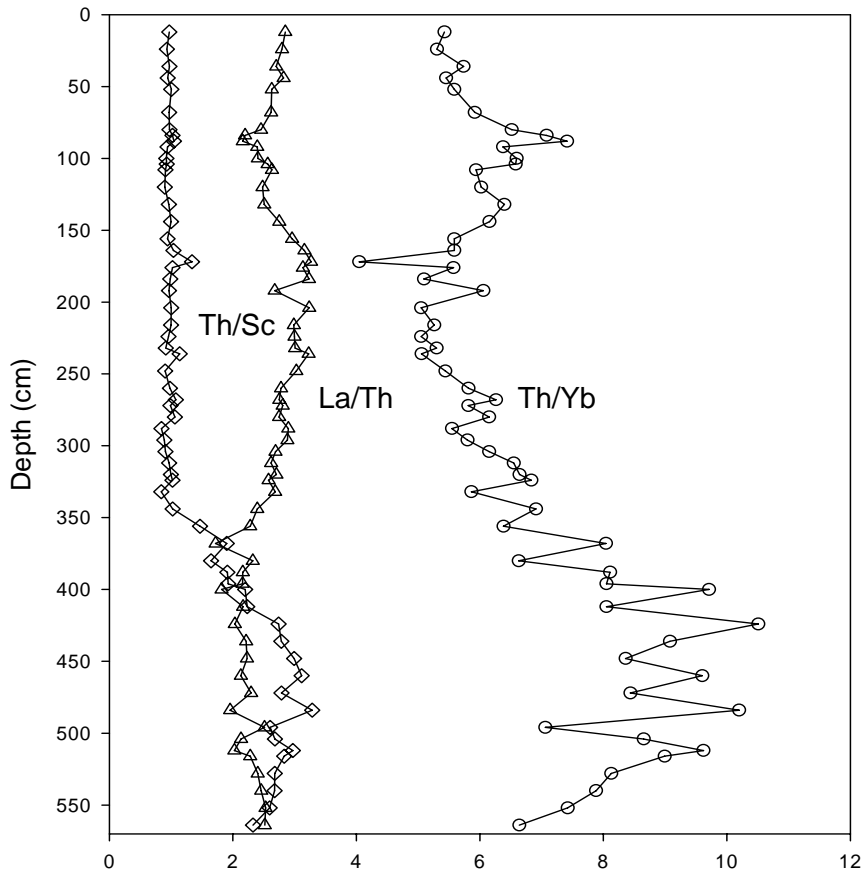
Fig. 8-7. Vertical variations of Th/Yb, La/Th and Th/Sc ratios of pit E55S20IV sediments, in the Jeongokri.
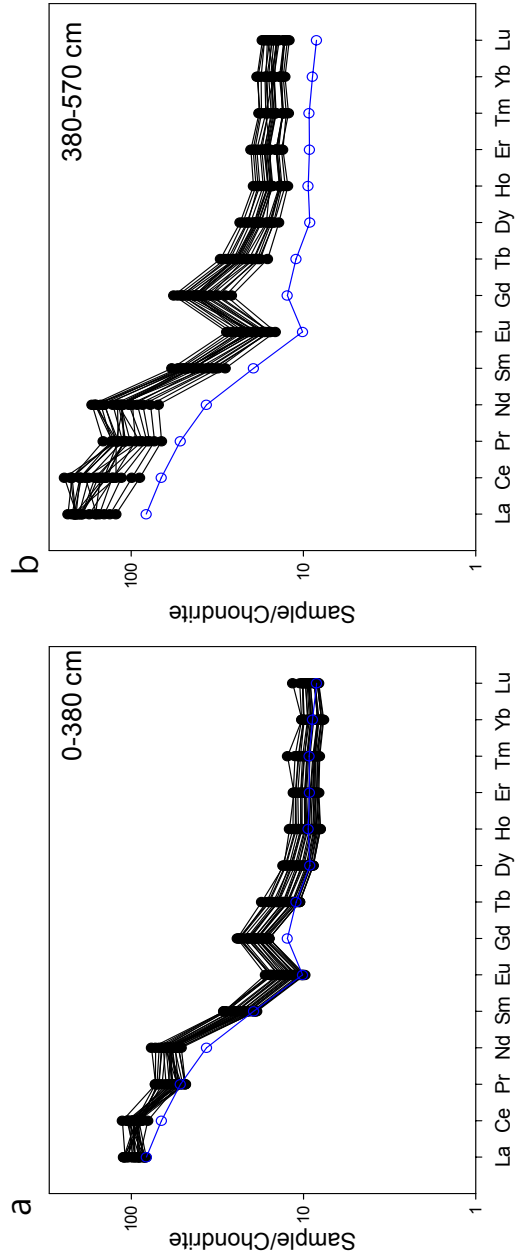
Fig. 8-8. REE distribution patterns are shown. All REE patterns are remarkably similar in shape, with enriched LREE and depleted and flat HREE profiles. These patterns resemble to that of average UCC (upper continental crust).

Table 8-1. Major element concentrations (wt%) of Jeongokri sediments

Sample depth (cm)	Al$_2$O$_3$	CaO	Fe$_2$O$_3$	K$_2$O	MgO	MnO	Na$_2$O	P$_2$O$_5$	SiO$_2$	TiO$_2$	Total
Recalculated compositions on a volatile-free basis											
12	18.19	0.28	7.02	2.24	1.61	0.14	0.22	0.11	69.11	1.09	98.99
24	17.78	0.23	6.71	2.21	1.80	0.13	0.30	0.10	69.69	1.04	98.85
36	17.96	0.24	7.17	2.21	1.76	0.16	0.24	0.10	69.07	1.07	93.28
44	17.57	0.24	6.83	2.00	1.73	0.15	0.22	0.10	70.07	1.08	101.80
52	17.45	0.22	6.62	2.06	1.57	0.14	0.16	0.10	70.57	1.10	94.33
68	17.67	0.23	6.85	2.19	1.57	0.14	0.18	0.10	69.98	1.11	97.68
80	17.56	0.24	6.92	2.22	1.46	0.11	0.14	0.10	70.16	1.09	99.25
84	18.77	0.25	7.29	2.27	1.49	0.12	0.10	0.11	68.51	1.08	96.41
88	19.41	0.26	7.60	2.28	1.54	0.14	0.10	0.12	67.47	1.08	98.89
92	18.79	0.25	7.29	2.26	1.49	0.12	0.11	0.11	68.50	1.09	99.14
100	19.78	0.28	7.63	2.27	1.57	0.13	0.10	0.12	67.07	1.05	93.10
104	19.11	0.28	7.43	2.24	1.63	0.12	0.12	0.12	67.86	1.08	100.13
108	18.11	0.27	7.05	2.31	1.51	0.12	0.11	0.11	69.32	1.10	93.09
120	17.99	0.26	7.25	2.33	1.45	0.14	0.12	0.11	69.25	1.10	98.88
132	18.14	0.26	7.44	2.35	1.45	0.11	0.13	0.12	68.91	1.09	98.62
144	17.96	0.28	7.30	2.38	1.52	0.14	0.14	0.12	69.06	1.09	93.02
156	17.49	0.31	6.75	2.45	1.55	0.15	0.20	0.11	69.91	1.07	92.86
164	16.68	0.31	6.42	2.40	1.55	0.16	0.22	0.10	71.06	1.09	99.19
172	17.25	0.35	6.61	2.41	1.63	0.14	0.24	0.11	70.17	1.08	98.91
176	17.08	0.35	6.79	2.44	1.55	0.13	0.23	0.11	70.19	1.13	95.07
184	18.46	0.35	7.19	2.31	1.58	0.17	0.17	0.13	68.57	1.08	99.64
192	18.55	0.28	7.35	2.29	1.54	0.13	0.14	0.12	68.51	1.08	99.44
204	18.00	0.33	6.86	2.28	1.49	0.14	0.15	0.12	69.53	1.09	99.68
216	19.40	0.34	7.52	2.27	1.50	0.19	0.10	0.14	67.46	1.10	98.85
224	20.73	0.33	7.89	2.29	1.50	0.14	0.06	0.14	65.83	1.08	98.90
232	20.65	0.38	7.74	2.36	1.59	0.13	0.11	0.13	65.80	1.09	93.31
236	18.78	0.36	7.54	2.35	1.55	0.16	0.12	0.13	67.92	1.09	99.07
248	20.28	0.36	7.80	2.35	1.53	0.13	0.10	0.14	66.22	1.09	99.29
260	17.90	0.28	7.06	2.30	1.20	0.15	0.08	0.11	69.80	1.12	93.63
268	17.92	0.32	7.97	2.58	1.21	0.12	0.08	0.11	68.43	1.25	92.83
272	18.79	0.29	7.25	2.33	1.24	0.12	0.07	0.11	68.69	1.11	99.20
280	18.42	0.30	7.10	2.30	1.28	0.18	0.07	0.11	69.13	1.12	98.68
288	17.73	0.29	7.07	2.32	1.23	0.16	0.09	0.11	69.88	1.12	99.34
296	17.58	0.28	7.15	2.32	1.16	0.17	0.07	0.11	70.03	1.12	92.97
304	19.44	0.29	7.68	2.16	1.17	0.08	0.05	0.13	67.89	1.10	99.40
312	20.20	0.31	7.70	2.15	1.22	0.12	0.04	0.14	66.99	1.11	99.10
320	19.84	0.30	7.58	2.23	1.21	0.12	0.07	0.16	67.36	1.11	93.84
324	20.30	0.31	7.81	2.30	1.22	0.13	0.04	0.15	66.62	1.11	93.74
332	20.61	0.32	7.88	2.26	1.24	0.16	0.06	0.16	66.22	1.11	99.09
344	19.83	0.30	7.63	2.28	1.21	0.13	0.06	0.15	67.28	1.13	99.36
356	20.70	0.31	7.82	2.31	1.18	0.12	0.05	0.17	66.21	1.13	91.19
368	21.75	0.30	8.12	2.34	1.22	0.11	0.04	0.17	64.86	1.09	99.18
380	21.23	0.29	7.86	2.54	1.26	0.13	0.05	0.16	65.37	1.11	93.84
388	23.18	0.30	8.14	2.59	1.34	0.16	0.05	0.17	63.01	1.07	97.71
396	23.67	0.31	8.29	2.72	1.40	0.17	0.06	0.17	62.14	1.08	99.17
400	23.95	0.31	8.35	2.71	1.41	0.14	0.07	0.17	61.81	1.09	96.44
412	23.02	0.29	7.76	3.03	1.41	0.11	0.08	0.15	63.10	1.06	99.47
424	24.45	0.30	7.77	3.18	1.47	0.12	0.12	0.16	61.43	1.00	98.05
436	23.88	0.29	7.46	3.36	1.43	0.13	0.14	0.15	62.21	0.95	99.07
448	23.20	0.28	7.46	3.22	1.35	0.17	0.12	0.14	63.05	1.02	93.64
460	22.70	0.28	7.52	3.27	1.32	0.11	0.13	0.12	63.53	1.02	99.20
472	22.97	0.27	7.72	3.24	1.28	0.11	0.13	0.13	63.14	1.00	99.12
484	23.99	0.29	7.45	3.20	1.32	0.10	0.12	0.13	62.40	1.00	98.89
496	22.27	0.28	7.49	3.08	1.24	0.14	0.07	0.14	64.27	1.04	99.17
504	25.05	0.30	8.09	2.71	1.21	0.16	0.05	0.17	61.25	1.01	98.98
512	25.62	0.32	7.73	2.63	1.23	0.20	0.05	0.16	61.07	0.99	98.78
516	25.69	0.32	7.80	2.66	1.20	0.19	0.04	0.16	60.95	1.00	90.63
528	25.61	0.32	8.33	2.64	1.28	0.30	0.04	0.18	60.30	1.00	99.43
540	25.73	0.32	8.03	2.69	1.26	0.16	0.05	0.17	60.57	1.02	96.22
552	26.07	0.34	8.64	2.60	1.34	0.24	0.04	0.19	59.51	1.03	99.32
564	24.45	0.34	8.08	2.91	1.34	0.22	0.08	0.15	61.38	1.04	90.75

Table 8-2 Trace and rare earth element compositions of Jeongokri sediments (ppm)

Sample depth (cm)	Ba	Cr	Sc	Sr	V	Zn	Zr	La	Ce	Pr	Nd	Sm	Eu	Gd	Tb	Dy	Ho	Er	Tm	Yb	Lu	Eu/Eu*	Ce/Ce*
12	496.0	21.8	13.7	48.4	90.8	90.5	180.1	103.6	98.7	62.9	65.2	25.7	13.8	21.4	14.5	12.1	10.7	10.8	10.4	9.9	10.1	0.6	1.2
24	484.9	26.4	13.3	48.7	87.6	92.1	186.9	94.4	105.9	58.6	59.9	24.5	13.4	20.4	14.0	11.6	10.2	10.2	9.9	9.4	9.8	0.6	1.4
36	482.6	19.5	13.3	47.2	88.0	93.6	184.1	95.2	97.7	57.5	62.2	23.2	12.6	19.6	13.1	11.0	9.8	9.8	9.6	9.1	9.4	0.6	1.3
44	479.7	19.9	13.6	48.2	85.7	92.4	195.5	98.6	95.1	60.1	62.8	24.7	13.4	20.8	14.2	11.8	10.4	10.4	10.1	9.5	9.7	0.6	1.2
52	455.1	13.6	12.5	45.0	84.4	87.2	199.3	89.9	103.3	54.2	57.7	21.9	11.7	18.7	12.8	10.7	9.6	9.7	9.5	9.1	9.3	0.6	1.5
68	467.1	17.2	13.2	45.4	94.0	86.5	186.6	91.5	92.6	54.7	59.2	21.7	11.6	18.5	12.3	10.3	9.2	9.3	9.2	8.7	9.2	0.6	1.3
80	459.0	17.4	13.1	45.2	95.4	84.6	186.6	85.1	92.1	50.2	56.1	19.3	10.1	16.5	10.8	9.0	8.2	8.4	8.3	7.9	8.3	0.6	1.4
84	462.8	21.2	13.5	44.8	95.8	88.2	212.6	82.6	99.5	48.3	53.5	18.6	9.8	15.8	10.5	8.9	8.1	8.4	8.3	7.9	8.3	0.6	1.6
88	466.8	19.9	13.6	42.9	85.5	89.0	180.6	83.5	94.8	48.9	53.0	18.9	9.9	15.8	10.5	8.8	8.0	8.2	8.1	7.7	8.2	0.6	1.5
92	468.0	17.8	13.7	44.8	94.9	86.3	197.7	83.9	104.9	51.1	60.8	19.4	10.3	16.8	10.9	9.1	8.4	8.6	8.6	8.1	8.6	0.6	1.6
100	461.7	24.3	13.6	43.7	96.6	94.4	180.7	81.9	90.4	48.4	51.2	18.9	10.1	15.8	10.5	8.8	8.0	8.1	8.1	7.6	8.1	0.6	1.4
104	470.3	23.6	13.8	46.6	99.2	96.2	153.6	89.7	90.6	54.6	58.1	21.0	11.2	17.5	11.5	9.4	8.4	8.6	8.5	7.9	8.3	0.6	1.3
108	462.9	12.7	13.4	45.2	95.4	89.3	200.7	87.0	98.8	54.0	63.5	20.6	11.0	17.8	11.5	9.5	8.6	8.9	8.7	8.2	8.6	0.6	1.4
120	479.3	16.9	13.7	45.6	94.3	88.1	217.7	83.2	97.7	52.0	61.0	19.9	10.5	17.1	11.1	9.3	8.5	8.7	8.6	8.2	8.6	0.6	1.5
132	466.3	25.3	13.6	45.4	96.7	89.3	204.5	89.5	80.2	53.5	55.5	21.1	11.2	17.4	11.6	9.6	8.7	8.9	8.7	8.3	8.6	0.6	1.2
144	474.1	17.8	12.7	45.2	89.8	89.3	180.2	94.9	96.9	57.8	59.0	23.1	12.3	18.8	12.5	10.1	9.0	9.1	8.8	8.3	8.6	0.6	1.3
156	490.9	19.6	13.0	49.3	89.3	90.6	223.0	98.5	103.2	60.6	59.3	24.3	13.1	19.5	13.0	10.7	9.4	9.6	9.3	8.8	9.1	0.6	1.3
164	495.6	17.6	12.0	49.6	91.7	85.9	216.1	106.8	87.7	66.2	63.2	26.4	14.1	21.1	14.0	11.2	9.8	9.9	9.5	9.0	9.3	0.6	1.0
172	495.1	20.0	13.0	51.6	87.2	92.1	226.6	154.5	109.2	92.6	92.4	42.1	22.6	38.2	23.6	19.6	17.0	17.9	16.7	17.3	16.5	0.6	0.9

Sample depth (cm)	Ba	Cr	Sc	Sr	V	Zn	Zr	La	Ce	Pr	Nd	Sm	Eu	Gd	Tb	Dy	Ho	Er	Tm	Yb	Lu	Eu/Eu*	Ce/Ce*
176	476.1	21.7	12.5	49.5	84.8	89.1	191.7	109.2	90.2	69.5	66.1	28.4	15.1	22.6	15.0	11.9	10.3	10.4	9.9	9.3	9.5	0.6	1.0
184	466.3	24.8	12.8	46.6	88.7	97.1	203.3	110.9	86.0	70.9	68.8	29.1	15.7	23.4	15.7	12.6	11.0	11.1	10.6	10.0	10.1	0.6	1.0
192	456.1	23.9	12.9	44.0	88.3	92.5	174.3	90.7	92.5	57.1	61.1	22.3	11.9	18.7	12.2	10.0	8.9	9.1	8.7	8.3	8.6	0.6	1.3
204	456.9	22.8	12.5	44.7	88.3	91.7	202.6	110.5	94.3	72.5	72.3	28.9	15.5	23.9	16.0	12.8	11.2	11.2	10.7	10.0	10.1	0.6	1.1
216	454.1	23.4	13.4	43.5	91.4	95.5	192.0	108.6	112.6	72.2	76.3	28.9	16.6	24.2	17.5	13.0	12.0	11.4	12.4	10.2	11.6	0.6	1.3
224	465.8	26.1	13.4	43.0	97.9	95.8	195.1	104.7	90.5	68.9	67.0	27.9	15.4	23.5	16.4	13.2	11.5	11.5	11.2	10.2	10.5	0.6	1.1
232	470.8	27.4	14.5	43.2	90.2	98.3	198.1	108.1	77.6	68.6	67.2	27.7	15.2	23.3	15.9	12.8	11.3	11.2	10.9	10.0	10.3	0.6	0.9
236	461.3	25.3	13.7	44.6	87.1	95.6	204.3	137.1	102.1	88.0	88.9	35.1	19.3	29.8	20.1	16.0	14.1	14.0	13.4	12.4	12.9	0.6	0.9
248	464.6	24.4	14.8	43.3	93.4	97.5	183.8	110.1	82.4	68.3	66.7	27.7	15.3	23.5	16.0	13.0	11.3	11.3	10.8	9.9	10.3	0.6	1.0
260	440.9	20.9	12.0	38.7	84.2	83.5	200.5	89.3	107.1	53.9	55.1	21.1	11.1	18.0	12.0	9.9	8.8	8.9	8.7	8.2	8.6	0.6	1.5
268	460.8	22.1	12.4	40.9	85.3	87.2	186.2	100.0	83.4	59.5	57.4	23.5	12.4	19.6	13.4	10.8	9.6	9.7	9.3	8.6	8.8	0.6	1.1
272	444.2	16.6	12.3	39.0	88.5	84.3	191.0	92.8	98.4	55.7	54.3	22.0	11.8	18.5	12.6	10.3	9.2	9.3	9.0	8.4	8.7	0.6	1.4
280	427.0	14.3	12.1	38.6	80.9	83.5	170.3	96.3	89.8	59.7	63.1	23.0	12.2	19.7	12.8	10.4	9.2	9.4	9.0	8.4	8.8	0.6	1.2
288	518.1	94.0	14.5	50.2	35.0	88.2	247.6	96.9	92.5	60.1	62.7	23.5	12.3	20.0	13.1	10.8	9.6	9.8	9.5	8.9	9.3	0.6	1.2
296	512.1	27.1	14.4	49.1	32.0	89.6	219.0	100.9	92.3	63.1	64.2	24.4	12.8	20.7	13.7	11.1	9.9	10.0	9.6	8.9	8.6	0.6	1.2
304	493.3	118.0	14.4	46.5	33.9	95.0	204.2	95.9	102.6	57.6	52.4	23.1	12.3	19.0	13.1	10.7	9.4	9.5	9.1	8.6	8.3	0.6	1.4
312	489.6	116.5	14.3	46.5	26.3	96.9	220.1	99.1	87.6	59.7	59.3	23.3	12.2	19.6	13.1	10.6	9.4	9.5	9.2	8.5	8.3	0.6	1.1
320	492.3	105.1	13.8	46.4	30.2	96.3	184.8	101.2	86.3	60.6	60.8	23.3	12.2	19.6	12.8	10.4	9.1	9.3	8.9	8.3	8.1	0.6	1.1
324	510.1	36.2	14.0	48.1	21.7	96.1	210.5	100.5	92.2	59.5	61.2	22.9	12.0	19.4	12.7	10.3	9.1	9.3	9.0	8.4	8.3	0.6	1.2
332	501.6	29.5	15.1	47.4	27.8	98.6	227.9	93.0	92.1	57.6	65.4	22.0	11.6	19.4	12.5	10.4	9.3	9.5	9.3	8.7	8.5	0.6	1.3

Sample depth (cm)	Ba	Cr	Sc	Sr	V	Zn	Zr	La	Ce	Pr	Nd	Sm	Eu	Gd	Tb	Dy	Ho	Er	Tm	Yb	Lu	Eu/Eu*	Ce/Ce*
344	516.9	82.1	14.9	47.5	24.6	98.4	241.9	99.5	90.3	60.0	65.2	22.8	11.6	19.8	12.8	10.7	9.6	9.8	9.5	8.9	8.7	0.5	1.2
356	506.3	85.2	14.5	48.0	25.1	100.5	205.7	132.8	99.0	73.3	77.2	31.2	16.0	28.3	17.8	14.9	13.3	13.9	13.3	13.5	12.9	0.5	1.0
368	499.5	124.9	13.7	43.5	22.5	100.2	213.5	122.5	89.1	66.7	69.5	28.4	14.5	26.1	16.1	13.9	12.3	13.2	12.6	13.1	12.4	0.5	1.0
380	540.7	24.2	13.7	44.7	14.8	104.0	211.9	143.1	114.0	78.1	85.5	33.1	15.5	31.3	18.5	15.4	13.6	14.2	13.1	13.8	13.0	0.5	1.1
388	589.0	100.0	14.3	44.2	less than	115.9	190.3	160.9	151.3	86.2	103.1	35.7	16.6	34.5	19.3	15.6	13.5	14.3	13.1	13.6	12.9	0.5	1.3
396	594.8	83.3	14.0	43.6	less than	119.8	176.1	158.7	184.3	89.3	119.4	36.3	16.9	37.2	19.6	15.7	13.7	14.4	13.2	13.5	12.9	0.5	1.5
400	594.7	86.4	14.0	43.6	less than	120.7	183.3	152.8	128.7	81.1	91.9	33.7	15.6	32.2	18.1	14.8	12.8	13.4	12.2	12.8	12.1	0.5	1.2
412	674.6	118.9	13.2	47.0	less than	121.0	285.5	174.7	127.4	94.3	98.4	38.5	17.7	34.8	21.9	16.4	15.6	15.5	16.6	14.8	16.1	0.5	1.0
424	727.7	100.9	12.7	49.0	less than	122.8	231.2	193.4	162.3	101.4	115.3	40.8	17.4	38.4	20.7	16.2	13.8	14.4	13.1	13.4	12.8	0.4	1.2
436	722.5	61.5	11.9	49.7	less than	115.7	264.6	200.6	176.6	112.3	127.7	44.1	18.9	42.7	22.8	17.8	15.1	15.8	14.4	14.8	14.1	0.4	1.2
448	695.5	75.8	11.4	48.0	less than	113.2	292.2	207.8	244.0	120.5	162.2	47.7	20.3	49.5	24.9	19.3	16.7	17.5	16.1	16.5	16.2	0.4	1.5
460	695.6	31.6	11.8	48.7	less than	113.5	290.9	213.7	194.7	122.1	142.5	47.9	19.5	46.5	24.2	18.4	15.6	16.4	14.7	15.5	14.8	0.4	1.2
472	659.8	111.0	12.0	48.1	less than	110.0	268.8	208.6	198.3	119.1	143.1	47.3	19.7	46.6	24.4	18.9	16.0	16.8	15.4	15.9	15.3	0.4	1.3
484	646.4	9.1	11.6	46.8	less than	110.6	249.7	202.5	138.8	110.8	112.5	44.0	18.8	40.4	22.2	17.5	15.2	15.9	14.5	15.0	14.4	0.4	0.9
496	568.0	112.8	11.9	44.7	less than	103.0	200.6	211.4	225.6	124.7	159.0	49.7	22.7	51.1	26.6	21.1	18.4	19.1	17.5	17.6	16.8	0.5	1.4
504	479.8	26.0	12.2	41.6	less than	105.2	159.7	190.9	156.0	107.3	118.4	43.7	20.9	42.1	23.5	18.8	16.0	16.6	14.9	15.3	14.2	0.5	1.1
512	465.3	91.1	11.9	42.1	less than	114.3	149.9	195.6	142.0	108.8	114.1	43.6	20.7	41.0	23.1	18.3	15.4	16.2	14.5	14.9	13.8	0.5	1.0
516	489.2	71.8	12.1	43.3	less than	115.9	139.9	212.8	143.9	119.2	119.9	46.7	22.2	43.1	24.5	19.2	16.1	17.0	15.2	15.3	14.2	0.5	0.9
528	483.1	44.2	12.6	41.9	less than	111.3	131.1	220.6	197.8	130.2	149.8	51.9	24.7	50.6	27.4	21.3	17.9	18.7	16.6	16.7	15.7	0.5	1.2
540	472.9	77.9	11.9	42.2	less than	111.9	141.6	213.9	122.5	122.2	111.1	48.8	23.5	42.9	25.4	20.3	17.1	17.9	16.0	16.3	15.2	0.5	0.8
552	472.3	40.9	13.0	44.6	less than	116.2	124.6	232.7	220.8	145.5	168.8	58.0	27.8	56.6	30.3	23.3	19.5	20.2	18.1	18.3	16.9	0.5	1.2
564	537.5	133.0	13.1	49.8	less than	107.9	141.7	210.0	220.6	128.5	162.1	53.4	26.3	53.6	28.4	22.5	18.8	19.6	17.8	18.6	17.3	0.5	1.3

whereas SiO_2 is generally enriched in sand-sized sediments because of quartz influx. In Jeongokri sediments, mean grain size of the upper part is smaller than that of the lower part, reflecting relatively higher clay and silt contents in the upper part (Fig. 8-3). However, in contrast to the general tendency of geochemical composition of sediment with grain size, the upper part containing high silt and clay contents has higher SiO_2 and lower Al_2O_3 concentrations than does the lower part containing higher sand contents (arrow shows a general trend; Fig. 8-9). REE concentrations also show different pattern with the general tendency of REE concentrations. In principle, the REE concentrations are generally enriched in clay and silt fractions, but depleted in sand fraction, because of dilution by quartz and carbonate minerals (Yang et al., 2002). But in Jeongokri sediments, total REE concentrations in the clay-rich upper part are lower than those of the sand-rich lower part (Fig. 8-8). These opposed and distinguished major and REE compositions between the upper and lower parts of the core represent that grain size is not a main factor controlling geochemical variation.

Among trace elements, Ba and Zr contents (ppm) well correlated with grain size distribution pattern (Fig. 8-6), which indicates that grain size affected the trace element compositions (r=0.82 and 0.31, respectively). Th/Yb, La/Th and Th/Sc ratios also show a similar pattern with grain size distribution pattern (r=0.41, 0.20 and 0.43, respectively; Fig. 8-7). However, increasing (Th/Yb and Th/Sc) and decreasing (La/Th) patterns occur from depth of approximately 330 cm. These trends are different with grain size distribution. Th/Yb and Th/Sc ratios are a distinctive indicator of source rock, which increase with influence of highly differentiated source rocks such as granitic rock (Taylor and McLennan, 1985; Lee, 2009). On the other hand, La/Th ratio decreases with more supply of felsic source materials. Gallet et al. (1998) suggested that there is no clear distinction of La/Th
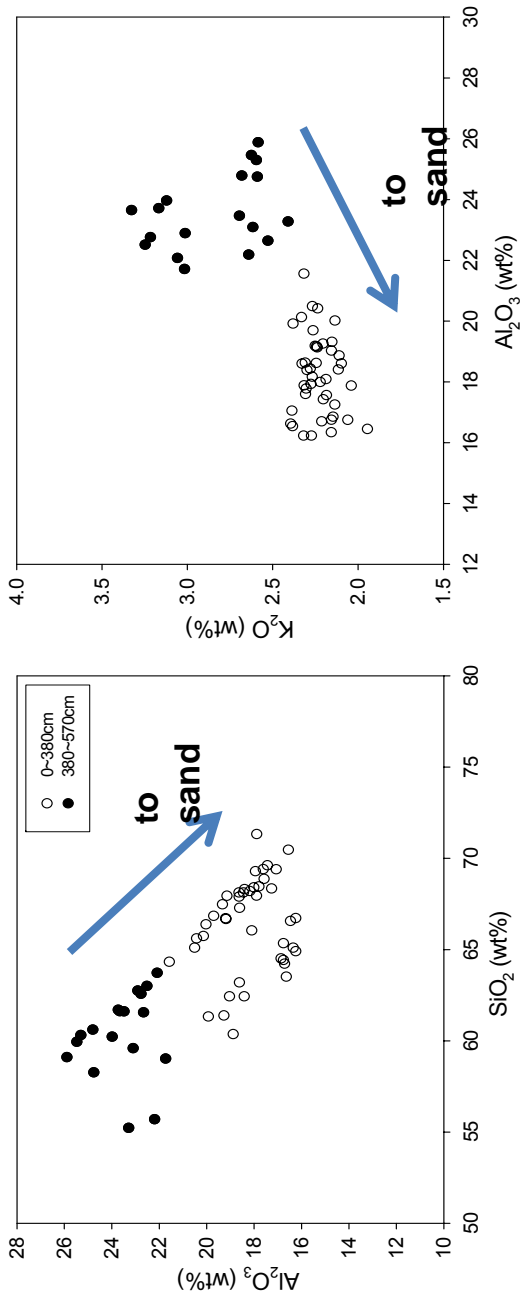
Fig. 8-9. Jeongokri sediments show an opposite trend to the general tendency of geochemical composition of sediment with grain size, which are well distinguished by 380 cm horizon.

ratio between whole-rock and size-fractions, representing that this ratio will be little affected by sedimentary sorting. In Jeongokri sediments, these ratios represent that influence of highly differentiated source rocks such as granitic rock was remarkably increased in the lower part, which is also supported by the presence of significant amount of feldspar in the lower part (Fig. 8-1).

8-5-2. Correlation between Chinese loess and Jeongokri sediments

To discriminate the origin of Jeongokri sediments, it is essential to characterize the compositions of possible source rocks. As mentioned above, many previous studies suggested that most of Quaternary sediments of the Korean Peninsula including the Jeongokri area were derived from the Chinese loess. If it is accepted, geochemical proxies of Quaternary sediments of the Korean Peninsula should be correlated with those of Chinese Loess Plateau sediments. However, to date reported geochemical proxies are not enough to accept this interpretation.

The difference of elemental concentrations between Chinese Loess Plateau sediments and Jeongokri sediments is compared using REE composition. The Chinese loess is from the Xining, Xifeng, Jixian and Luochuan areas and all of REE data are from Gallet et al. (1996) and Jahn et al. (2001) (Fig. 8-10). All Chinese loess and Jeongokri sediments have similar chondrite-normalized REE distribution patterns with relative LREE enrichment and HREE depletion and a negative Eu anomaly (Figs. 8-8 and 8-10). Also, REE patterns of the upper part of the Jeongokri core and Chinese Loess Plateau sediments resemble to that of UCC (upper continental crust). However, detailed comparison of REE patterns has a limit in these REE patterns to correlate the provenance. More reliable provenance indicators are REE ratio diagrams. The degree of fractionation of REE patterns can be expressed by a ratio between the concentration of a light REE (La or Ce) and the
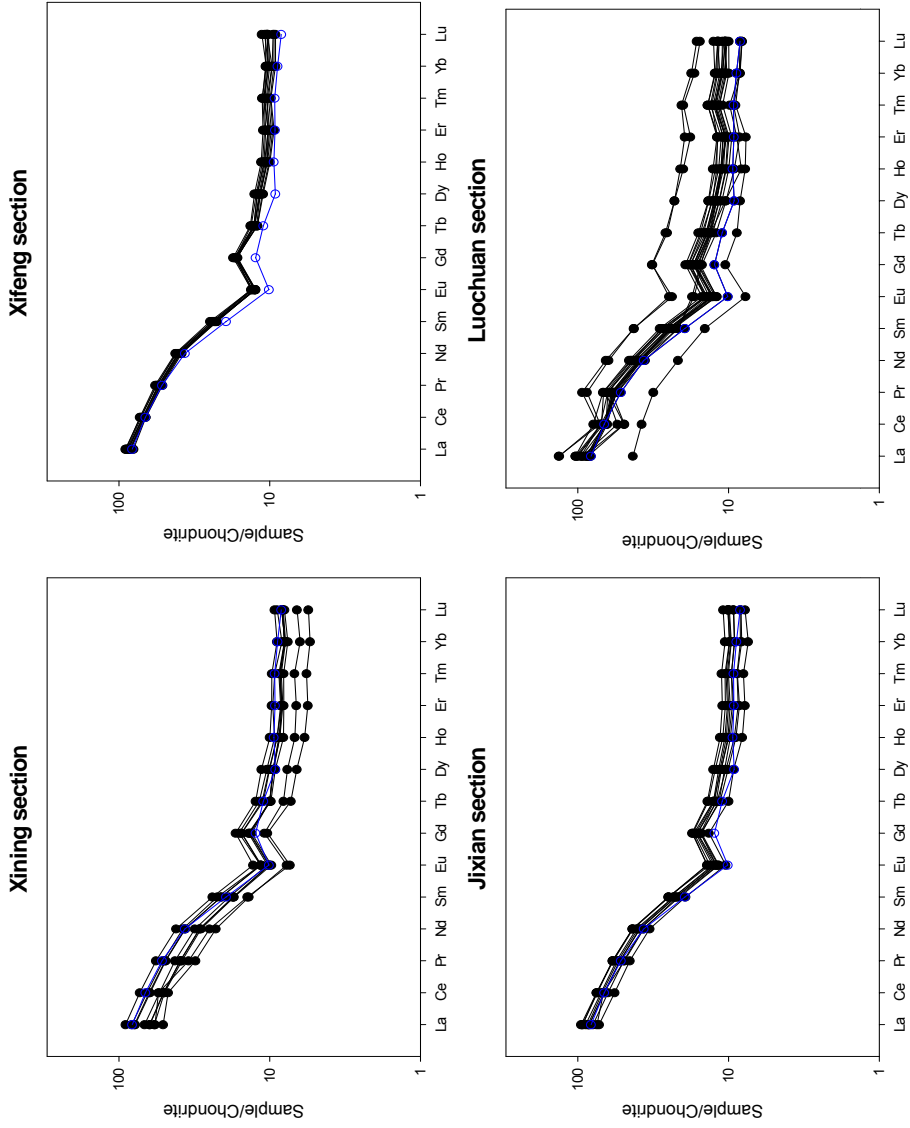
Fig. 8-10. Chondrite-normalized REE distribution patterns of Chinese loess and UCC (blue line) (Gallet et al., 1996; Jahn et al., 2001).

concentration of a heavy REE (Yb or Y). The ratio (La/Yb)$_N$ is plotted against La$_N$ and Ce$_N$ on a bivariate graph and is a measure of the degree of REE fractionation with changing REE content (Rollinson, 1993). Also, individual REE characteristics can be compared by Eu anomaly [(Eu/Eu*) vs (La/Sm)$_N$]. Fig. 8-11 illustrates the REE ratios between the Chinese loess and Jeongokri sediments.

All diagrams show remarkable difference between the upper and lower parts of the core, or between the lower part of the core and Chinese Loess Plateau sediments (Fig. 8-11). In a [(La/Yb)$_N$ vs. La$_N$] diagram, plots for Chinese loess and the upper part of the core (~380 cm) are slightly overlapped (Fig. 8-11a). Also, plots for Chinese loess are similar to those of UCC (Taylor and McLennan, 1981). However, the lower part (380~570 cm) is plotted in a different field, and shows broad range of plots. [(La/Yb)$_N$ vs Ce$_N$] and [(Eu/Eu*) vs (La/Sm)$_N$] diagrams show that plots of the upper part were close to those of Chinese loess. However, plots of each sediment are not overlapped (Fig. 8-11 b and c).

The lower part containing a large contribution of sand-sized sediments was interpreted as a fluvial origin (Shin et al., 2004). REE ratios of this part are remarkably distinguished from those of the upper part of the core and Chinese Loess Plateau sediments. To confirm the origin of the lower part, REE patterns are compared with those of the recent Imjin-Hantan River sediments. Fig. 8-12a shows very similar REE patterns between lower part of Jeongokri sediments and Imjin-Hantan River sediments. It indicates that the lower part of the core was derived from local origin of fluvial source.

On the other hand, REE compositions of the upper part of the core show similar REE ratios with those of Chinese loess, but not exactly coincident. In all diagrams, plots of the upper part distribute in the middle part between those of Chinese loess and lower part of the core. It might be a result of a mixture of origin from the lower
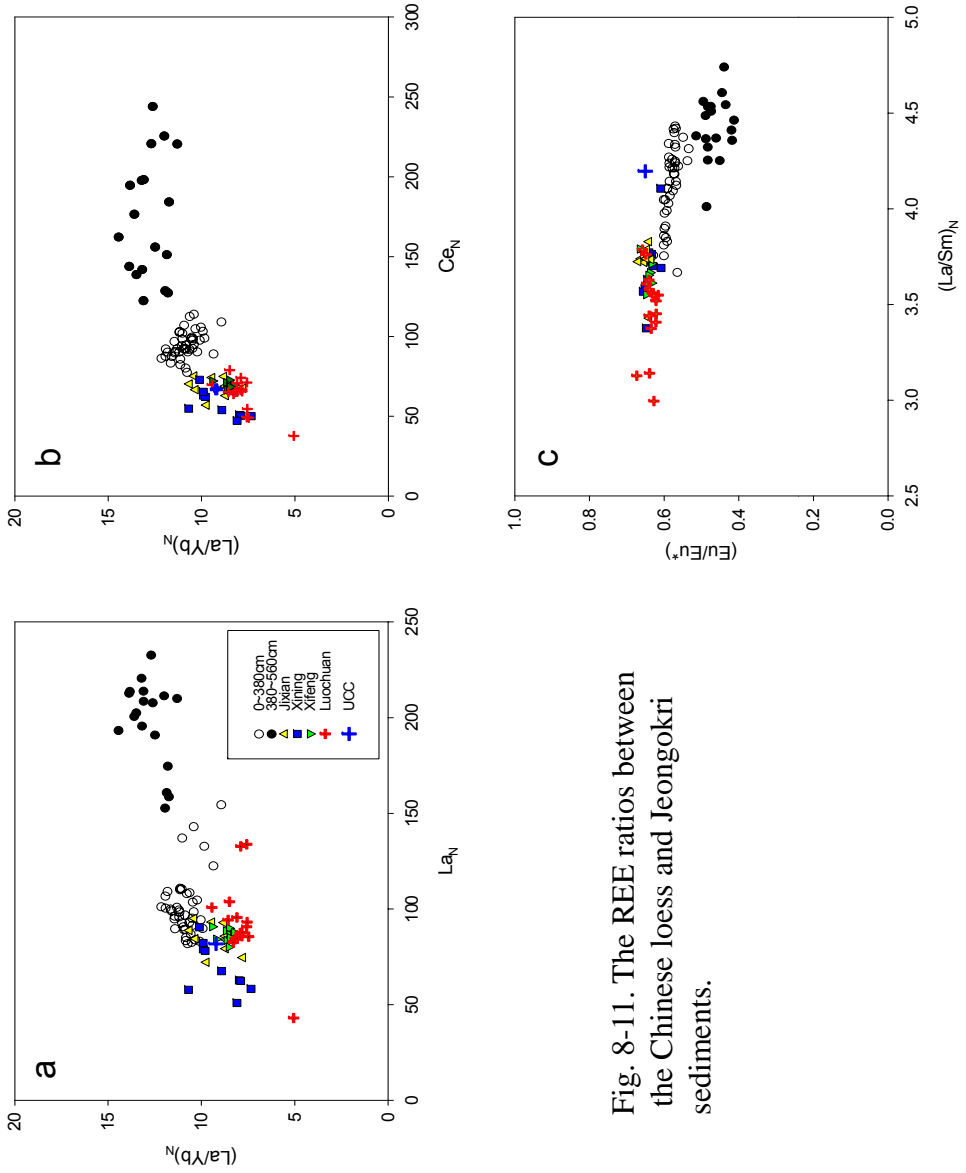
Fig. 8-11. The REE ratios between the Chinese loess and Jeongokri sediments.
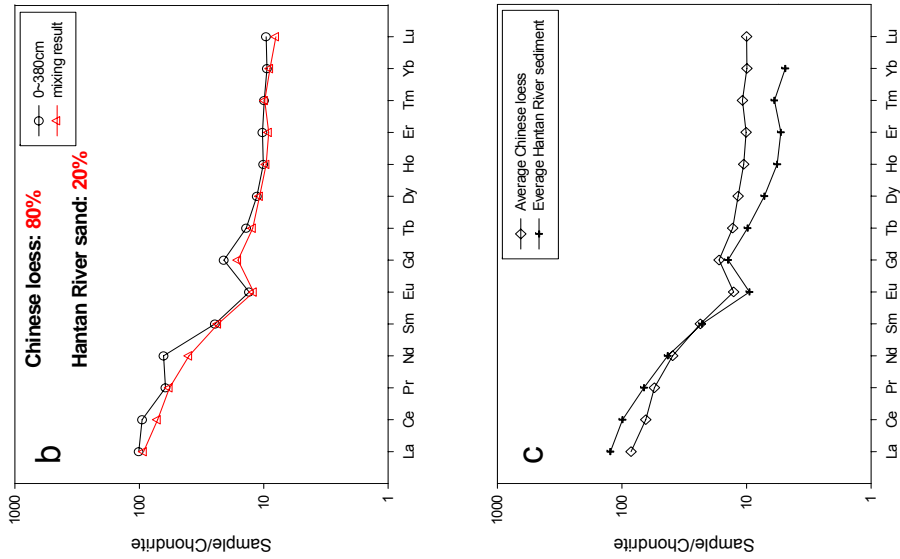
Fig. 8-12. a) Chondrite-normalized REE distribution patterns between lower part of Jeongokri sequence and surface sediments of Hantan River.
b) the results of mixing calculations between Chinese loess and surface sediments of Hantan River. c) Average REE patterns of Chinese loess and surface sediments of Hantan River.

part of the core and Chinese Loess Plateau sediments. To estimate the relative contribution of these two potential sources quantitatively, mixing calculations (Le Maitre, 1981; Lee, 2009) were applied in this study. The chondrite-normalized REE patterns of average compositions along with the results of mixing calculation between Chinese loess and the lower part of the core show in Fig. 8-13. Also, mixing calculation between Chinese loess and Imjin-Hantan River sediments shows in Fig. 8-12b and c.

The results of mixing calculations show that the Chinese Loess Plateau sediments might be the most dominant source (80%). The lower part of the core contributed 20% of the source of upper part of the core. Mixing calculations between Chinese Loess Plateau sediments and Imjin-Hantan River sediments also imply that 20% of the composition of upper part was derived from Imjin-Hantan River sediments. Accordingly, the origin of the upper part of the Jeongokri sediments is mixed sources, which is mainly from Chinese loess and partially from local origins of the Korean Peninsula.

8-5-3. Possible source area

Kim et al. (2009c) has proven that Jeongokri sediments were mainly deposited during MIS 6 and 7 periods. The upper part of the core mainly belongs to MIS 6, while the lower part of the core belongs to MIS 7. Different depositional time is closely related to sedimentary environments. Sedimentary environments are also related to climate change. MIS 7 period in East Asia was interglacial period of warm and humid. During this period, the improved vegetation covered the possible source area, dust might be entrapped in source area and dust supply was significantly decreased. On the contrary, increased rainfall contributed sediments deposition primarily of fluvial origin. Depositional environments of the lower part
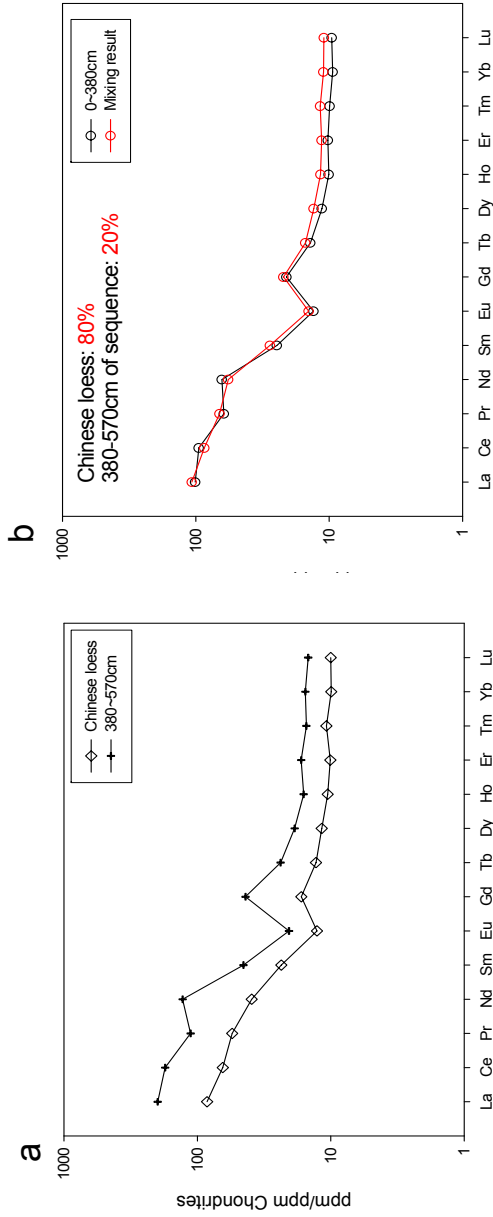
Fig. 8-13. a) Chondrite-normalized average REE distribution patterns between lower part of Jeongokri sequence and Chinese loess. b) the result of mixing calculations between Chinese loess and the lower part of Jeongokri sequence.

of the core are consistent with these environments. On the other hand, during cold and dry glacial period of MIS 6, winter monsoon was much stronger than summer monsoon. Accordingly, dust supply from Chinese Loess Plateau was relatively increased, which was one possible source for the upper part of the Jeongokri sediments.

Mixed sources of the upper part represent that local area nearby the Jeongokri was also possible source area. Another possible source area for the interpretation of mixed contributions is Yellow Sea area. The Yellow Sea is located between China and the Korean Peninsula (Fig. 1-1), which is the place for tremendous sediment load from China and the Korean Peninsula. Many researches suggested clearly that sediments of the Yellow Sea are "multi-sourced deposits" on the basis of mineral and geochemical compositions and oceanographic observations (Qin and Li, 1983; Gao et al., 1996; Zhao et al., 1990; 1997; 2001; Wei et al., 2000). Muddy sediments in the central-western part of the Yellow Sea are derived ultimately from Chinese rivers, especially the Huanghe River, whereas the eastern sandy sediments primarily came from Korean rivers during the postglacial transgression (Yang and Youn, 2007). However, large sediment budget and high accumulation rate in the Yellow Sea are attributable to the supply of considerable amount of sediments from the Huanghe River because nearby Korean rivers are not so large to supply huge amounts of sediments (Schubel et al., 1984; Wells, 1988; Ren and Shi, 1986; Alexander et al., 1991; Chang et al., 1996; Park et al., 2000). Huanghe River sediments are largely inherited from widely distributed loess deposits (Yang et al., 2002). Because, the Huanghe River originates on the northeastern Tibetan Plateau of Northwestern China and then flows across the dry loess plateau of north China; about 90% of its sediment load is derived from the loess plateau deposits (Liu et al., 2009). These results support that possible source area of mixed contribution is

Yellow Sea area.

Considerable distance between Chinese Loess Plateau and Korean Peninsula is unlikely to direct transport of loess plateau sediments by wind. On the other hand, Yellow Sea area is closer to the Korean Peninsula. The Yellow Sea experienced dramatic glacio-eustatic sea-level fluctuations during the late Quaternary (Yang et al., 2003). A dry and cold paleoclimate prevailed during glacial periods such as MIS 6 and Yellow Sea area was sub-aerially exposed because of low sea level (c.f. Yang et al., 2008). In that time, winter monsoon was considerably strengthened, and exposed Yellow Sea area was located in the path of winter monsoonal wind direction. In that period of time, tremendous sediments in Yellow Sea area were exposed and transported by winter monsoonal wind. These environments during MIS 6 could cause an important aeolian source for Jeongokri sediments.

8-6. Summary

In contrast to the general tendency of geochemical composition of sediment with grain size, Jeongokri sediments show an opposite trend, and the upper and lower parts are well distinguished by 380 cm horizon. All Chinese loess and Jeongokri sediments have similar chondrite-normalized REE distribution patterns with relative LREE enrichment and HREE depletion and a negative Eu anomaly The lower part of the sequence containing a large contribution of sand-sized sediments indicates a fluvial origin. The upper part of Jeongokri sequence might be a result of a mixture of fluvial origin and Chinese loess with constant ratio. One possible source area for the interpretation of mixed contributions is Yellow Sea area.

APPENDIX

A. Sample preparation

After collection of samples in the field, they are opened in the laboratory. The laboratory should be a red-light condition. Therefore, samples do not expose to any sunlight before have any luminescence measurements. However, to ensure that the sample used for dating was completely unexposed, the sediment at both ends of the tube was removed to a depth of 5cm. This removed part was used for dosimetry measurements. All samples pre-treatment were undertaken in red-light conditions.

A-1. Size fraction for coarse grain dating

For coarse grain dating, removal of fine grains is necessary. In this study, quartz grains (90-250 μm) were used for OSL dating. To remove all particles <90 μm and >250 μm in diameter, the sediment samples were wet-sieved through 90 μm and 250 μm sieve. The sieve was washed through with tap water until the water running through the sieve was clear.

A-2. Size fraction for fine grain dating

For fine grain dating (4~11 μm), two methods were used from Jeongokri sediments. First method is using Sodium Pyrophosphate decahydrate ($Na_4O_7P_2.10H_2O$). Sodium Pyrophosphate decahydrate acts as a deflocculating agent and disperses the clays particles (Helena, 2006). A 0.5% solution of Sodium Pyrophosphate decahydrate was made up by mixing 5g of Sodium Pyrophosphate decahydrate with 100 ㎖ of distilled water. A beaker containing the sample was filled with a 5% solution of Sodium Pyrophosphate decahydrate and stirred

vigorously. This was allowed to settle for 2 hours, and then the liquid and material in suspension were removed. Another 5% Sodium Pyrophosphate decahydrate solution was added to the sample in the beaker until the liquid appeared clear and colorless after settling.

Second method is using Sodium Oxalate ($Na_2C_2O_4$). Sodium Oxalate also acts as a deflocculating agent allowing each particle to settle individually. A 0.01 Normal solution of Sodium Oxalate was made up by mixing 6.7g of Sodium Oxalate with 10 litres of distilled water. Following "Stokes's Law" the settling times for different grain sizes were calculated; over a depth of 20cm it takes 20 minutes for particles <11 μm to settle, and 4 hours for particles <4 μm to settle. For the fine grain samples from the Jeongokri, approximately 100g of sediment was put in a 1 litre cylinder, which was filled with the Sodium Oxalate solution to a depth of 20cm. The measuring cylinder was put in a sonic bath for 10 minutes followed by 1 minute of hand shaking. It was then placed in the fume cupboard and wait to settle for 20 minutes to remove all particles greater than 11 μm. And then, pour (<11 μm) liquid fraction into another cylinder and settle for 4 hours. This procedure was repeatedly performed on each 100g of sediment at least three times. The remaining sediment was washed three times with distilled water to remove the Sodium Oxalate.

Either methods 1 and 2 were equally employed for each sample in order to use the fine grain (4~11 μm) sediment. This method is very time-consuming due to the number of times it has to be performed for each sample.

A-3. Removal of carbonates and organic materials

The preparation of samples with a treatment of dilute hydrochloric (HCl) acid (10%) was used to remove all carbonates. After adding HCl to the sediment, if

there are any carbonates then there should be a reaction. HCl was normally added up until the reaction subsided. After the HCl treatment, the sediments were rinsed three times with distilled water (wait to settle in between rinses). The % loss of material can be used as an indication of the carbonates contents.

The next treatment was with 33% hydrogen peroxide (H_2O_2) to digest any organics. After adding H_2O_2 to the sediments, if any organics were present, a reaction will be visible. More H_2O_2 were added if there were any reaction. The samples were rinsed three times with distilled water after finish this treatment.

A-4. Density separation for coarse grain samples

Quartz separated from the remaining sample by density separation using sodium polytungstate at two densities. First, density of 2.62 is used to separate quartz from potassium and sodium feldspars and second density of 2.70 to separate the quartz fraction from any heavy minerals such as zircons or appetites. The remaining grains are 2.62 g/cm^3< ρ <2.70 g/cm^3). In this study, density separation didn't use.

A-5. HF etching for coarse (90-250 μm) grain sediment

HF etching was treated with 40% hydrofluoric acid (HF) for approximately 1 hour to remove any remaining feldspar grains as well as to etch away the outer alpha irradiated layer of the grains. Following the HF treatment the sample was washed in 10% HCl and distilled water to remove any fluoride precipitates.

A-6. Hydrofluorosilicic Acid (H_2SiF_6) treatment for fine (4-11 μm) grain sediment

Quartz grains were isolated from this fraction using 1 week of hydrofluorosilicic acid (H_2SiF_6) treatment at room temperature to preferentially

etch of feldspathic material. The material was then resieved using 11 μm diameter mesh to remove grains that had been reduced in size by the etching. 1 week of treatment with H_2SiF_6 was sufficient to remove any significant feldspar signal from these sediments.

A-7. Disc preparation

Coarse grain (90-250 μm) sediments mounted on 9.8 mm diameter aluminium discs using silicone spray. Each disc should carry only a monolayer. Two mask sizes with hole diameters of 2 and 5 mm can be used, and are termed small and large aliquots respectively.

Fine grains (4-11 μm) are deposited from suspension in acetone. Equality of weight between discs can be achieved by weighing grains. For fine grain (4-11 μm) sediments, sample was used 1 mg per each disc. First, 1 ㎖ acetone was filled to glass bottle (1 cm diameter), and then 1 ㎖ acetone mixed with 1mg sample putted into same bottle. It can delay the settling time of sediments. This bottle kept in the oven 1 day for dry.

B. Dose rate calculation

B-1. Introduction

The rate at which trapped electrons are accumulated is proportional to the rate at which energy is absorbed by a grain from the flux of radiation to which it is exposed. The dose is defined as the energy absorbed per kilogram and the unit of measurement is the *gray* (Gy); 1 Gy=1 Jkg^{-1}. The natural dose-rate is expressed as gray per thousand years (Gy Ka^{-1}) or as milligray per year (mGy a^{-1}) (Aitken, 1998). An ionizing radiation field is derived from three main areas; an internal dose from

within the grains themselves, an external dose from the bulk sediment matrix (K^{40}, Rb, U and Th) and a contribution from cosmic radiation. Fig. B-1 shows the decay chains and emissions for ^{235}U, ^{238}U and ^{232}Th (Aitken, 1985).

The external sources of radiation consist of alpha (α) particles from the decay chains of U and Th, beta (β) particles from the U, Th, K and Rb decay series, and gamma (γ) rays from U, Th, K, as well as a small contribution from cosmic radiation (Helena, 2006). The internal dose rate for quartz is generally assumed to be zero (Aitken, 1998; Simon J. Armitage, 2002), because quartz contains very low levels of U, Th and K contents. This study assumes that the internal dose-rate of the quartz grains is negligible.

B-1-1. External dose-rate

In this study, external dose-rate was calculated by emission counting methods which measure α, β and γ emissions. This allows the concentration of the parent radionuclides to be calculated. In this study, dose rate investigation also performed using high-resolution gamma spectrometry. This technique has been used for detect the disequilibrium of decay chain (Olley et al., 1996). Disequilibrium of the decay chain occurs when an isotope is added to or removed from a system without its parent or a daughter isotope (Osmond and Cowart, 1982). Weathering processes in surficial environments can cause disequilibria by three processes: solution and precipitation reaction, emanation of radon isotopes and alpha particle recoil (Olley et al., 1996).

Alpha, beta and gamma radiation are able to penetrate different thickness of sediment. Although the maximum penetration for each type of radiation is dependent upon the energy it carries, some generalizations can be made. Fig. B-2 illustrates the different penetrating powers of these radiations (Aitken, 1998).
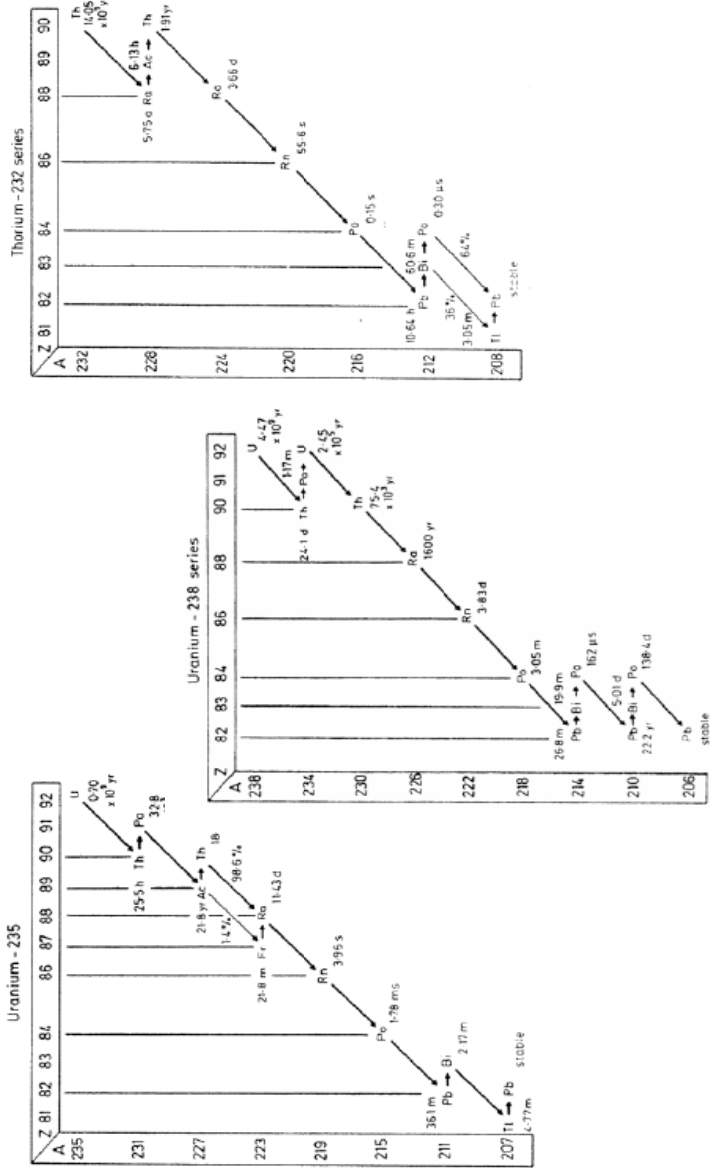
Fig. B-1. Decay series for ^{232}Th, ^{235}U and ^{238}U. Long arrows represent alpha decay and short one beta decay (Aitken, 1985).

174
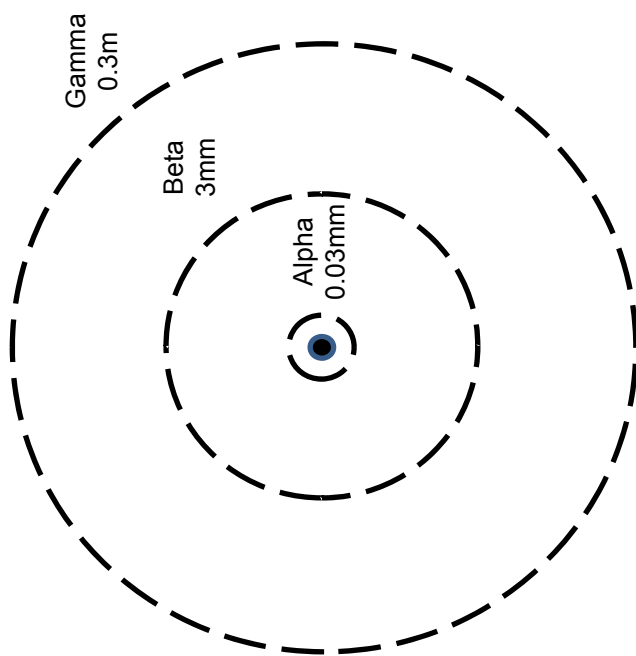
Fig. B-2. Spheres of influence of relevant nuclear radiations (Aitken, 1998)

Alpha particles are highly ionizing and lose their energy rapidly within the order of 0.025 mm (25 μm) of the emitting nucleus. Beta particles and gamma rays are less strongly ionizing and have longer ranges: a few millimeters and a few tenths of a metre respectively. This is because alpha particles ionize heavily, and hence lose their energy rapidly; this is in contrast to the lightly ionizing nature of the other two types (Aitken, 1998).

B-1-2. Cosmic radiation

The contribution of cosmic rays to the environmental dose-rate is generally small, but should be included in estimates of the external dose-rate (Aitken, 1985). Cosmic radiation consists of two types of components: the 'soft' component (electrons and photons) which is absorbed by the top 150 g/cm^3 (~0.6m) of overburden; and the 'hard' component, which is mostly composed of muons (Aitken, 1998).

The penetration of cosmic radiation is dependent upon the bulk density of the sample. For a given overburden density, the cosmic ray dose rate can be estimated from the depth of the sample. Geographic location and altitude may also affect the cosmic radiation. All samples were taken within 60m of sea-level and hence no correction for sample altitude was required. Assuming an overburden density is 1.85g/cm^3 (Brady, 1990).

B-2. Methods for assessing radioisotope concentrations

Thick-source alpha counting (TSAC) and Geiger-Muller-beta counting (GM-beta) has been used for dose rate estimation.

B-2-1. Thick Source Alpha Counting (TSAC)

Thick source alpha counting (TSAC) measures the alpha emissions from a sample due to the decay of members of the uranium and thorium decay chains. The total alpha particles emitted from the decay of the U and Th decay chains. In this study, TSAC was undertaken at the Aberystwyth Luminescence Laboratory using Daybreak 582 and 583 alpha-counters. A refinement of the basic TSAC method is to measure the number of coincident pairs of alpha emissions due to the rapid decay of ^{216}Po to ^{212}Pb following its formation from ^{220}Rn, an isotope in the ^{232}Th decay chain (Fig. B-1). Thorium and uranium concentrations can be calculated by comparing the "pairs" count rate with the total alpha count rate (Simon, 2002).

B-2-2. Geiger-Muller-beta (GM-beta) counting

Beta counting at the Aberystwyth Luminescence Laboratory was performed using the Risø GM-25-5 beta counter (Bøtter-Jensen and Mejdahl, 1988). Three dried, ground 1g subsamples of each sample were measured for a period of not less than 24 hours.

B-2-3. High-Resolution Gamma Spectrometry (HRGS)

High-resolution gamma spectrometry (HRGS) gives information on the concentrations of some of the parent and daughter nuclides in the U, Th and K decay chains (Helena, 2006). The radionuclide concentrations of the samples were measured using low-level high resolution gamma spectrometry at Korea Basic Science Institute (KBSI), Korea. Conversion to dose rates used the data presented by Olley et al. (1996). Cosmic ray contributions were calculated using the equations given in Prescott and Hutton (1994).

B-3. Calculation of dose rates

Dose rates were calculated from radioisotope concentrations using the dose-rate conversion factors (Table B-1) of Olley et al. (1996).

B-3-1. Water content correction

Water absorbs some of the radiation that would reach the constituent mineral grains of a sample. This significantly reduces the α, β and γ dose rates experienced by mineral grains, relative to those evaluated using dry dosimetry samples. Attenuation factor of dry dose-rate should be divided in order to obtain wet dose rates. They are given by (1+HWF) where H=1.50 for alpha, 1.25 for beta, and 1.14 for gamma;.

$$\beta_w = \beta_d/(1+1.25WF), \quad \gamma_w = \gamma_d/(1+1.14WF)$$

W is the saturation water content (defined here as the weight of water divided by the dry weight of sediment) and F is the fraction of saturation corresponding to the assumed average water content over the entire burial period (Aitken, 1998). The values given for H are those proposed by Zimmerman (1971); those for beta and gamma have also been discussed by Aitken and Xie (1990).

B-3-2. Attenuation of the beta dose-rate

The degree of attenuation within the grain is dependent on a range of diameter of quartz grains as well as water content of the sediment. The appropriate values for the grain size of quartz used for OSL analysis can be selected to calculate the attenuation. The HF etching for coarse grain sediments will have a disproportionate effect on the beta dose-rate. This is because the exterior of the grain will have a

Nuclide		Specific activity conversion factors		
		Alpha	**Beta**	**Gamma**
Uranium series	**U-238**	0.00973	0.00435	0.00032
	U-234	0.0124	0	0.00007
	Th-230	0.0122	0.00005	0.00006
	Ra-226	0.0125	0.00002	0.00003
	Rn-222	0.0774	0.00481	0.00844
	Pb-210	0.0151	0.00211	0.00001
Thorium series	**Th-232**	0.0437	0.00259	0.00472
	Rn-220	0.0786	0.00451	0.00757
Potassium	**K-40**	0	0.00263	0.00079

Table B-1. Conversion factors used to determine dose rates (Olley et al., 1996), data based on Murray (1981). Conversion of Bq kg^{-1} to counts ksec^{-1}, assuming the count rate is taken on a ZnS screen of 42 mm diameter, conversion from counts ksec-' to dose rate imGy year-') is carried out using euation 4.15 in Aitken (1985).

higher absorbed fraction than the centre of the grain (Mejdahl, 1979). For 4~11 μm fine grain sediment, attenuation of alpha and beta dose is small enough to be negligible (Aitken, 1985).

B-4. The comparison of dose rates between the different methods

　　The dose-rate can be compared from thick source alpha counting and GM-beta counting (TSAC&GM-beta) and high resolution gamma spectrometry (HRGS). The results from TSAC&GM-beta, to those obtained from HRGS are detailed in Table B-2. The ratios of alpha count rate obtained using different methods are close to unity (Fig. B-3). Also, Beta dose-rate of the HRGS method is consistent with those from TSAC&GM-beta (Fig. B-4). The average ratios for the spectrometry methods compared to TSAC&GM-beta are consistent with unity (Beta dose rates are within 3% on average; Alpha counts are within 7% on average) (Table B-3). Therefore, all dose rates are equally suitable for calculate of the dose-rate.

B-5. Dose rate calculation: an example (0519-0)

　　Dose rate of 0519-0 was estimated by measuring Th, U and K concentrations using high resolution gamma spectrometer.

* 0519-0

Nuclide		Ra-226	Ra-228	K-40
Energy	keV	295+392+609	338+911	1460.7
Name	Bq/Kg	58.5	143.1	724
	+/-	0.7	2.7	24.2

➢ U-238~Ra-226 were derived from Ra-226,

➢ Rn-222~Pb-210 were derived from Ra-226 x 0.8 (Radon escape)

➢ Th-232 and Rn220 were derived from Ra-228 (Radon escape was assumed to be negligible)

Nuclide	Activity		Alpha		Beta		Gamma	
	Bq/kg	error	count/ks	error	Gy/ka	error	Gy/ka	error
U-238	58.500	0.700	0.569	0.007	0.254	0.003	0.019	0.000
U-234	58.500	0.700	0.725	0.009	0.000	0.000	0.004	0.000
Th-230	58.500	0.700	0.714	0.009	0.003	0.000	0.004	0.000
Ra-226	58.500	0.700	0.731	0.009	0.001	0.000	0.002	0.000
Rn-222	46.800	0.560	3.622	0.043	0.225	0.003	0.395	0.005
Pb-210	46.800	0.560	0.707	0.008	0.099	0.001	0.000	0.000
Th-232	143.100	2.700	6.253	0.118	0.371	0.007	0.675	0.013
Rn-220	143.100	2.700	11.248	0.212	0.645	0.012	1.083	0.020
K-40	724.000	24.200	0.000	0.000	1.904	0.064	0.572	0.019
Sum			24.570	0.247	3.503	0.065	2.754	0.031

Ex) Error on alpha dose-rate:

$(\sqrt{(0.007^2+0.009^2+0.009^2+0.009^2+0.043^2+0.008^2+0.118^2+0.212^2})$

➢ In this study, conversion factors used to determine dose rates, which data based on Olley et al. (1996).

* Conversion factors used to determine dose rates (Olley et al., 1996), data based on Murray (1981).

1) α contribution

➢ Alpha particles are highly ionizing and lose their energy rapidly. Consequently they have very short ranges. For coarse grain method, α dose rate is assumed to be negligible, because the outer $10\mu m$ of each grain remove due to the HF etch. However, alpha contribution in fine grain sediment (4-11μm) is relatively more important than in coarse grain.

➢ The thermoluminescence per unit length of alpha particle track is independent of particle energy.

- a value: 0.04+/- 0.02 (Rees-Jones, 1995)
- Conversion from counts $ksec^{-1}$ to dose rate ($mGy\ year^{-1}$) is carried out using this equation (Aitken, 1985).
- $D\alpha=1280*a\ value*alpha\ count\ rate$ (Aitken, 1985; equation 4.15).
- Conversion of $Bq\ kg^{-1}$ to $mGy\ year^{-1}$

D_α= 1.280 * 0.04 * 24.570 = 1.258 Gy/ka^{-1}

D_α error= 1.280 * 0.02 * 24.570 = 0.628 Gy/ka^{-1}

- The uncertainty in the alpha dose rate includes random error and associated with measurement on systematic error (3%) associated with conversion factor.

D_α=1±0.03 * 1.258±0.628=1.258 Gy/ka

D_α error= 1.258$\sqrt{(0.03/1)^2+(0.628/1.258)^2}$= 0.630 Gy/ka

D_α = 1.258 ± 0.630 Gy/ka

- Attenuation of alpha dose
  - In this study, we used 4~11μm fine grain sediment. In this grain size, attenuation of alpha dose is small enough to be negligible and is close to 5% (Aitken, 1985; Fig. C.2).
  - Thus, the alpha dose rate is assumed to be negligible in this study.

2) β contribution
  - Attenuation of beta dose in fine grain (4~11μm) sediment shows negligible

attenuation less than 5%. Thus, the beta dose rate is assumed to be negligible in this study (Aitken, 1985).

D_β= 3.503 ± 0.065 Gy/ka

➢ The uncertainty in the beta dose rate includes random error and associated with measurement on systematic error associated with conversion factor.

3% systematic error

D_β=1±0.03 * 3.503±0.063=3.503

D_β error= 3.503√$(0.03/1)^2$+$(0.063/3.503)^2$= 0.124

D_β= 3.503 ± 0.124 Gy/ka

3) γ contribution

➢ No significant attenuation of γ occurs due to grain size.

D_γ= 2.754 ± 0.031 Gy/ka^{-1}

➢ The uncertainty in the gamma dose rate includes random error and associated with measurement on systematic error associated with conversion factor.

3% systematic error

D_γ=1±0.03 * 2.754±0.031=2.754

D_γ error= 2.754√$(0.03/1)^2$+$(0.031/2.754)^2$= 0.088

D_γ= 2.754 ± 0.0883 Gy/ka
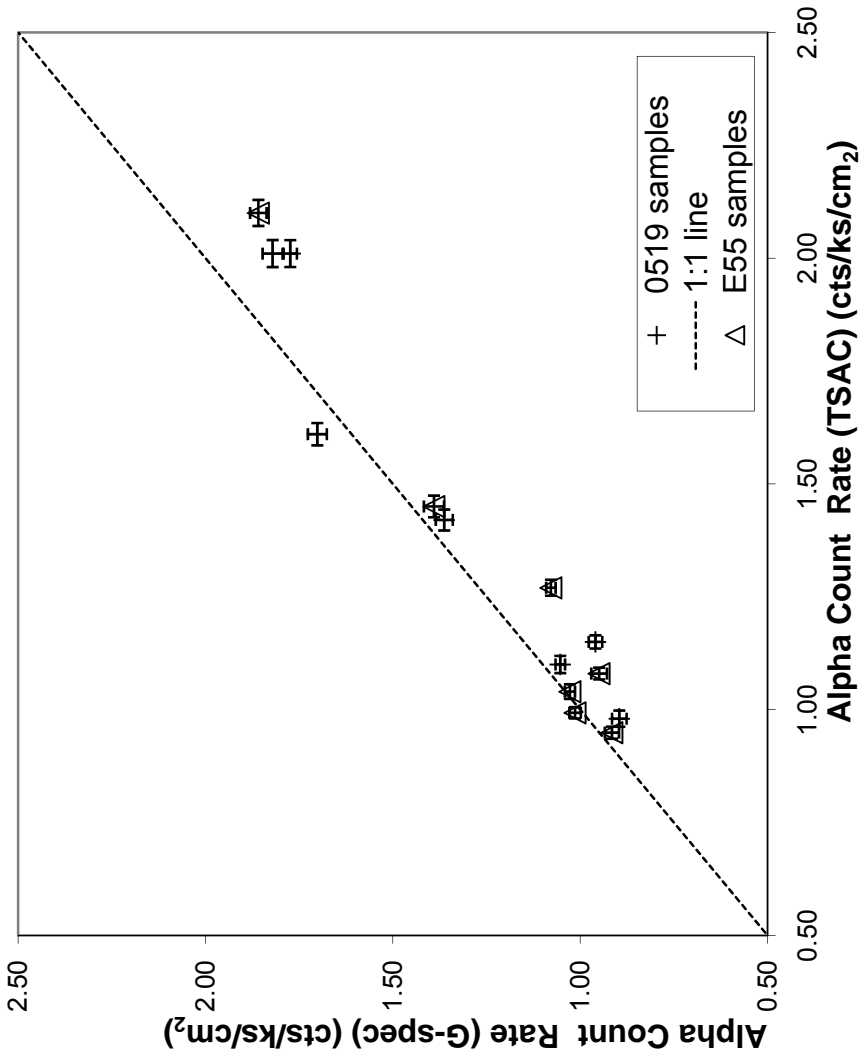
Fig. B-3. The ratios of alpha count rate obtained using thick source alpha counting and GM-beta counting (TSAC&GM-beta) and high resolution gamma spectrometry (HRGS)
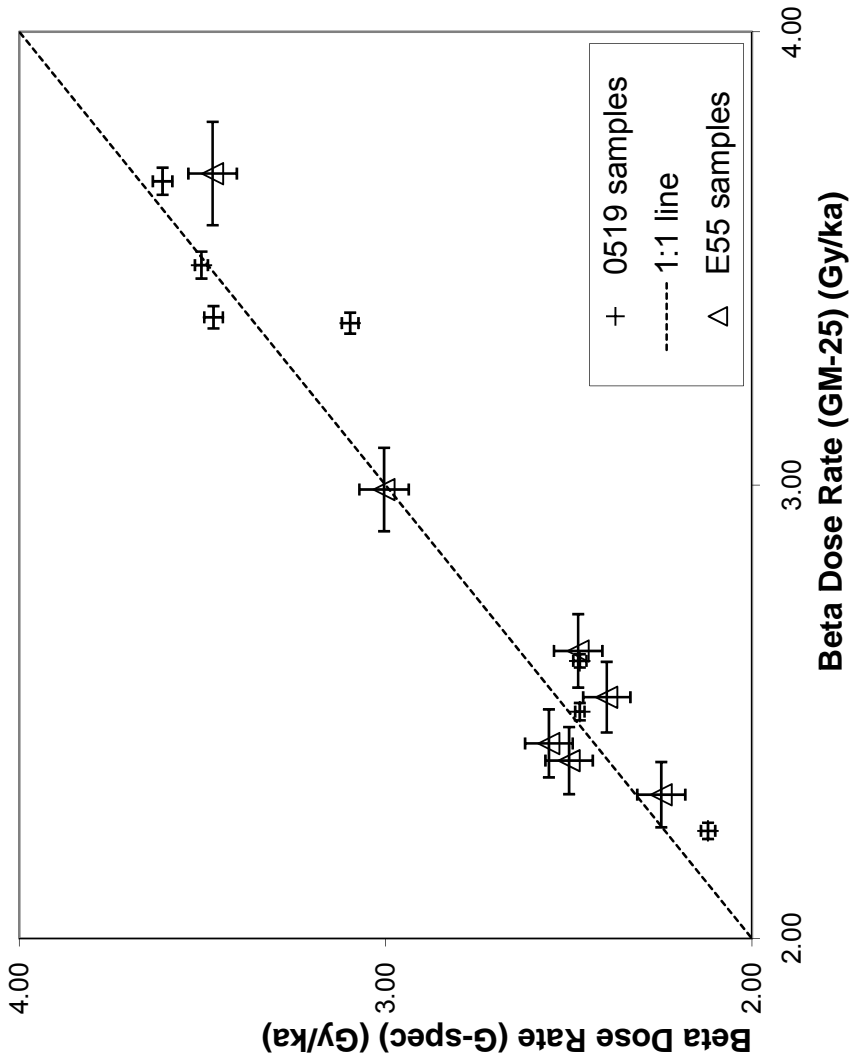
Fig. B-4. The ratios of beta dose rate obtained using thick source alpha counting and GM-beta counting (TSAC&GM-beta) and high resolution gamma spectrometry (HR GS)

Alpha and beta counting results (TSAC&GM-beta)

Samples	Alpha count rate (cts/ks/cm²)		Beta dose rate (Gy/ka)	
0519-0	2.01	± 0.03	3.485	±0.107
0519-1	2.01	± 0.03	3.670	±0.113
0519-2	1.61	± 0.02	3.370	±0.103
0519-3	1.42	± 0.02	3.357	±0.104
0519-4	1.10	± 0.02	2.500	±0.078
0519-5	1.15	± 0.01	2.612	±0.080
0519-6	0.98	± 0.02	2.237	±0.070

High resolution gamma spectrometry results (HRGS)

Alpha count rate (cts/ks)		Alpha count rate (cts/ks/cm²)		Beta Dose Rate (Gy/ka)	
24.570	± 0.247	1.774	± 0.018	3.503	± 0.065
25.221	± 0.369	1.821	± 0.027	3.609	± 0.067
23.569	± 0.351	1.702	± 0.025	3.470	± 0.067
18.878	± 0.315	1.363	± 0.023	3.097	± 0.066
14.589	± 0.176	1.053	± 0.013	2.470	± 0.065
13.289	± 0.250	0.959	± 0.018	2.470	± 0.065
12.409	± 0.269	0.896	± 0.019	2.120	± 0.066

Alpha and beta counting results (TSAC&GM-beta) | | | **High resolution gamma spectrometry results (HRGS)** | |

Sample	Alpha count rate (cts/ks/cm²)		Beta dose rate (Gy/ka)		Alpha count rate (cts/ks)		Alpha count rate (cts/ks/cm²)		Beta Dose Rate (Gy/ka)	
E55S20IV-2	0.95	± 0.01	2.317	±0.072	12.681	± 0.26	0.916	± 0.019	2.248	± 0.066
E55S20IV-3	1.08	± 0.01	2.634	±0.081	13.154	± 0.29	0.950	± 0.021	2.474	± 0.066
E55S20IV-4	0.99	± 0.01	2.430	±0.075	14.044	± 0.21	1.014	± 0.015	2.554	± 0.065
E55S20IV-5	1.04	± 0.02	2.392	±0.074	14.233	± 0.19	1.028	± 0.013	2.499	± 0.065
E55S20IV-6	1.27	± 0.02	2.532	±0.078	14.936	± 0.18	1.078	± 0.013	2.396	± 0.065
E55S20IV-7	1.45	± 0.02	2.990	±0.092	19.259	± 0.37	1.391	± 0.027	3.004	± 0.067
E55S20IV-9	2.10	± 0.03	3.687	±0.114	25.748	± 0.30	1.859	± 0.022	3.472	± 0.066

Table B-2. The dose rate results from TSAC&GM-beta, to those obtained from HRGS.

	Alpha Count Rate	Beta dose rate
Sample	Ratio (G-Spec/TSAC)	Ratio (G-Spec/GM-25)
E55S20IV-2	0.96	0.97
E55S20IV-3	0.88	0.94
E55S20IV-4	1.02	1.05
E55S20IV-5	0.99	1.04
E55S20IV-6	0.85	0.95
E55S20IV-7	0.96	1.00
E55S20IV-9	0.89	0.94
Average	**0.94**	**0.99**

	Alpha Count Rate	Beta dose rate
Sample	Ratio (G-Spec/TSAC)	Ratio (G-Spec/GM-25)
0519-0	0.88	1.01
0519-1	0.91	0.98
0519-2	1.06	1.03
0519-3	0.96	0.92
0519-4	0.96	0.99
0519-5	0.83	0.95
0519-6	0.91	0.95
Average	**0.93**	**0.97**

Table B-3. The dose rate ratios between the thick source alpha counting and GM-beta counting (TSAC&GM-beta) and high resolution gamma spectrometry.

Aberystwyth LDB2005

Dose Rates (Gy/ka)

Sample	Water Content (%)	Depth (m)	Alpha		Beta		Gamma		Cosmic		Total (Gy/ka)	
0519-0	50 ± 5	7	0.953	±0.492	2.125	±0.105	1.917	±0.203	0.092	±0.009	5.086	±0.543
0519-1	45 ± 5	6.3	1.001	±0.517	2.327	±0.118	2.017	±0.211	0.099	±0.010	5.444	±0.571
0519-2	40 ± 5	5.3	0.859	±0.436	2.225	±0.115	1.758	±0.123	0.110	±0.011	4.952	±0.468
0519-3	35 ± 5	4.3	0.773	±0.393	2.313	±0.124	1.671	±0.119	0.123	±0.013	4.881	±0.429
0519-4	35 ± 5	3.3	0.608	±0.311	1.723	±0.092	1.295	±0.103	0.139	±0.015	3.765	±0.341
0519-5	25 ± 5	2.3	0.693	±0.355	1.972	±0.112	1.422	±0.123	0.157	±0.017	4.244	±0.393
0519-6	25 ± 5	1.3	0.599	±0.311	1.688	±0.096	1.277	±0.131	0.178	±0.018	3.742	±0.351

Assuming: a value 0.04±0.02, assume sample density : 1.85 g/cm^3

Dose rates are calculated for 4-11 micron grains of quartz, with the specified water content and burial depth. An error of ±0.2m was used on the depth value.

Dose conversion factors are those from Adamiec and Aitken (1998).

Table B-4. The total dose rate results for 0519 series from TSAC&GM-beta (Aberystwyth LDB2005).

Aberystwyth LDB2005

Dose Rates (Gy/ka)

Sample	Water Content (%)	Depth (m)	Alpha		Beta		Gamma		Cosmic		Total (Gy/ka)	
E55S20IV-2	21 ± 5	0.9	0.608	±0.311	1.818	±0.106	1.259	±0.100	0.187	±0.019	3.873	±0.344
E55S20IV-3	21 ± 5	1.5	0.698	±0.361	2.067	±0.121	1.571	±0.144	0.173	±0.018	4.509	±0.407
E55S20IV-4	20 ± 5	2.1	0.635	±0.327	1.926	±0.113	1.328	±0.120	0.161	±0.017	4.050	±0.366
E55S20IV-5	22 ± 5	2.7	0.644	±0.331	1.859	±0.108	1.350	±0.124	0.149	±0.016	4.002	±0.370
E55S20IV-6	25 ± 5	3.3	0.759	±0.389	1.911	±0.108	1.508	±0.135	0.139	±0.015	4.317	±0.426
E55S20IV-7	26 ± 5	3.9	0.906	±0.461	2.236	±0.126	1.703	±0.125	0.129	±0.014	4.974	±0.494
E55S20IV-9	35 ± 5	5.1	1.113	±0.565	2.541	±0.136	2.192	±0.153	0.113	±0.012	5.959	±0.601

Assuming: a value 0.04±0.02, assume sample density : 1.85 g/cm^3

Dose rates are calculated for 4-11 micron grains of quartz, with the specified water content and burial depth. An error of ±0.2m was used on the depth value.

Dose conversion factors are those from Adamiec and Aitken (1998).

Table B-5. The total dose rate results for 0519 series from TSAC&GM-beta (Aberystwyth LDB2005).

sample	Alpha		Beta		Gamma		Cosmic		Total (Gy/ka)	
0519-0	0.719	± 0.361	2.155	± 0.113	1.754	± 0.085	0.092	± 0.005	**4.721**	**±0.388**
0519-1	0.771	± 0.388	2.310	± 0.123	1.855	± 0.093	0.099	± 0.005	**5.035**	**±0.417**
0519-2	0.754	± 0.379	2.313	± 0.127	1.833	± 0.094	0.111	± 0.006	**5.011**	**±0.411**
0519-3	0.634	± 0.319	2.154	± 0.123	1.599	± 0.085	0.124	± 0.006	**4.511**	**±0.352**
0519-4	0.490	± 0.247	1.718	± 0.101	1.220	± 0.064	0.140	± 0.007	**3.568**	**±0.274**
0519-5	0.495	± 0.249	1.882	± 0.117	1.271	± 0.072	0.157	± 0.008	**3.804**	**±0.285**
0519-6	0.462	± 0.233	1.615	± 0.104	1.133	± 0.066	0.178	± 0.009	**3.388**	**±0.263**
	Alpha		Beta		Gamma		Cosmic		Total (Gy/ka)	
E55S20IV-2	0.494	± 0.249	1.780	± 0.115	1.233	± 0.073	0.187	± 0.009	**3.695**	**± 0.284**
E55S20IV-3	0.512	± 0.258	1.960	± 0.125	1.308	± 0.077	0.174	± 0.009	**3.954**	**± 0.297**
E55S20IV-4	0.553	± 0.279	2.043	± 0.130	1.390	± 0.080	0.161	± 0.008	**4.148**	**± 0.318**
E55S20IV-5	0.548	± 0.276	1.960	± 0.124	1.344	± 0.076	0.150	± 0.007	**4.002**	**± 0.312**
E55S20IV-6	0.556	± 0.280	1.826	± 0.114	1.349	± 0.075	0.140	± 0.007	**3.870**	**± 0.312**
E55S20IV-7	0.709	± 0.357	2.267	± 0.137	1.696	± 0.096	0.130	± 0.007	**4.803**	**± 0.394**
E55S20IV-9	0.864	± 0.435	2.416	± 0.136	1.975	± 0.103	0.113	± 0.006	**5.369**	**± 0.467**

Table B-6. The total dose rate results for 0519 and E55S20IV series from high resolution gamma spectrometer (KBSI 2005).

4) Cosmic dose rate

➤ Cosmic rays can be calculated from the thickness of the sediment overlying the sample.

➤ The cosmic dose rate (Gy/ka) is calculated using equation from Prescott and Hutton (1994). Dc(Gy/ka) is derived from the thickness of the overburden $x(hg/cm_2)$

x= (density of overburden (g/cm^3) * thickness of overburden (cm))/100

Assume sample density: 1.85 g/cm^3, sample depth: 700 cm

D_c=0.21exp(-0.070x+0.0005x^2)

D_c= 0.21exp(-0.070*((1.85*700)/100)+0.0005*((1.85*700)/100)^2)

D_c= 0.0922 ± 0.0046 (5 % of D_c value)

5) Correction for moisture content

➤ Correction of the dry dose rates for moisture content were made using the following equations,

D_α= D_α,dry / 1+1.50WF

D_β= D_β,dry / 1+1.25WF

D_γ= D_γ,dry / 1+1.14WF

➤ D_α, D_β and D_γ are the corrected α, β and γ dose rates.

➤ W is the water content (mass of water/mass of dry sediment).

Water content of 0519-0: 50±5 %

- Alpha dose rate

$D_{\alpha}= 1.258 \pm 0.629$ Gy/ka^{-1}

Corrected alpha dose rate (Gy/ka) = 1.258 / (1+1.5*0.50) = 0.719

Error on alpha dose rate (Gy/ka) =

X=1.5 * 0.5=0.75

$\Delta X= X*\sqrt{(0/1.5)^2+(0.05/0.5)^2}=0.075$

Y=1+X=1.75

$\Delta Y=\sqrt{(0)^2+\Delta X^2}$

$\Delta Y= \Delta X$

$\Delta Y=0.075$

Z=Dα dry/Y

$\Delta Z=Z\sqrt{(\Delta\,D\alpha\,dry/\,D\alpha\,dry)^2+(\,\Delta Y/Y)^2}$

Z=1.258/1.75=0.719 Gy/ka

$\Delta Z=0.719\sqrt{(0.629/1.258)^2+(0.075/1.75)^2}$

$\Delta Z=0.361$ Gy/ka

Error on alpha dose rate (Gy/ka) =0.361 Gy/ka

Corrected D$_{\alpha}$ = 0.719±0.361 Gy/ka

- Beta dose rate

$D_\beta = 3.503 \pm 0.124$ Gy/ka^{-1}

Corrected beta dose rate (Gy/ka) = 3.503/ (1+1.25*0.50) = 2.155

Error on beta dose tate (Gy/ka)   =

X=1.25 * 0.5= 0.625

$\Delta X = X*\sqrt{(0/1.25)^2+(0.05/0.5)^2} = 0.0625$

Y=1+X= 1.625

$\Delta Y = \sqrt{(0)^2 + \Delta X^2}$

$\Delta Y = \Delta X$

$\Delta Y = 0.0625$

Z=Dβ dry/Y

$\Delta Z = Z\sqrt{(\Delta D\beta\ dry/ D\beta\ dry)^2 + (\Delta Y/Y)^2}$

Z=3.503/1.625=2.155 Gy/ka

$\Delta Z = 2.155\sqrt{(0.124 /3.503)^2+(0.0625/1.625)^2}$

$\Delta Z = 0.113$ Gy/ka

Error on beta dose rate (Gy/ka) =0.113 Gy/ka

Corrected D$_\beta$= 2.155±0.113 Gy/ka

- Gamma dose rate

$D_\gamma = 2.754 \pm 0.088$ Gy/ka^{-1}

Corrected gamma dose rate (Gy/ka) = 2.754/ (1+1.14*0.50) = 1.754

Error on gamma dose tate (Gy/ka)=

X=1.14 * 0.5= 0.57

$\Delta X= X*\sqrt{(0/1.14)^2+(0.05/0.5)^2}= 0.057$

Y=1+X= 1.57

$\Delta Y=\sqrt{(0)^2+\Delta X^2}$

$\Delta Y= \Delta X$

$\Delta Y=0.057$

Z=Dγ dry/Y

$\Delta Z=Z\sqrt{(\Delta D\gamma\ dry/ D\gamma\ dry)^2+(\Delta Y/Y)^2}$

Z=2.754 /1.57=1.754 Gy/ka

$\Delta Z=1.754\ \sqrt{(0.088 /2.754)^2+(0.057/1.57)^2}$

$\Delta Z=0.085$ Gy/ka

Error on gamma dose rate (Gy/ka) =0.085 Gy/ka

Corrected D_γ= 2.754 ±0.085 Gy/ka

6) Total dose rate

Error on total dose-rate (Gy/ka)

$(\sqrt{0.361^2+0.113^2+0.085^2+0.0046^2})$ =0.388 Gy/ka

0.719+2.155+1.754+0.0922 = 4.72±0.388 Gy/ka

Nuclide	Activity		Alpha		Beta		Gamma	
Bq/kg	count/ks	error	Gy/ka	error	Gy/ka	error	Gy/ka	error
U-238	64.400	1.200	0.627	0.012	0.280	0.005	0.021	0.000
U-234	64.400	1.200	0.799	0.015	0.000	0.000	0.005	0.000
Th-230	64.400	1.200	0.786	0.015	0.003	0.000	0.004	0.000
Ra-226	64.400	1.200	0.805	0.015	0.001	0.000	0.002	0.000
Rn-222	51.520	0.960	3.988	0.074	0.248	0.005	0.435	0.008
Pb-210	51.520	0.960	0.778	0.014	0.109	0.002	0.001	0.000
Th-232	142.600	4.000	6.232	0.175	0.369	0.010	0.673	0.019
Rn-220	142.600	4.000	11.208	0.314	0.643	0.018	1.079	0.030
K-40	743.500	30.300	0.000	0.000	1.955	0.080	0.587	0.024
sum			25.221		3.609		2.806	

Table B-7. Th, U and K concentrations for 0519-1 from high resolution gamma spectrometer (KBSI 2005).

Nuclide	Activity		Alpha		Beta		Gamma	
Bq/kg	count/ks	error	Gy/ka	error	Gy/ka	error	Gy/ka	error
U-238	57.200	1.200	0.557	0.012	0.249	0.005	0.018	0.000
U-234	57.200	1.200	0.709	0.015	0.000	0.000	0.004	0.000
Th-230	57.200	1.200	0.698	0.015	0.003	0.000	0.003	0.000
Ra-226	57.200	1.200	0.715	0.015	0.001	0.000	0.002	0.000
Rn-222	45.760	0.960	3.542	0.074	0.220	0.005	0.386	0.008
Pb-210	45.760	0.960	0.691	0.014	0.097	0.002	0.000	0.000
Th-232	136.200	3.800	5.952	0.166	0.353	0.010	0.643	0.018
Rn-220	136.200	3.800	10.705	0.299	0.614	0.017	1.031	0.029
K-40	735.100	29.600	0.000	0.000	1.933	0.078	0.581	0.023
sum			23.569		3.470		2.669	

Table B-8. Th, U and K concentrations for 0519-2 from high resolution gamma spectrometer (KBSI 2005).

Nuclide	Activity		Alpha		Beta		Gamma	
Bq/kg	count/ks	error	Gy/ka	error	Gy/ka	error	Gy/ka	error
U-238	45.200	1.100	0.440	0.011	0.197	0.005	0.014	0.000
U-234	45.200	1.100	0.560	0.014	0.000	0.000	0.003	0.000
Th-230	45.200	1.100	0.551	0.013	0.002	0.000	0.003	0.000
Ra-226	45.200	1.100	0.565	0.014	0.001	0.000	0.001	0.000
Rn-222	36.160	0.880	2.799	0.068	0.174	0.004	0.305	0.007
Pb-210	36.160	0.880	0.546	0.013	0.076	0.002	0.000	0.000
Th-232	109.700	3.400	4.794	0.149	0.284	0.009	0.518	0.016
Rn-220	109.700	3.400	8.622	0.267	0.495	0.015	0.830	0.026
K-40	710.300	28.700	0.000	0.000	1.868	0.075	0.561	0.023
sum			18.878		3.097		2.237	

Table B-9. Th, U and K concentrations for 0519-3 from high resolution gamma spectrometer (KBSI 2005).

Nuclide Bq/kg	Activity		Alpha		Beta		Gamma	
	count/ks	error	Gy/ka	error	Gy/ka	error	Gy/ka	error
U-238	42.600	0.600	0.414	0.006	0.185	0.003	0.014	0.000
U-234	42.600	0.600	0.528	0.007	0.000	0.000	0.003	0.000
Th-230	42.600	0.600	0.520	0.007	0.002	0.000	0.003	0.000
Ra-226	42.600	0.600	0.533	0.008	0.001	0.000	0.001	0.000
Rn-222	34.080	0.480	2.638	0.037	0.164	0.002	0.288	0.004
Pb-210	34.080	0.480	0.515	0.007	0.072	0.001	0.000	0.000
Th-232	77.200	1.900	3.374	0.083	0.200	0.005	0.364	0.009
Rn-220	77.200	1.900	6.068	0.149	0.348	0.009	0.584	0.014
K-40	569.400	19.900	0.000	0.000	1.498	0.052	0.450	0.016
sum			14.589		2.470		1.707	

Table B-10. Th, U and K concentrations for 0519-4 from high resolution gamma spectrometer (KBSI 2005).

Nuclide	Activity		Alpha		Beta		Gamma	
Bq/kg	count/ks	error	Gy/ka	error	Gy/ka	error	Gy/ka	error
U-238	36.800	0.900	0.358	0.009	0.160	0.004	0.012	0.000
U-234	36.800	0.900	0.456	0.011	0.000	0.000	0.003	0.000
Th-230	36.800	0.900	0.449	0.011	0.002	0.000	0.002	0.000
Ra-226	36.800	0.900	0.460	0.011	0.001	0.000	0.001	0.000
Rn-222	29.440	0.720	2.279	0.056	0.142	0.003	0.248	0.006
Pb-210	29.440	0.720	0.445	0.011	0.062	0.002	0.000	0.000
Th-232	72.300	2.700	3.160	0.118	0.187	0.007	0.341	0.013
Rn-220	72.300	2.700	5.683	0.212	0.326	0.012	0.547	0.020
K-40	604.600	24.800	0.000	0.000	1.590	0.065	0.478	0.020
sum			13.289		2.470		1.633	

Table B-11. Th, U and K concentrations for 0519-5 from high resolution gamma spectrometer (KBSI 2005).

Nuclide	Activity		Alpha		Beta		Gamma	
Bq/kg	count/ks	error	Gy/ka	error	Gy/ka	error	Gy/ka	error
U-238	36.500	1.000	0.355	0.010	0.159	0.004	0.012	0.000
U-234	36.500	1.000	0.453	0.012	0.000	0.000	0.003	0.000
Th-230	36.500	1.000	0.445	0.012	0.002	0.000	0.002	0.000
Ra-226	36.500	1.000	0.456	0.013	0.001	0.000	0.001	0.000
Rn-222	29.200	0.800	2.260	0.062	0.140	0.004	0.246	0.007
Pb-210	29.200	0.800	0.441	0.012	0.062	0.002	0.000	0.000
Th-232	65.400	2.900	2.858	0.127	0.169	0.008	0.309	0.014
Rn-220	65.400	2.900	5.140	0.228	0.295	0.013	0.495	0.022
K-40	491.300	23.000	0.000	0.000	1.292	0.060	0.388	0.018
sum			12.409		2.120		1.456	

Table B-12. Th, U and K concentrations for 0519-6 from high resolution gamma spectrometer (KBSI 2005).

Nuclide	Activity		Alpha		Beta		Gamma	
Bq/kg	**count/ks**	**error**	**Gy/ka**	**error**	**Gy/ka**	**error**	**Gy/ka**	**error**
U-238	34.500	1.000	0.336	0.010	0.150	0.004	0.011	0.000
U-234	34.500	1.000	0.428	0.012	0.000	0.000	0.002	0.000
Th-230	34.500	1.000	0.421	0.012	0.002	0.000	0.002	0.000
Ra-226	34.500	1.000	0.431	0.013	0.001	0.000	0.001	0.000
Rn-222	27.600	0.800	2.136	0.062	0.133	0.004	0.233	0.007
Pb-210	27.600	0.800	0.417	0.012	0.058	0.002	0.000	0.000
Th-232	69.600	2.800	3.042	0.122	0.180	0.007	0.329	0.013
Rn-220	69.600	2.800	5.471	0.220	0.314	0.013	0.527	0.021
K-40	536.100	23.700	0.000	0.000	1.410	0.062	0.424	0.019
sum			12.681		2.248		1.529	

Table B-13. Th, U and K concentrations for E55S20IV-2 from high resolution gamma spectromet er (KBSI 2005).

Nuclide	Activity		Alpha		Beta		Gamma	
Bq/kg	count/ks	error	Gy/ka	error	Gy/ka	error	Gy/ka	error
U-238	37.100	1.100	0.361	0.011	0.161	0.005	0.012	0.000
U-234	37.100	1.100	0.460	0.014	0.000	0.000	0.003	0.000
Th-230	37.100	1.100	0.453	0.013	0.002	0.000	0.002	0.000
Ra-226	37.100	1.100	0.464	0.014	0.001	0.000	0.001	0.000
Rn-222	29.680	0.880	2.297	0.068	0.143	0.004	0.250	0.007
Pb-210	29.680	0.880	0.448	0.013	0.063	0.002	0.000	0.000
Th-232	70.900	3.100	3.098	0.135	0.184	0.008	0.335	0.015
Rn-220	70.900	3.100	5.573	0.244	0.320	0.014	0.537	0.023
K-40	609.000	26.900	0.000	0.000	1.602	0.071	0.481	0.021
sum			13.154		2.474		1.621	

Table B-14. Th, U and K concentrations for E55S20IV-3 from high resolution gamma spectrometer (KBSI 2005).

Nuclide	Activity		Alpha		Beta		Gamma	
Bq/kg	count/ks	error	Gy/ka	error	Gy/ka	error	Gy/ka	error
U-238	39.200	0.800	0.381	0.008	0.171	0.003	0.013	0.000
U-234	39.200	0.800	0.486	0.010	0.000	0.000	0.003	0.000
Th-230	39.200	0.800	0.478	0.010	0.002	0.000	0.002	0.000
Ra-226	39.200	0.800	0.490	0.010	0.001	0.000	0.001	0.000
Rn-222	31.360	0.640	2.427	0.050	0.151	0.003	0.265	0.005
Pb-210	31.360	0.640	0.474	0.010	0.066	0.001	0.000	0.000
Th-232	76.100	2.300	3.326	0.101	0.197	0.006	0.359	0.011
Rn-220	76.100	2.300	5.981	0.181	0.343	0.010	0.576	0.017
K-40	617.400	22.900	0.000	0.000	1.624	0.060	0.488	0.018
sum			14.044		2.554		1.707	

Table B-15. Th, U and K concentrations for E55S20IV-4 from high resolution gamma spectrometer (KBSI 2005).

Nuclide	Activity		Alpha		Beta		Gamma	
Bq/kg	count/ks	error	Gy/ka	error	Gy/ka	error	Gy/ka	error
U-238	43.500	0.700	0.423	0.007	0.189	0.003	0.014	0.000
U-234	43.500	0.700	0.539	0.009	0.000	0.000	0.003	0.000
Th-230	43.500	0.700	0.531	0.009	0.002	0.000	0.003	0.000
Ra-226	43.500	0.700	0.544	0.009	0.001	0.000	0.001	0.000
Rn-222	34.800	0.560	2.694	0.043	0.167	0.003	0.294	0.005
Pb-210	34.800	0.560	0.525	0.008	0.073	0.001	0.000	0.000
Th-232	73.400	2.000	3.208	0.087	0.190	0.005	0.346	0.009
Rn-220	73.400	2.000	5.769	0.157	0.331	0.009	0.556	0.015
K-40	587.400	20.800	0.000	0.000	1.545	0.055	0.464	0.016
sum			14.233		2.499		1.681	

Table B-16. Th, U and K concentrations for E55S20IV-5 from high resolution gamma spectrometer (KBSI 2005).

Nuclide	Activity		Alpha		Beta		Gamma	
Bq/kg	count/ks	error	Gy/ka	error	Gy/ka	error	Gy/ka	error
U-238	39.300	0.600	0.382	0.006	0.171	0.003	0.013	0.000
U-234	39.300	0.600	0.487	0.007	0.000	0.000	0.003	0.000
Th-230	39.300	0.600	0.479	0.007	0.002	0.000	0.002	0.000
Ra-226	39.300	0.600	0.491	0.008	0.001	0.000	0.001	0.000
Rn-222	31.440	0.480	2.433	0.037	0.151	0.002	0.265	0.004
Pb-210	31.440	0.480	0.475	0.007	0.066	0.001	0.000	0.000
Th-232	83.300	1.900	3.640	0.083	0.216	0.005	0.393	0.009
Rn-220	83.300	1.900	6.547	0.149	0.376	0.009	0.631	0.014
K-40	537.500	18.800	0.000	0.000	1.414	0.049	0.425	0.015
sum			14.936		2.396		1.733	

Table B-17. Th, U and K concentrations for E55S20IV-6 from high resolution gamma spectrometer (KBSI 2005).

Nuclide	Activity		Alpha		Beta		Gamma	
Bq/kg	count/ks	error	Gy/ka	error	Gy/ka	error	Gy/ka	error
U-238	52.400	1.300	0.510	0.013	0.228	0.006	0.017	0.000
U-234	52.400	1.300	0.650	0.016	0.000	0.000	0.004	0.000
Th-230	52.400	1.300	0.639	0.016	0.003	0.000	0.003	0.000
Ra-226	52.400	1.300	0.655	0.016	0.001	0.000	0.002	0.000
Rn-222	41.920	1.040	3.245	0.080	0.202	0.005	0.354	0.009
Pb-210	41.920	1.040	0.633	0.016	0.088	0.002	0.000	0.000
Th-232	105.700	4.000	4.619	0.175	0.274	0.010	0.499	0.019
Rn-220	105.700	4.000	8.308	0.314	0.477	0.018	0.800	0.030
K-40	658.600	30.400	0.000	0.000	1.732	0.080	0.520	0.024
sum			19.259		3.004		2.199	

Table B-18. Th, U and K concentrations for E55S20IV-7 from high resolution gamma spectrometer (KBSI 2005).

Nuclide	Activity		Alpha		Beta		Gamma	
Bq/kg	count/ks	error	Gy/ka	error	Gy/ka	error	Gy/ka	error
U-238	72.300	1.000	0.703	0.010	0.315	0.004	0.023	0.000
U-234	72.300	1.000	0.897	0.012	0.000	0.000	0.005	0.000
Th-230	72.300	1.000	0.882	0.012	0.004	0.000	0.004	0.000
Ra-226	72.300	1.000	0.904	0.013	0.001	0.000	0.002	0.000
Rn-222	57.840	0.800	4.477	0.062	0.278	0.004	0.488	0.007
Pb-210	57.840	0.800	0.873	0.012	0.122	0.002	0.001	0.000
Th-232	139.100	3.300	6.079	0.144	0.360	0.009	0.657	0.016
Rn-220	139.100	3.300	10.933	0.259	0.627	0.015	1.053	0.025
K-40	671.100	25.400	0.000	0.000	1.765	0.067	0.530	0.020
sum			25.748		3.472		2.763	

Table B-19. Th, U and K concentrations for E55S20IV-9 from high resolution gamma spectromet er (KBSI 2005).

References

Adamiec, G., Bailey, R.M., Wang, X.L., Wintle, A.G., 2008. The mechanism of thermally transferred optically stimulated luminescence in quartz. Journal of Physics D: Applied Physics 41, 135503.

Aitken, M.J., 1985. Themoluminescence dating. Academic, London.

Aitken, M.J., Xie, J., 1990. Moisture correction for annual gamma dose. Ancient TL, v. 8, p. 6-9.

Aitken, M.J., 1998. An Introduction to Optical Dating. Oxford University Press, Oxford.

Alexander, C.R., DeMaster, D.J., Nittrouer, C.A., 1991. Sediment accumulation in a modern epicontinental-shelf setting: the Yellow Sea. Marine Geology, v. 98, p. 51-72.

An, Z., 2000. The history and variability of the East Asian paleomonsoon climate. Quaternary Science Reviews, v.19, p. 171-187.

Bae, K.D., 1988. The significance of the Chongokni industry in the tradition of Paleolithic culture in East Asia. Department of Anthropology, University of California. Berkeley, unpublished Ph.D. thesis.

Bae, K.D., 1989. Excavation Report of Chongokni (Campaign in 1986). Museum of Seoul National University, Seoul. (In Korean)

Bae, K.D., 1992. Palaeolithic tradition of East Asia: Chongoknian. In Proceedings of 1st International Symposium on Cultural Properties. pp. 193-211, National Institute of Cultural Properties of Korea, Seoul.

Bae, K.D., Hong, M.Y., Lee, H.Y., Kim, Y.Y., 2001. Report of Test-Pits Excavation of the Chongok Paleolithic Site in 2000-2001. The Institute of Cultural Properties of Hanyang University, Yeoncheon. (In Korean)

Bailey, R.M., Smith, B.W., Rhodes, E.J., 1997. Partial bleaching and decay form characteristics of quartz OSL. Radiation Measurements, v. 27, p. 123-136.

Bailey, S.D., Wintle, A.G., Duller, G.A.T., Bristow, C.S., 2001. Sand deposition during the last millennium at Aberffraw, Anglesey, North Wales as determined by OSL dating of quartz. Quaternary Science Review, v. 20, p. 701-704.

Balashov, Y.A., Ronov, A.B., Migdisov, A.A., Turanskaya, N.V., 1964. The effect of climate and facies environment on the fractionation of the rare earth elements during sedimentation. Geochemistry International, v. 1, p. 951-969.

Banerjee, D., Murray, A.S., Bøtter-Jensen, L., Lang, A., 2001. Equivalent dose estimation using a single aliquot of polymineral fine grains. Radiation Measurements v. 33, p. 73-94.

Berger, G.W., Luternauer, I.J., 1987. Preliminary field work for thermoluminescence dating studies at the Fraser River delta, British Columbia. Geological Survey of Canada Paper v. 87/IA, p. 901-904.

Bøtter-Jensen, L., Mejdahl, V., 1988. Assessment of beta dose-rate using a GM multicounter system. Nuclear Tracks and Radiation Measurements, v. 14, p. 187-191.

Bøtter-Jensen, L., McKeever, S.W.S., Wintle, A.G., 2003. Optically Stimulated Luminescence Dosimetry. Elsevier, Amsterdam.

Blair, M.W., Yukihara, E.G., McKeever, S.W.S., 2005. Experiences with single-aliquot OSL procedures using coarse-grain feldspars. Radiation Measurements v. 39, p. 361-374.

Boles, J.R., Franks, S.G., 1979. Clay diagenesis in Wilcox sandstones of southwest Texas: implications of smectite diagenesis on sandstone cementation. Journal of Sedimentary Petrology, v. 49, p. 55-70.

Brady, N.C., 1990. Nature and Properties of Soils, 10th edition. Macmillan, New York.

Buylaert, J.P., Murray, A.S., Huot, S., Vriend, M.G.A., Vandenberghe, D., De Corte, F., van den Haute, P., 2006. A comparison of quartz OSL and isothermal TL measurements on Chinese loess. Radiation Protection Dosimetry v. 119, p. 474-478.

Burbidge, C.I., Duller, G.A.T., Roberts, H.M., 2006. D_e determination for young samples using the standardised OSL response of coarse-grain quartz. Radiation Measurements v. 41, p. 278–288.

Chang, J.H., Park,Y.A., Han, S.J., 1996. Late quaternary stratigraphy and sea-level change in the tidal flat of Gomso Bay, west coast of Korea. The Sea: J. Korean Soc. Oceanogr, v. 1, p. 59–72 (in Korean).

Choi, J.H., Murray, A.S., Jain, M., Cheong, C.S., Chang, H.W., 2003. Luminescence dating of well-sorted marine terrace sediments on the southeastern coast of Korea. Quaternary Science Reviews, v. 22, p. 407-421.

Choi, J.H., 2004. Luminescence ages of Quaternary marine sediments on the Eastern coast of Korea and their geomorphic implications. Unpublished Ph.D thesis, Seoul National University, Korea.

Choi, et al., 2004. Age estimate of the Chongok Basalt with Luminescence dating: preliminary result. In Proceedings of Annual Joint Conference, p. 7-9, Petrological Society and Mineralogical Society of Korea, Cheongju.

Choi, J.H., Murray, A.S., Cheong, C.-S., Hong, D.G., Chang, H.W., 2006. Estimation of equivalent dose using quartz isothermal TL and the SAR procedure. Quaternary Geochronology, v. 1, p. 101-108.

Chung, Y-H., 1996. Problems of studies of North Korean Palaeolithic cave sites. In Proceedings of International Symposium on the Palaeolithic Cave Sites and Culture in Northeast Asia. Edited by Yung-Jo Lee. p. 23- 37, Chungbuk National University Museum, Cheongju. (In Korean)

Coe, R.S., Singer, B.S., Pringle, M.S., Zhao, X.X., 2004. Matuyama–Brunhes reversal and Kamikatsura event on Maui: paleomagnetic directions, 40Ar/39Ar ages and implications. Earth and Planetary Science Letters v. 222, p. 667–684.

Colls, A.E., Stokes, S., Blum, M.D., Straffin, E., 2001. Age limits on the Late Quaternary evolution of the upper Loire River. Quaternary Science Reviews, v. 20, p. 743-750.

Danhara, T., Bae, K., Okada, T., Matsufuki, K., Hwang, S., 2002. What is the real age of the Chongokni Paleolithic site? A new approach by fission track dating, K-Ar dating and tephra analysis. In: Bae, K. and Lee, J. (Eds.), Paleolithic Archaeology in Northeast Asia. The Institute of Cultural Properties, Hanyang University, p. 77-116.

Davies, B.E., 1980. Applied Soil Trace Elements. New York, Wiley, 482p.

Duller, G.A.T., Bøtter-Jensen, L., 1993. Luminescence from potassium feldspars stimulated by infrared and green light. Radiation Protection Dosimetry, v. 47, p. 683-688.

Duller, G.A.T., 1994. Luminescence dating of poorly bleached sediments from Scotland. Quaternary Geochronology, v. 13, p. 521-524.

Duller, G.A.T., Bøtter-Jensen L., Kohsiek P., Murray A.S., 1999a. A high sensitivity optically stimulated luminescence scanning system for measurement of single sand-sized grains. Radiation protection Dosimetry, v. 84, p. 325-330.

Duller, G.A.T., Bøtter-Jensen L., Murray A.S and Truscott A.J., 1999b. Single grain laser luminescence (SGLL) measurements using a novel automated reader. Nuclear Instruments and Methods. v. 155, p. 506-514.

Duller, G.A.T., Murray, A.S., 2000. Luminescence dating of sediments using individual mineral grains. GEOLOGOS, v. 5, p. 88-106.

Duller, G.A.T., 2003. Distinguishing quartz and feldspar in single grain luminescence measurements. Radiation Measurements, v. 37, p. 161-165.

Duller, G.A.T., 2007. Assessing the error on equivalent dose estimates derived from single aliquot regenerative dose measurements. Ancient TL, v. 25, p. 15-24.

Fuller, I.C., Wintle, A.G., Duller, G.A.T., 1994. Test of the partial bleach methodology as applied to the infra-red stimulated luminescence of an alluvial sediment from the Danube, Radiation Measurements, v. 23, p. 539-544.

Gallet, S., Jahn, B-M., Torii, M., 1996. Geochemical characterization of the Luochuan loess-paleosol sequence, China, and paleoclimatic implications. Chemical geology, v. 133, p. 67-88.

Gallet, S., Jahn, B-M., Lanoë, V.V., Dia, A., Rossello, E., 1998. Loess geochemistry and its implications for particle origin and composition of the upper continental crust. Earth and Planetary Science Letters, v. 156, p. 157-172.

Gao, S., Park, Y.A., Zhao, Y.Y., Qin, Y.S., 1996. Transport and resuspension of fine-grained sediments over the southeastern Yellow Sea. In: Lee, C.B., Zhao, Y.Y. (Eds.), Proceedings of the Korean-China international seminar on Holocene and late Pleistocene environments in the Yellow Sea Basin, Nov. 20-22, 1996. Seoul National University, Seoul, Korea, p. 83-98.

Goble, R.J., Rittenour, T.M., 2006. A linear modulation OSL study of the unstable ultrafast component in samples from Glacial Lake Hitchcock, Massachusetts, USA, *Ancient TL*, v. 24, p. 37–46.

Godfrey-Smith, D.I., Huntley, D.J., Chen, W-H., 1988. Optical dating studies of quartz and

feldspar sediment extracts. Quaternary Science Review, v. 7, p. 373-380.

Helena, R., 2006. Developing a luminescence chronology for late Quaternary fluvial change in South African floodplain wetlands. Unpublished Ph.D thesis, University of Wales, Aberystwyth.

Huntley, D.J., Godfrey-Smith, D.I., Thewalt, M.L.W., 1985. Optical dating of sediments. Nature, v. 313, p. 105-107.

Huntley, D.J., Lamothe, M., 2001. Ubiquity of anomalous fading in K-feldspars and the measurement and correction for it in optical dating. Canadian Journal of Earth Sciences, v. 38, p. 1093-1106.

Imbrie, J., Hays, J.D., Martinson, D.G., McIntyre, A., Mix, A.C., Morley, J.J., Pisias, N.G., Prell, W.L., Shackleton, N.J., 1984. The orbital theory of Pleistocene climate: support from a revised chronology of the marine $\delta^{18}O$ record. Berger, A.L. et al. (Eds.), Milankovitch and Climate, Part 1. D. Reidel. 269-305.

Jahn, B-M., Gallet, S., Han, J., 2001. Geochemistry of the Xining, Xifeng and Jixian sections, Loess Plateau of China: eolian dust provenance and paleosol evolution during the last 140 ka. Chemical Geology, v. 178, p. 71-94.

Jain, M., Tandon, S.K., Bhatt, S.C., Singhvi, A.K., Mishra, S., 1999. Alluvial and aeolian sequences along the River Luni, Barmer district: physical stratigraphy and feasibility of luminescence chronology methods. Memoir Geological Society of India, v. 42, p. 273-295.

Jain, M., Bøtter-Jensen, L., Murray, A.S., Jungner, H., 2002. Retrospective dosimetry: dose evaluation using unheated and heated quartz from a radioactive waste storage building. Radiation Protection Dosimetry, v. 101, p. 525-530.

Jain, M., Murray, A.S., Bøtter-Jensen, L., 2003. Characterisation of blue-light stimulated luminescence components in different quartz samples: implications for dose measurement. Radiation Measurements, v. 37, p. 441-449.

Jain, M., Murray, A.S., Bøtter-Jensen, L., Wintle, A.G., 2005. A single-aliquot regenerative-dose method based on IR (1.49 eV) bleaching of the fast OSL component in quartz. Radiation Measurements, v. 39, p. 309-318.

Kim, W.Y., Chung, Y-H., Choi, M-J., 1981. Study of Korean Palaeolithic Culture. Korean Institute of Humanistic Study, Seoul (In Korean).

Kim, K.H., Kim, O.J., Min, K.D., Lee, Y.S., 1984. Structural, paleomagnetic and petrological studies of the Chugaryeong Rift Valley, Journal of Mining Geology, v. 17, p. 215-230.

Kim, J.C., Duller, G.A.T., Roberts, H.M., Wintle, A.G., Lee, Y.I., Yi, S.B., 2009a. Dose dependence of thermally transferred optically stimulated luminescence signals in quartz. Radiation Measurements, doi:10.1016/j.radmeas.2008.12.001.

Kim, J.C., Roberts, H.M., Duller, G.A.T., Lee, Y.I., Yi, S.B., 2009b. Assessment of diagnostic tests for evaluating the reliability of SAR D_e values from polymineral and quartz fine grains. Radiation Measurements, doi:10.1016/j.radmeas.2009.01.003.

Kim, J.C., Duller, G.A.T., Roberts, H.M., Wintle, A.G., Lee, Y.I., Yi, S.B., 2009c. Re-evaluation of the chronology of the palaeolithic site at Jeongokri, Korea, using OSL and TT-OSL signals from quartz. Quaternary Geochronology, doi:10.1016/j.quageo.2009.02.005.

Kojima, M., 1983. Dating of the basalt from the Chongokni Palaeolithic site. In Chongokni, p. 586- 588, National Institute of Cultural Properties of Korea, Seoul. (In Japanese)

Kuhns, C.K., Agersnap Larsen, N., McKeever, S.W.S., 2000. Characteristics of LM-OSL from several different types of quartz. Radiation Measurements, v. 32, p. 413-418.

Kukla, G., Heller, F., Liu, X.M., Liu, T.S., An, Z.S., 1988. Pleistocene climates in China dated by magnetic susceptibility, Geology, v. 16, p. 811–814.

Kukla, G., An, Z.S., 1989. Loess stratigraphy in central China. Palaeography, Palaeoclimatology, Palaeoecology, v. 72, p. 203–225.

Lai, Z.-P., 2006. Testing the use of an OSL standardised growth curve (SGC) for D_e determination on quartz from the Chinese Loess Plateau. Radiation Measurements, v. 41, p. 9–16.

Lai, Z.-P., Brückner, H., Zöller, L., Fülling, A., 2007. Existence of a common growth curve for silt-sized quartz OSL of loess from different continents. Radiation Measurements, v. 42, p. 1432–1440.

Lamothe, M., Auclair, M., 1999. A solution to anomalous fading and age shortfalls in optical dating of feldspar minerals. Earth and Planetary Science Letters, v. 171, p. 319-323.

Lee, D.S., Ryu, K.J., Kim, G.H., 1983. Geotectonic interpretation of Choogaryong Rift Valley, Korea. Journal of the Geological Society of Korea, v. 19, p. 19-38.

Lee, S.H., Lee, Y.I., Yoon, H,I., Yoo, K-C., 2008. East Asian monsoon variation and climate changes in Jeju Island, Korea, during the latest Pleistocene to early Holocene. Quaternary Research, v. 70, p. 265-274.

Le Maitre, R.W., 1981. GENMIX – a generalized petrological mixing model program. Comput. Geosci, v. 7, p. 229-247.

Lee, Y.I., Y, S., 2002. Characteristics of Pyeongchang-ri Paleolithic-site paleosols, Yongin-si, Gyeonggi-do, Korea: implications for archaeogeological application. Journal of the Geological Society of Korea, v. 38, p. 471-489.

Lee, Y.I., 2009. Geochemistry of shales of the Upper Cretaceous Hayang Group, SE Korea: Implications for provenance and source weathering at an active continental margin. Sedimentary Geology, doi:10.1016/j.sedgeo.2008.12.004.

Li, B., Li, S.-H., 2006. Studies of thermal stability of charges associated with thermal transfer of OSL from quartz. Journal of Physics D: Applied Physics 39, 2941–2949.

Li, B., Li, S.-H., Wintle, A.G., 2006. Observations of thermal transfer and the slow component of OSL signals from quartz. Radiation Measurements, v. 41, p. 639–648.

Liu, T.S et al., 1985. Loess and the Environment. China Ocean Press, Beijing, p. 191-208.

Liu, T.S., Ding, Z.L., 1998. Chinese loess and the paleomonsoon. Annual Review of Earth and Planetary Sciences, v. 26, p. 111-145.

Liu, J., Saito, Y., Kong, X., Wang, H., Zhao, L., 2009. Geochemical characteristics of sediment as indicators of post-glacial environmental changes off the Shandong Peninsula in the Yellow Sea. Continental Shelf Research, v. 29, p. 846-855.

Machida, H., Arai, F., 1992. Atlas of tephra in and around Japan. Univ. Tokyo Press, p. 1-276.

Machida, H., 1999. Quaternary widespread tephra catalog in and around Japan: Recent progress. The Quaternary Research (Daiyonki-kenkyu), v. 38, p. 194-201.

McKeever, S.W.S., Chen, R., 1997. Luminescence models. Radiation Measurements, v. 27, p. 625-661.

McLennan, S.M., 2001. Relationships between the trace element composition of sedimentary rocks and upper continental crust. Geochemistry Geophysics Geosystems, v.2, p. 2000GC000109.

Mejdahl, v., 1979. Thermoluminescence dating: beta-dose attenuation in quartz grains. Archaeometry, v. 21, p. 61-72.

Miyairi, Y., Yoshida, K., Miyazaki, Y., Matsuzaki, H., Kaneoka, I., 2004. Improved ^{14}C dating of a tephra layer (AT tephra, Japan) using AMS on selected organic fractions. Nuclear Instruments and Methods in Physics Research Section B: Beam Interactions with Materials and Atoms, v. 223-224, August 2004, p. 555-559

Movius, H.L. Jr., 1948. The Lower Palaeolithic cultures of southern and eastern Asia. Transactions of the American Philosophical Society, v. 38, p. 329-420.

Movius, H.L. Jr., 1949. The Lower Palaeolithic Cultures of Southern and Eastern Asia. Transactions of the American Philosophical Society, N. S. 38: 329-420.

Murray, A.S., 1981. Environmental Radioactivity Studies; Relevant to Thermoluminescence Dating. Unpublished D.Phil. thesis, Oxford University.

Murray, A.S., Olley, J.M., Caitcheon, G.G., 1995. Measurement of equivalent doses in quartz from contemporary water-lain sediments using optically stimulated luminescence. Quaternary Science Reviews, v. 14, p. 365-371.

Murray, A.S., Roberts, R.G., 1998. Measurement of the equivalent dose in quartz using a regenerative-dose single-aliquot protocol. Radiation Measurements, v. 29, p. 503-515.

Murray, A.S., Wintle, A.G., 1998. Factors controlling the shape of the OSL decay curve in quartz. Radiation Measurements, v. 29, p. 65-79.

Murray, A.S., Wintle, A.G., 2000. Luminescence dating of quartz using an improved single-aliquot regenerative-dose protocol. Radiation Measurements, v. 32, p. 57-73.

Murray, A.S., Clemmensen, L.B., 2001. Luminescence dating of Holocene aeolian sand movement, Thy, Denmark, Quaternary Science Review, v. 20, p. 751-754.

Murray, A.S., Olley, J.M., 2002. Precision and accuracy in the optically stimulated

luminescence dating of sedimentary quartz: a status review. Geochronometria, v. 21, p. 1-15.

Murray, A.S., Funder, S., 2003. Optically stimulated luminescence dating of a Danish Eemian coastal marine deposit: a test of accuracy. Quaternary Science Reviews, v. 22, p. 1177-1183.

Murray, A.S., Wintle, A.G., 2003. The single-aliquot regenerative dose protocol: potential for improvements in reliability. Radiation Measurements, v. 37, p. 377-381.

Murray, A.S., Svendsen, J.I., Mangerud, J., Astakhov, V.I., 2007. Testing the accuracy of quartz OSL dating using a known-age Eemian site on the river Sula, northern Russia. Quaternary Geochronology, v. 2, p. 102–109.

Murray, A., Buylaert, J.-P., Henriksen, M., Svendsen, J.-I., Mangerud, J., 2008. Testing the reliability of quartz OSL ages beyond the Eemian. Radiation Measurements, v. 43, p. 776–780.

Naruse, T., Bae, K., Matsufuji, K., Danhara, T., Hayashida, A., Hwang, S., Yu, K.M., Yum, J.G., Shin, J.B., 2003. Loess-paleosol sequence in the Chongokni Paleolithic site. In: Bae, K. (Ed.), Paleolithic Archaeology in Northeast Asia, Hanyang University, v. 2, p. 143-156.

Nesbitt, H.W., 1979. Mobility and fractionation of rare earth elements during weathering of a granodiorite. Nature, v. 279, p. 206-210.

Nesbitt, H.W., Young, G.M., McLennan, S.M., Keays, R.R., 1996. Effects of chemical weathering and sorting on the petrogenesis of siliciclastic sediments, with implication for provenance studies. Journal of Geology, v. 104, p. 525-542.

Norton, C.J., Bae, K., Harris, J.W.K., Lee, H., 2006. Middle Pleistocene handaxes from the Korean Peninsula. Journal of Human Evolution, v. 51, p. 527-536.

Olley, J., Murray, A. S., Roberts, R. G., 1996. The effects of disequilibria in the uranium and thorium decay chains on burial dose rates in fluvial sediments. Quaternary Geochronology, v. 15, p. 751-760.

Olley, J.M., Caitcheon, G.G., Murray, A.S., 1998. The distribution of apparent dose as determined by optically stimulated luminescence in small aliquots of fluvial quartz: implications for dating young sediments. Quaternary Science Reviews, v. 17, p. 1033-1040.

Olley, J.M., Caitcheon G.G., Roberts R.G., 1999. The origin of dose distributions in fluvial sediments, and the prospect of dating single grains from fluvial deposits using optically stimulated luminescence. Radiation Measurements, v. 30, p. 207-217.

Osmond, J. K., Cowart, J. B., 1982. Groundwater. In "Uranium Series Disequilibrium: Applications to Environmental Problems". M. lvanovich and R. S. Harmon. Oxford, Clarendon Press.

Packman, S.C., Mauz, B., Rousseau, D.-D., Antoine, P., Rossignol, J., Lang, A., 2007. Implications of broad dose distributions obtained with the single-aliquot regenerative-dose method on quartz fine-grains from loess. Quaternary Geochronology, v. 2, p. 39-44.

Pagonis, V., Wintle, A.G., Chen, R., Wang, X.L., 2008. A theoretical model for a new dating protocol for quartz based on thermally transferred OSL (TT-OSL). Radiation Measurements, v. 43, p. 704-708.

Park, C-S., Yoon, S-O., Hwang, S., 2007. Properties and Provenance of Loess-paleosol Sequence at the Daebo Granite Area of Buan, Jeonbuk Province, South Korea. Journal of the Korean Geographical Society, v. 42, p.898-913.

Park, D.W., 1987. The loess-like red yellow soils of the south western coastal area of Korea in comparison with the loess of China and Japan. Geojournal, v. 15, p. 197-200.

Park, S.C., Lee, H.H., Han, H.S., Lee, G.H., Kim, D.C., Yoo, D.G., 2000. Evolution of late Quaternary mud deposits and recent sediment budget in the southeastern Yellow Sea. Marine Geology, v. 170, p. 271– 288.

Pawley, S.M., Bailey, R.M., Rose, J., Moorlock, B.S.P., Hamblin, R.J.O., Booth, S.J., Lee, J.R., 2008. Age limits on Middle Pleistocene glacial sediments from OSL dating, north Norfolk, UK. Quaternary Science Reviews, v. 27, p. 1363–1377.

Rees-Jones, J. 1995. Optical dating of young sediments using fine-grain quartz. Ancient TL 13, 9-14.

Porat, N., Zilberman. E., Amit. R., Enzel. Y., 2001. Residual ages of modern sediments in an hyperarid region, Israel. Quaternary Science Reviews, v. 20, p. 795-798.

Porat, N., Duller, G.A.T., Roberts, H.M., Wintle, A.G., 2009. A simplified SAR protocol for TT-OSL. Radiation Measurements, doi:10.1016/j.radmeas.2008.12.004.

Porter, S.C., An, Z., 1995. Correlation between climate events in the North Atlantic and China during the last glaciation. Nature, v. 375, p. 305-308.

Porter, S.C., Hallet, B., Wu, X.H., An, Z.S., 2001. Dependence of nearsurface magnetic susceptibility on dust accumulation rate and precipitation on the Chinese Loess Plateau. Quaternary Research, v. 55, p. 271– 283.

Prescott, J.R. and Hutton, J.T., 1994, Cosmic ray contribution to dose rates for luminescence and ESR dating: large depths and long-term time variation. Radiation Measurements, v. 23, p. 497-500.

Qin, Y.S., Li, F., 1983. Study of influence of sediment loads discharged from the Huanghe River on sedimentation in the Bohai sea and the Huanghe sea. Sedimentation on the Continental Shelf: With Special Reference to the East China Sea 2. China Ocean Press, Qingdao, p. 83-92.

Ren, M.E., Shi, Y.L., 1986. Sediment discharge of the Yellow River (China) and its effect on the sedimentation of the Bohai and the Yellow Sea. Cont. Shelf Res, v. 6, p. 785-810.

Rhodes, E.J., Bailey, R.M., 1997. The effect of thermal transfer on the zeroing of the luminescence of quartz from recent glaciofluvial sediments. Quaternary Science Review, v. 16, p. 291-298.

Rhodes, E.J., 2000. Observations of thermal transfer OSL signals in glacigenic quartz. Radiation measurement, v. 32, p. 595-602.

Richardson, C.A., 1994. Effects of bleaching on the sensitivity to dose of the infrared-stimulated luminescence of potassium-rich feldspars from Ynyslas, Wales. Radiation Measurements, v. 23, p. 587-592.

Rittenour, T., 2008. Luminescence dating of fluvial deposits: applications to geomorphic, paleoseismic and archaeologic research. Boreas, v. 37, p. 613–635.

Roberts, H.M., Wintle, A.G., 2001. Equivalent dose determinations for polymineralic fine-grains using the SAR protocol: application to a Holocene sequence of the Chinese Loess Plateau. Quaternary Science Reviews, v. 20, p. 859-863.

Roberts, H.M., Wintle, A.G., 2003. Luminescence sensitivity changes of polymineral fine grains during IRSL and [post-IR] OSL measurements. Radiation Measurements, v. 37, p. 661-671.

Roberts, H.M., Duller, G.A.T., 2004. Standardised growth curves for optical dating of sediment using multiple-grain aliquots. Radiation Measurements, v. 38, p. 241-252.

Roberts, H.M., 2006. Optical dating of coarse-silt sized quartz from loess: Evaluation of equivalent dose determinations and SAR procedural checks. Radiation Measurements, v. 41, p. 923-929.

Roberts, H.M., 2007. Assessing the effectiveness of the double-SAR protocol in isolating a luminescence signal dominated by quartz. Radiation Measurements, v. 42, p. 1627–1636.

Rollinson, H.R., 1993. Using Geochemical Data: Evaluation, Presentation, Interpretation. Longman Singapore Publishers. 352p.

Rutter, N., Ding, Z.L., Evans, M.E., 1990. Magnetostratigraphy of the Baoji loess-paleosol section in the north-central China Loess Plateau. Quaternary International, v. 7-8, p. 97-102.

Schubel, J.R., Shen, H.T., Park, M.J., 1984. A comparison of some characteristic sedimentation processes of estuaries entering the Yellow Sea. In: Park, Y.A., Pilkey, O.H., Kim, S.W. (Eds.), Marine Geology and Physical Processes of the Yellow Sea, p. 286-308.

Shin, J.B., 2004. Loess-Paleosol Stratigraphy of Dukso and Hongcheon Areas and Correlation with Chinese Loess-Paleosol Stratigraphy: Application of Quaternary loess-paleosol stratigraphy to the Chongokni Paleolithic site. Unpublished Ph.D thesis, Yensei University, Korea.

Shin, J.B., Yu, K.M., Naruse, T., Hayashida, A., 2004. Study on loess-paleosol stratigraphy of Quaternary unconsolidated sediments at E55S20-IV pit of Chongokni Paleolithic Site. Journal of the Geological Society of Korea, v. 40, p. 369-381.

Simon, J.A., 2002. Testing and application of luminescence techniques using sediment from the southeast African coast. Unpublished PhD thesis. University of Wales, Aberystwyth.

Singarayer, J.S., Bailey, R.M., 2003. Further investigations of the quartz optically stimulated luminescence components using linear modulation. Radiation Measurements, v. 37, p. 451-458.

Singarayer, J.S., Bailey, R.M., 2004. Component-resolved bleaching spectra of quartz optically stimulated luminescence: preliminary results and implications for dating. Radiation Measurements, v. 38, p. 111-118.

Smith, B.W., Rhodes, E.J., 1994. Charge movements in quartz and their relevance to optical dating. Radiation Measurements, v. 23. p. 329-333.

Spalletti, L.A., Queralt, I., Matheos, S.D., Colombo, F., Maggi, J., 2008. Sedimentary petrology and geochemistry of siliciclastic rocks from the upper Jurassic Tordillo Formation (Neuquen Basin, western Argentina): Implications for provenance and tectonic setting, Journal of South American Earth Sciences, v. 25, p. 440-463.

Spooner, N.A., 1994a. On the optical dating signal from quartz. Radiation Measurements, v. 23, p. 593-600.

Spooner, N.A., 1994b. The anomalous fading of infrared-stimulated luminescence from feldspars. Radiation Measurements, v. 23, p. 625-632.

Stevens, T., Thomas, D.S.G., Armitage, S.J., Lunn, H.R., Lu, H., 2007. Reinterpreting climate proxy records from late Quaternary Chinese loess: a detailed OSL investigation. Earth Science Reviews, v. 80, p. 111–136.

Stokes, S., Bray, H.E., Blum, M.D., 2001. Optical resetting in large drainage basins: tests of zeroing assumptions using single-aliquot procedures. Quaternary Science Reviews, v. 20, p. 879-885.

Stokes, S., Hetzel, R., Bailey, R.M., Tao, M.X., 2003. Combined IRSL-OSL single aliquot regeneration (SAR) equivalent dose (D_e) estimates from source proximal Chinese loess. Quaternary Science Reviews, v. 22, p. 975-983.

Taylor, S.R., McLennan, S.M., 1981. The composition and evolution of the continental crust: rare earth element evidence from sedimentary rocks. *Phil. Trans. R. Soc.*, A301, 381-399.

Taylor, S.R., McLennan, S.M., 1985. The Continental Crust: Its Composition and Evolution. Blackwell, London, 312pp.

Thomas, P.J., Murray, A.S., Sandgren, P., 2003. Age limit and age underestimation using different OSL signals from lacustrine quartz and polymineral fine grains. Quaternary Science Reviews, v. 22, p. 1139-1143.

Thomas, P.J., Jain, M., Juyal, N., Singhvi, A.K., 2005. Comparison of single-grain and small-aliquot OSL dose estimates in <3000 years old river sediments from South India. Radiation Measurements, v. 39, p. 457-469.

Tsukamoto, S., Rink, W.J., Watanuki, T., 2003. OSL of tephric loess and volcanic quartz in Japan and an alternative procedure for estimating D_e from a fast OSL component. Radiation Measurements, v. 37, p. 459-465.

Tsukamoto, S., Duller, G.A.T., Wintle, A.G., 2008. Characteristics of thermally transferred optically stimulated luminescence (TT-OSL) in quartz and its potential for dating sediments. Radiation Measurements, v. 43, p. 1204-1218.

Wallinga, J., Murray. A.S., Duller, G.A.T., 2000. Underestimation of equivalent dose in single-aliquot optical dating of feldspars caused by preheating. Radiation Measurements, v. 32, p. 691-695.

Wallinga, J., Murray, A.S., Duller, G.A.T., Tornqvist, T.E., 2001. Testing optically stimulated luminescence dating of sand-sized quartz and feldspar from fluvial deposits. Earth and Planetary Science Letters, v. 193, p. 617-630.

Wallinga, J., 2002. Optically stimulated luminescence dating of fluvial deposits: a review. Boreas, v.31, p. 303-222. Oslo. ISSN 0300-9483.

Wang, X.L., Wintle, A.G., Lu, Y.C., 2006a. Thermally transferred luminescence in fine-grained quartz from Chinese loess: Basic observations. Radiation Measurements, v. 41, p. 649-658.

Wang, X.L., Lu, Y.C., Wintle, A.G., 2006b. Recuperated OSL dating of fine-grained quartz in Chinese loess. Quaternary Geochronology, v. 1, p. 89-100.

Wang, X.L., Lu, Y.C., Zhao, H., 2006c. On the performances of the single-aliquot regenerative-dose (SAR) protocol for Chinese loess: fine quartz and polymineral grains. Radiation Measurements, v. 41, p. 1-8.

Wang, X.L., Wintle, A.G., Lu, Y.C., 2007. Testing a single-aliquot protocol for recuperated OSL dating. Radiation Measurements, v. 42, p. 380-391.

Ward, S., Stokes, S., Bailey, R., Singarayer, J., Goudie, A., Bray, H., 2003. Optical dating of quartz from young samples and the effects of pre-heat temperature. Radiation Measurements, v. 37, p. 401–407.

Watanuki, T., Murray, A.S., Tsukamoto, S., 2003. A comparison of OSL ages derived from silt-sized quartz and polymineral grains from Chinese loess. Quaternary Science Reviews, v. 22, p. 991-997.

Watanuki, T., Murray, A.S., Tsukamoto, S., 2005. Quartz and polymineral luminescence dating of Japanese loess over the last 0.6 Ma: Comparison with an independent chronology. Earth and planetary Science Letters, v. 240, p. 774-789.

Wee, S.M., 1996. Geochemical Characteristics of the Quaternary Jungok basalt in Choogaryong rift valley, mid-Korean Peninsula. Journal of Economic and Environmental Geology, v. 29, p. 171-182.

Wei, J.W., Shi, X.F., Xin, C.Y., Chen, Z.H., 2000. Distribution patterns of clay minerals in the Yellow Sea and their significance. Yellow Sea: epicontinent shelf in Asia. Proceedings of First Korea–China Symposium on Sedimentary Processes and Depositional Environments, Ansan, Korea, April 6– 9, 2000. Seoul, Korea, pp. 179– 186.

Wells, J., 1988. Distribution of suspended sediment in the Korea Strait and southeastern Yellow Sea: onset of winter monsoons. Marine Geology, v. 83, p. 273-284.

Wintle, A.G., 1973. Anomalous fading of thermoluminescence in mineral samples. Nature, v. 245, p. 143-144.

Wintle, A.G., Murray, A.S., 1999. Luminescence sensitivity changes in quartz. Radiation Measurements, v. 30, p. 369-391.

Wintle, A.G., Murray, A.S., 2006. A review of quartz optically stimulated luminescence characteristics and their relevance in single-aliquot regeneration dating protocols. Radiation Measurements, v. 41, p. 369-391.

Wintle, A.G., 2008. Luminescence dating: where it has been and where it is going. Boreas, v. 37, p. 471-482.

Won, J.K., 1983. A study on the Quaternary volcanism in the Korean Peninsula – in the Choogaryong Rift valley, Journal of the Geological Society of Korea, v. 19, p. 159-168.

Won, J.K., Kim, Y.K., Lee, M.W., 1990. The study on the geochemistry of Choogaryong alkari basalt, Journal of the Geological Society of Korea, v. 26, p. 70-81.

Yang, S.Y., Jung, H.S., Choi, M.S., Li, C.X., 2002. The rare earth element compositions of the Changjiang (Yangtze) and Huanghe (Yellow) river sediments. Earth and Planetary Science Letters, v. 201, p. 407-419.

Yang, S.Y., Jung, H.S., Lim, D.I., LI, C.X., 2003. A review on the provenance discrimination of sediments in the Yellow Sea. Earth-Science Reviews, v. 63, p. 93-120.

Yang, S., Youn, J-S., 2007. Geochemical compositions and provenance discrimination of the central south Yellow Sea sediments. Marine Geology, v. 243, p. 229-241.

Yang. S.Y., Yim, W.W-S., Huang, G., 2008. Geochemical composition of inner shelf Quaternary sediments in the northern South China Sea with implications for provenance discrimination and paleoenvironmental reconstruction, Global and Planetary Change, v. 60, p. 207-221.

Yi, S., Clark, G.A., 1983. Observation on the Lower Palaeolithic of Northeast Asia. Current Anthropology, v. 24(2), p. 181-202.

Yi, S.B., 1984. Geoarcheology of Chongokni, Korea. In Chon-gok-ri, edited by Institute of Cultural Properties, p. 531-561. Institute of Cultural Properties, Seoul (in Korean).

Yi, S., 1986. Lower and Middle Palaeolithic of Northeast Asia: a geoarchaeological review. Department of Anthropology, Arizona State University, unpublished Ph.D. thesis.

Yi, S., 1989. The Study of Northeast Asian Palaeolithic. Seoul National University Press, Seoul (In Korean).

Yi, S., Soda, T., Arai, F., 1998. New discovery of Aira-Tn ash (AT) in Korea. Journal of the Korean Geographic Society, v. 33, p. 447-454.

Yi, S., 2005. New data on the formation of the basalt plain in the Imjin River basin. Journal of the Geomorphological Association of Korea, v. 12(3), p. 29-48. (in Korean).

Yi, S, Lee, Y.I., Lim, H.S., 2005. A Preliminary Study on the Geological Background of the Formation Process of Imjin Basin Palaeolithic Sites. v. I., Seoul National University Museum, Seoul.

Yoo, Y.W., 1997. On the characteristics of Handaxes from Imjin-Hantan Riverine Area.

Journal of the Korean Archaeological Society, v. 36, p. 147-80. (In Korean with English Abstract).

Yoo, Y.W., 2007. Long-Term Changes in the Organization of Lithic Technology : A Case Study from the Imjin-Hantan River Area, Korea. Department of Anthropology, McGill University, Montreal. unpublished Ph.D. thesis.

Yoon, S-O., Park, C-S., Hwang, S., Naruse, T., 2007. Weathering characteristics of Loess-Paleosol Sequence at the Daecheon area, South Korea. Journal of the Geological Society of Korea, v. 43, p. 281-296.

Yu, K-M., Shin, J-B., Naruse, T., 2008. Loess-paleosol stratigraphy of Dukso area, Namyangju City, Korea (South). Quaternary International, v. 176-177. P. 96-103.

Zhao, Y.Y., Qin, Z.Y., Li, F.Y., Chen, Y.W., 1990. On the source and genesis of the mud in the central area of the south Yellow Sea. Chin. J. Oceanol. Limnol, v. 8, 66-73.

Zhao, Y.Y., Park, Y.A., Qin, Y.S., Gao, S., Zhang, F.G., Yu, J.J., 1997. Recent development in the southern Yellow Sea sedimentology: China-Korea joint investigation. The Yellow Sea, v. 3, p. 47-51.

Zhao, Y.Y., Park, Y.A., Qin, Y.S., Choi, J.Y., Gao, S., Li, F.Y., Cheng, P., Jiang, R.H., 2001. Material source for the Eastern Yellow Sea Mud: evidence of mineralogy and geochemistry from China-Korea joint investigations. The Yellow Sea, v. 7, p. 22-26.

Zhang, J.F., Zhou, L.P., Yue, S.Y., 2003. Dating fluvial sediments by optically stimulated luminescence: selection of equivalent doses for age calculation. Quaternary Science Reviews, v. 22, p. 1123-1129.

Zhang, Z.F., Zhou, L.P., 2007. Optimization of the 'double SAR' procedure for polymineral fine grains. Radiation Measurements, v. 42, p. 1475-1482.

Zhang, Z.F., Fan, C.F., Wang, H., Zhou, L.P., 2007. Chronology of an oyster reef on the coast of Bohai Bay, China: constraints from optical dating using different luminescence signals from fine quartz and polymineral fine grains of coastal sediments. Quaternary Geochronology, v. 2, p. 71-76.

Zimmerman, D.W., 1971. Thermoluminescent dating using fine grains from pottery, Archaeometry, v. 13, p. 29-52.

요약 (국문초록)

 이 연구는 전곡리 고고학 유적지 일대에서 수집된 제 4기 미고화 퇴적물의 퇴적연대 측정과 지구 화학적 특성에 관한 연구이다. 수십년 동안, 많은 고고학 유물들이 이 지역에서 발견되었고 이러한 유물들은 아슐리안 석기와 유사한 형태를 보이기 때문에 동아시아의 전기 구석기 유적의 일부분으로 생각되어왔다. 이번 연구는 전곡리 고고학 유적지 일대의 12지점으로부터 연대 측정과 지구화학 분석을 위한 샘플링을 실시하였다. 또한, 이번 연구에서는 지표와 전곡 현무암층의 해발 고도가 측정되었다. 측정된 전곡 현무암층의 해발고도를 고려할 때 최소 3회 이상의 서로 다른 현무암 분출이 있었음을 나타낸다 (해발고도 48~49 m, 52 m, 53~54 m). 이러한 결과는 이 지역에 다수의 용암이 서로 다른 시간 간격으로 흘렀음을 지시한다. 총 12지점 중 3지점에서 25개의 시료로부터 연대측정이 실시되었다. 이번 연구에서는 광여기루미네선스 연대측정법이 활용되었다. 전곡리 시료 지점 1의 하성 퇴적층으로부터 수집된 시료의 경우 약 3만 4천년에서 6만 6천년의 넓은 연대분포를 보인다. 한편 시료 지점 2와 3번에서 수집된 세립질의 퇴적물로부터 얻은 연대값은 약 10만년에서 20만년 사이의 연대를 지시한다. 반면에 10만년 이내의 연대값들은 시료지점 2와 3에서 얻을 수 없었다. 이전 전곡 현무암에 대한 연대측정 결과들은 용암이 약 50만년부터 10만년까지 분출하였음을 지시한다. 전곡 현무암 상부에 분포하는 미고화 퇴적물을 이용한 이번 연대측정 결과는 미고화 퇴적물의 연대가 최소 20만년 전부터 형성되었음을 지시한다. 또한 전곡리 고고학 유적지의 유물 층준의 하한은 20만년 이내로 측정되었기 때문에 전곡리의 인류 기원은 20만년을 넘지는 않을 것으로 생각된다.

 제 4기 동안의 한반도의 고환경은 몬순의 영향을 받았다. 지화학 분석을 통한 전곡리 제4기 층의 기원 결과는 중국의 뢰스 기원과 한반도의 기반암

222

기원이 서로 혼합되어 유래되었음을 지시한다. 또한 가능성 있는 기원지는 중국과 한반도 사이에 위치한 황해지역이며 중국의 뢰스 퇴적물과 한반도에서 유입된 기반암 기원의 퇴적물들이 혼합된 후 재이동 되었을 가능성을 제시한다.

감사의 글

긴 시간이 흘러 졸업에 다가섰습니다. 석사 학위 이후 많은 갈등과 번민도 있었습니다. 하지만, 많은 분들의 도움으로 제가 이 자리까지 오지 않았나 싶습니다. 짧은 글로나마 고마움을 대신하고자 합니다.

제일 먼저 지도 교수님이신 이용일 교수님께 감사를 드립니다. 학문을 임하는 자세와 학문에 대한 열정을 몸소 보여주셨습니다. 선생님께서 가르쳐주신 많은 것들 잊지 않겠습니다. 학부 과정에 지도 교수님이셨고 또한 이번 학위 논문의 심사위원이셨던 정대교 교수님께 감사를 드립니다. 항상 관심 가져주시고 마음 써 주셔서 감사합니다. 이번 학위의 심사위원이셨던 이선복교수님과 이성근 교수님께 감사를 드립니다. 이선복 교수님께선 이 논문의 연구지역인 전곡리 일대를 처음 접할 수 있는 기회를 주셨으며 고고학에 대한 많은 조언을 해 주셨습니다. 이성근 교수님께선 항상 많은 관심과 지지를 보내주셨습니다. 또 다른 심사위원이셨던 최정헌 박사님께도 감사를 드립니다. 학위 과정 동안 많은 조언을 해주신 길영우 박사님과 박영윤 박사님께도 감사를 드립니다. 학위 과정을 무사히 마칠 수 있도록 많은 지원과 격려를 해주신 지질자원연구원 지표환경변화연구실 양동윤실장님과 김주용 박사님을 비롯한 많은 연구원들께도 감사를 드립니다. Professor Wintle, Professor Duller, Dr. Helen, Dr. Tsukamoto께 감사를 드립니다. 제가 1년 남짓 영국에서 공부할 때 정말로 많은 가르침과 도움을 받았

습니다. 서울대학교 퇴적시스템연구실 선후배님들께 감사를 드립니다. 모자란

저를 많이 챙겨 주시고 도와주셨습니다. 많지 않지만 소중한 제 삶의 활력소인

친구들에게도 심심한 감사를 드립니다. 항상 같이 하길 바랍니다.

저의 소중한 가족들에게 감사를 드립니다.

먼저 저의 어머니께 무한한 감사를 드립니다. 학위 과정 동안 많이 답답하셨을

텐데 묵묵히 지켜봐 주시고 응원해 주셔서 감사합니다. 앞으로 효도 많이 할께

요. 건강하세요. 사랑하는 누나들과 매형들 그리고 소중한 조카들에게도 감사를

드립니다. 저에게 정말로 커다란 힘이 되어 주었습니다. 장인어른과 장모님 그

리고 처남께 감사를 드립니다. 많이 부족한 저를 믿고 소중한 가정을 이루도록

허락해 주셔서 감사합니다. 소중한 저의 아내 임선에게 감사를 드립니다. 항상

옆에서 든든한 버팀목이 되어주었네요. 이제 갓 태어난 우리 딸 예지에게도 감

사를 드립니다. 마지막으로 하늘에 계신 아버지께서 줄곧 보살펴 주신 것 같습

니다. 변변치 못한 논문이지만 아버지께 바칩니다.